JBR–BTR, 2007, 90: 396.

Case 1
Patient presents with nodular swelling at the carpal region.
On radiography (Fig. A), there are multiple erosive lesions at the carpal bones (arrows).
On T1-weighted MR image (Fig. B) there are multiple soft tissue nodules of intermediate signal intensity, the osseous lesions having the same signal intensity when compared with the soft tissue nodules. A gradient echo-sequence is performed to confirm the presumed diagnosis (Fig. C).

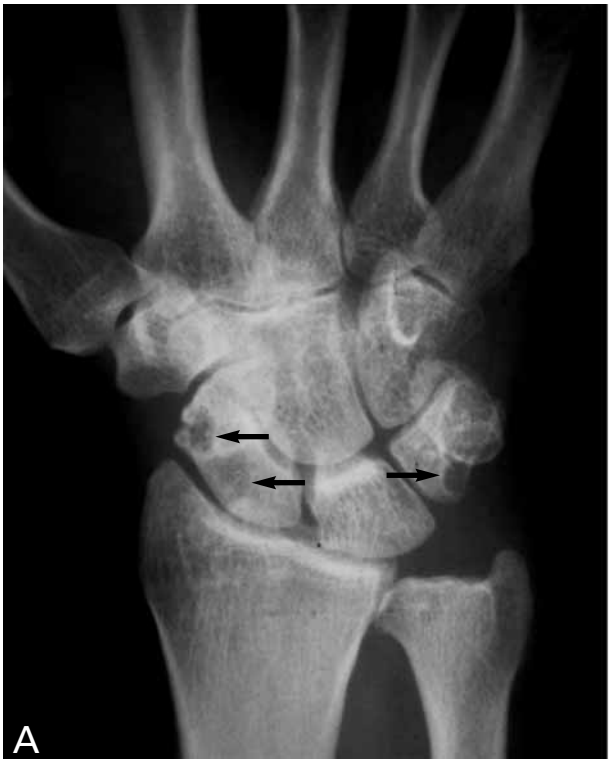

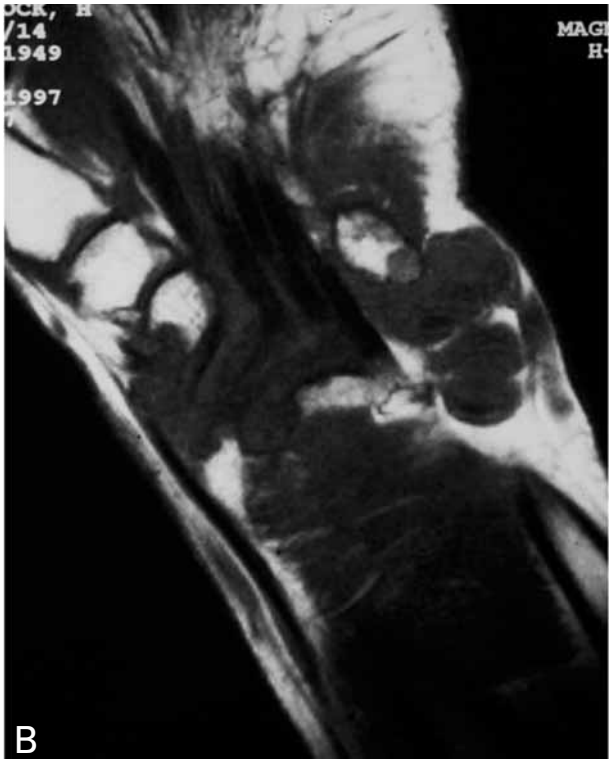

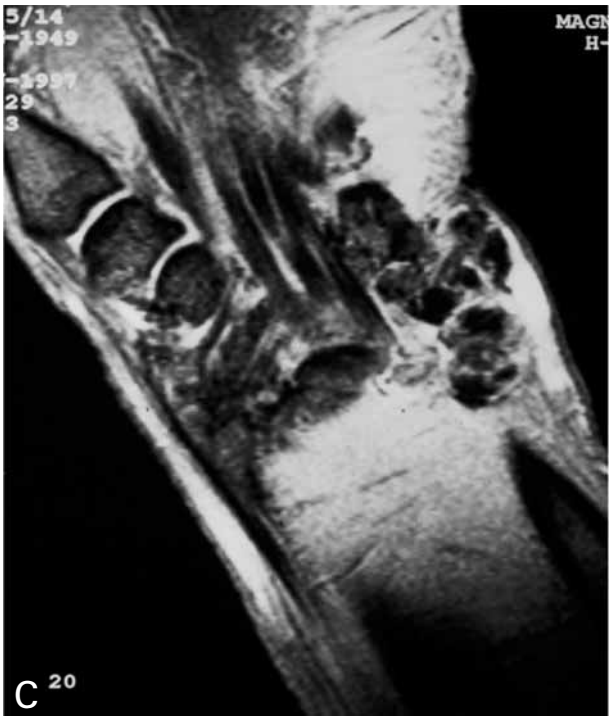

The combination of soft tissue and osseous lesions, the intra-articular localization, and the low signal intensity together with the presence of susceptibility artifacts (blooming effect) on gradient echo-sequence are almost diagnostic for a **pigmented villonodular synovitis**.

JBR–BTR, 2007, 90: 397.

Case 2
Twenty two-year-old patient. Radiography (Fig. A) shows a large lytic lesion in the distal half of the diaphysis and metaphysis of the fourth metacarpal without epiphyseal involvement. There is diffuse cortical disruption and considerable expansion. Most of the lesion is outlined by a paper-thin shell of bone, which is confirmed by the CT-scan (Fig. B). On T2-weighted MR-images (Fig. C) the lesion is multiloculated and several fluid-fluid levels are visible (arrows).

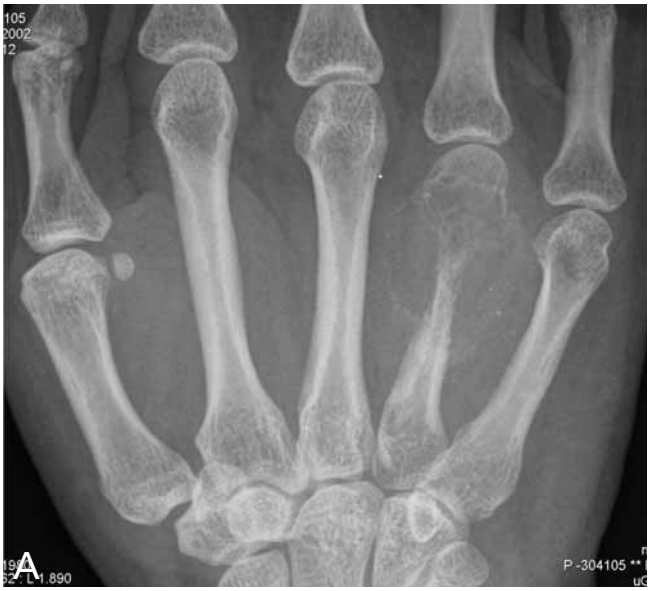

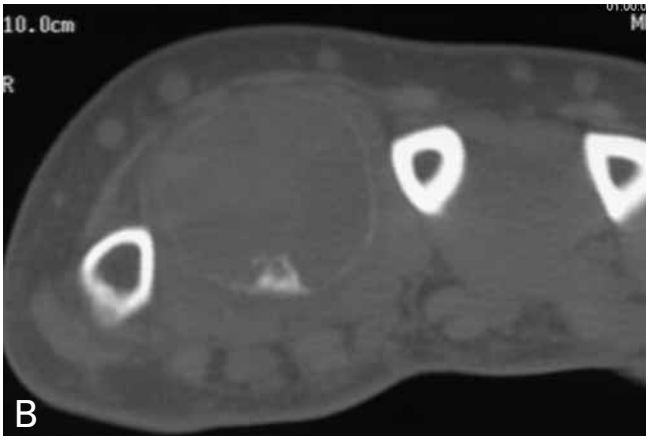

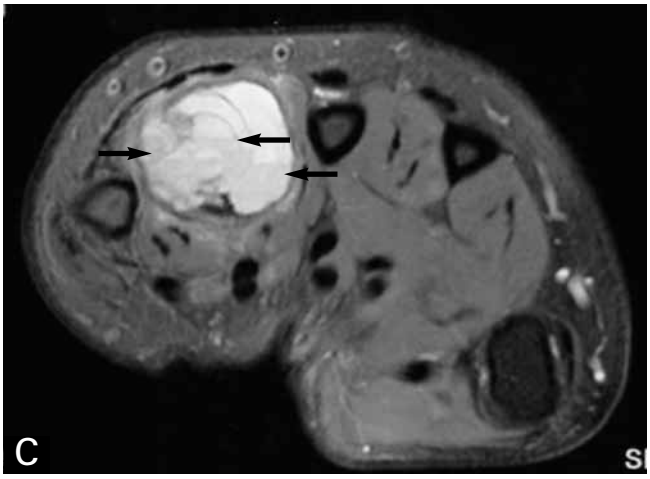

Histological examination after curettage revealed a typical **aneurysmal bone cyst**.
The blowout or ballooning with a thin shell of surrounding periosteal bone together with the fluid-fluid levels are characteristic features of an aneurysmal bone cyst.

JBR–BTR, 2007, 90: 398.

Case 3
A young boy presents with a mass lesion at the carpal tunnel. On T1- (Fig. A) as well as on T2- weighted (Fig. B) MR image there is a mixture of low and high signal intensity components.On both sequences there is a characteristic "fascicular sign". On sagittal T1-weighted image (Fig. C) low signal intensity components have a linear shape and longitudinal course.

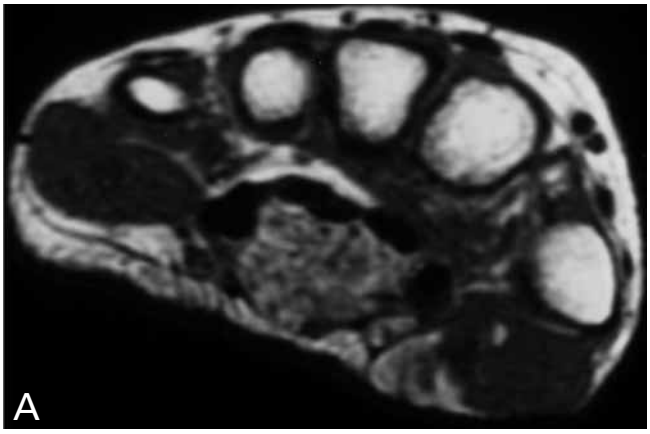

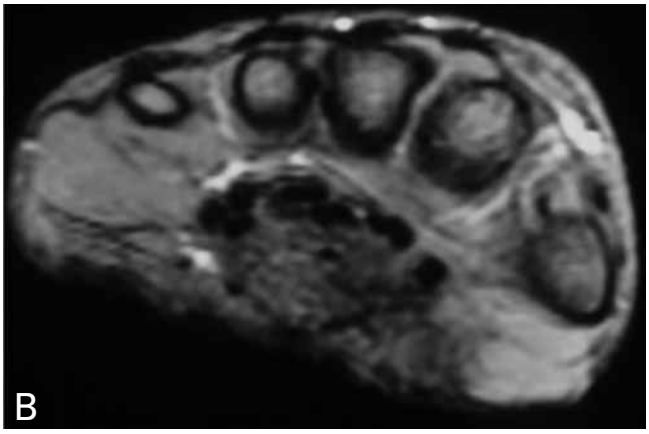

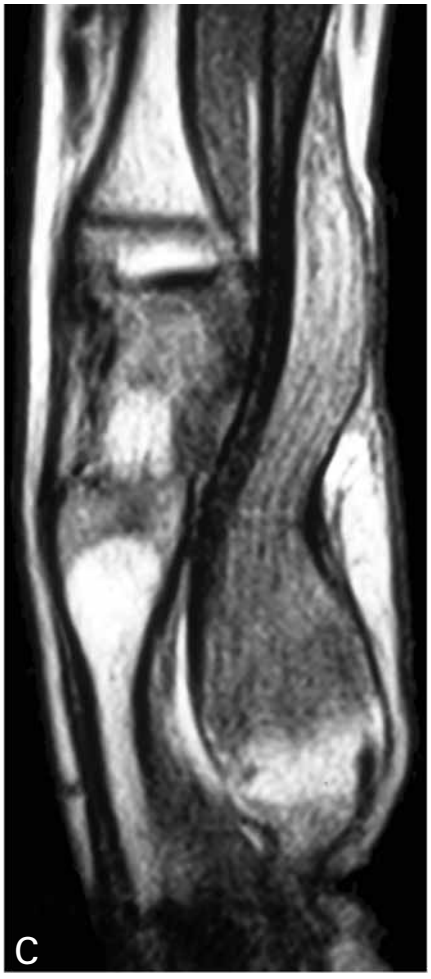

Fibrous and fatty components are responsible for the mixed signal intensity of the lesion as well on T1- as on T2-WI. Longitudinally coursing nerve bundles are responsible for the fascicular sign on axial images and for the spaghettilike appearance on longitudinal images. MR features, morphology and location are characteristic for **lipomatosis of the median nerve (fibrolipohamartoma).**

JBR–BTR, 2007, 90: 399.

Case 4
Conventional radiography of both hands (Fig. A) shows diffuse demineralisation of bone and subperiosteal bone resorption at the radial aspects of the middle phalanges and phalangeal tufts. Paraarticular soft tissue deposits of tumoral calcinosis and vascular calcifications are also seen.

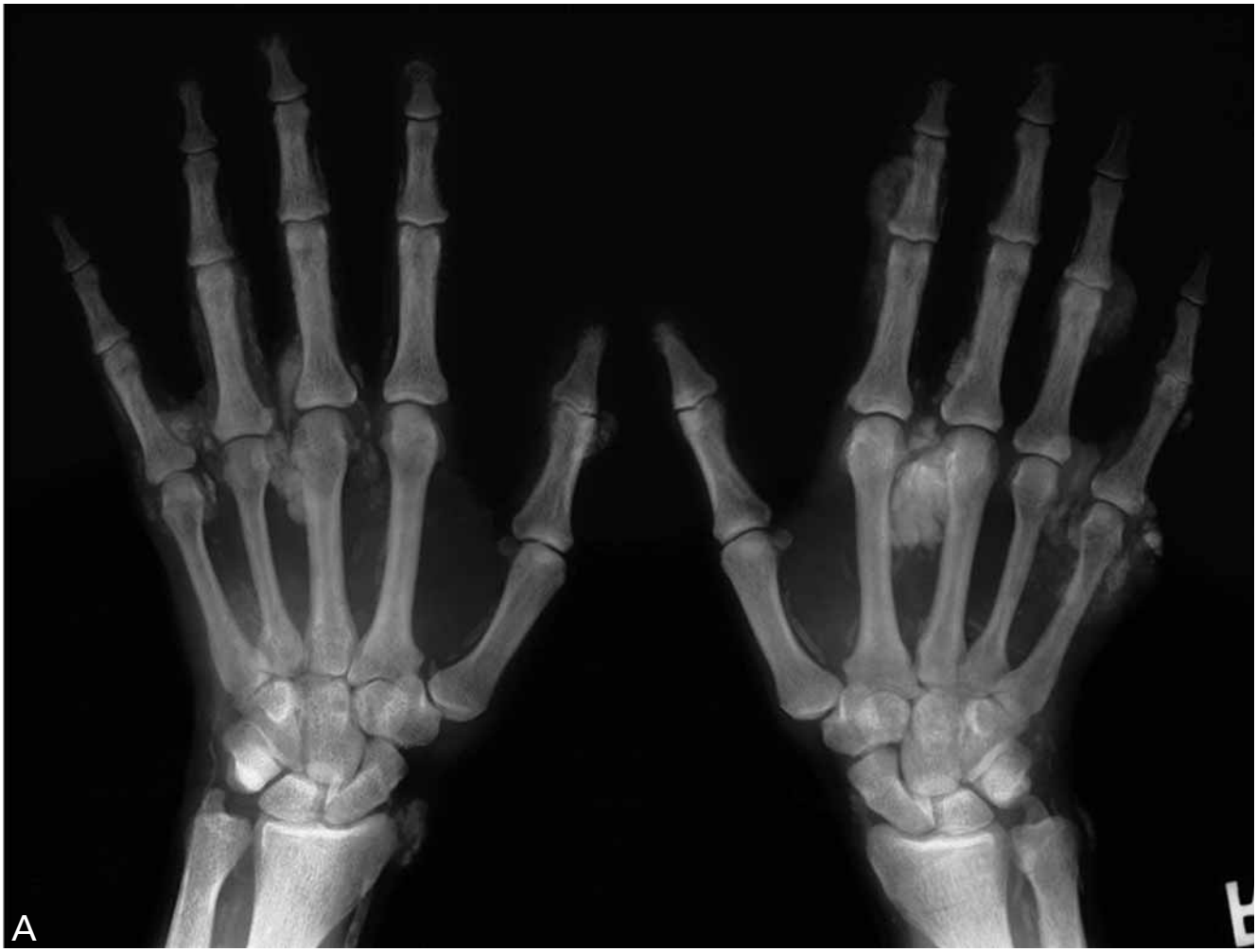

The diagnosis of **renal osteodystrophy** was established. Renal osteodystrophy occurs in patients with chronic renal failure. Renal failure results in hyperphosphatemia and increased synthesis of parathyroid hormone. Because normal kidney function is fundamental to the proper metabolism of vitamin D, renal diseases can lead to rickets and osteomalacia. Musculoskeletal abnormalities of renal osteodystrophy may show features of hyperparathyroidism, rickets and osteomalacia, and soft tissue and vascular calcifications.

JBR–BTR, 2007, 90: 400.

Case 5
Patient presenting with radiating finger pain elicited by changes in temperature. MRI shows a well defined, subungual lesion of low to intermediate signal intensity on T1-weighted image (not shown), homogeneous high signal intensity on T2-weighted images (Fig. A and B) and marked enhancement after administration of Gadolinium chelates (Fig. C).

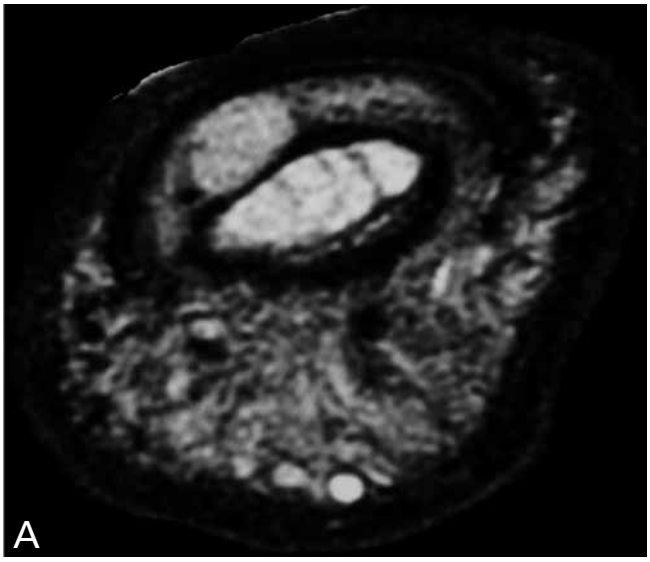

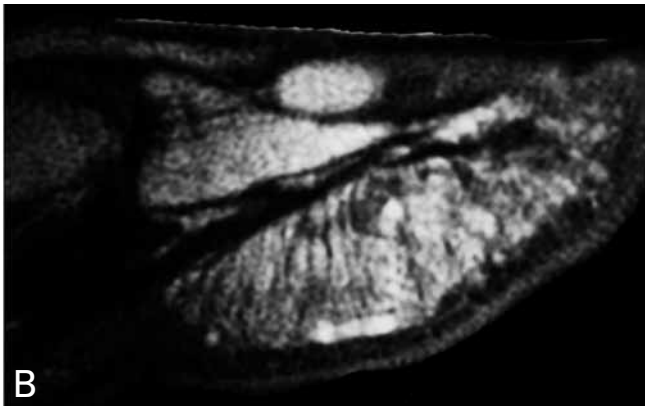

Location of the lesion (subungual), clinical history and MR findings are highly suggestive for a **glomus tumor**

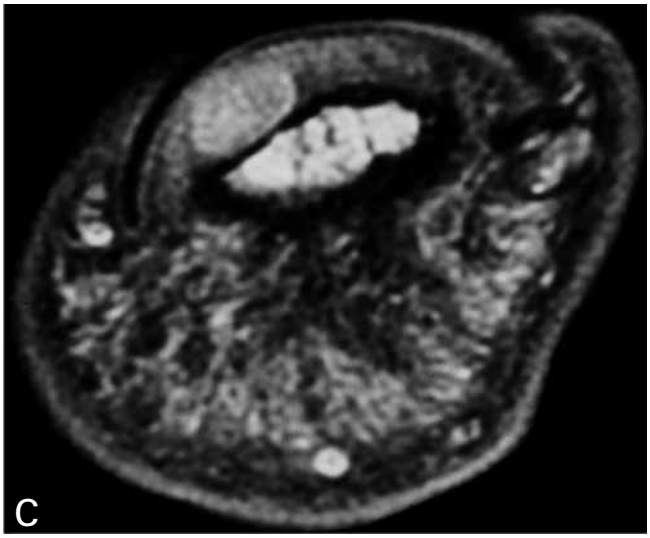

JBR–BTR, 2007, 90: 401.

Case 6
A 37-year-old man had a swelling at the volar side of the middle phalanx of the third digit of the right hand.
Radiography (Fig. A) showed a well defined compact calcification, arising from the periost. No flaring of the cortex or medullary continuity was noted.

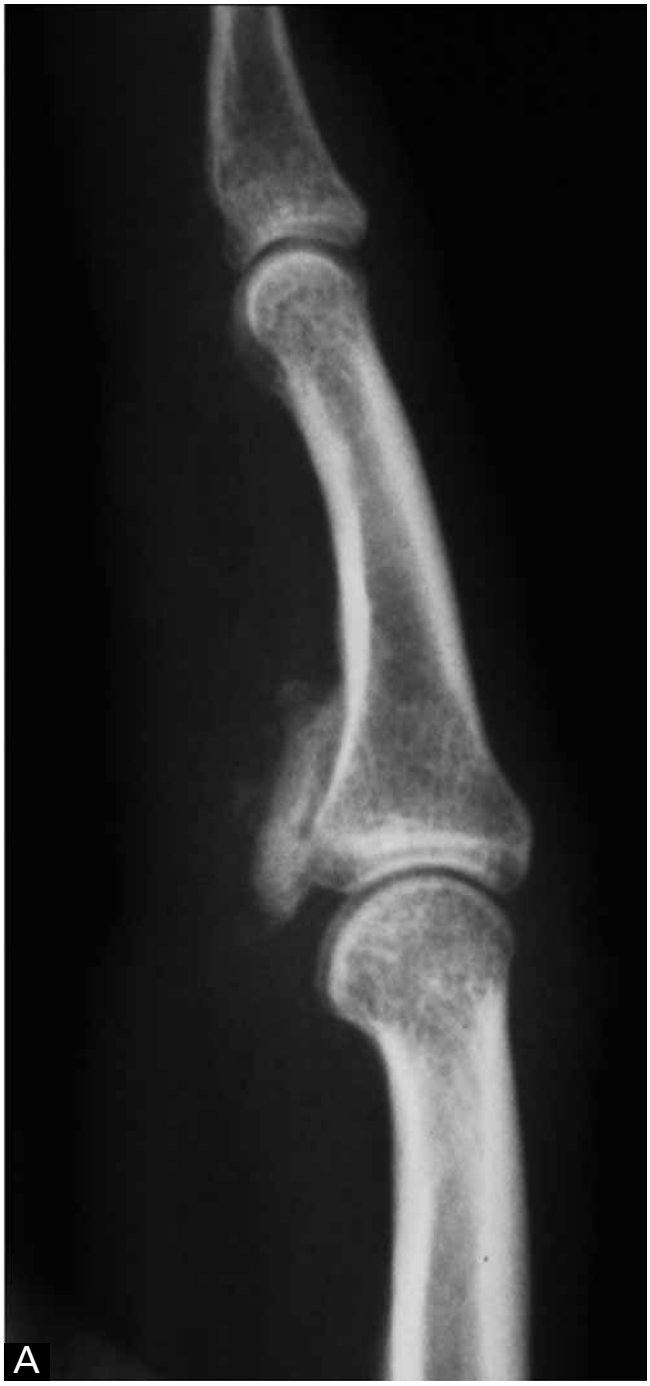

This is an example of a **Nora's lesion**, which can be defined as a well marginated mass of heterotopic mineralization arising from the periosteal aspect of an intact cortex, without medullary changes.
It has a distinct radiological appearance and is part of a spectrum of reactive lesions, which includes florid reactive periostitis and turret exostosis.

JBR–BTR, 2007, 90: 402.

Case 7
Patient presenting with mildly painful nodules at the third ray of the hand. On T1-weighted MR images the lesions are hardly visible (not shown), on T2-weighted images with fat suppression there are at least six small nodules of high signal intensity (Fig. A and B), which enhance markedly after administration of Gadolinium chelates (Fig. C).

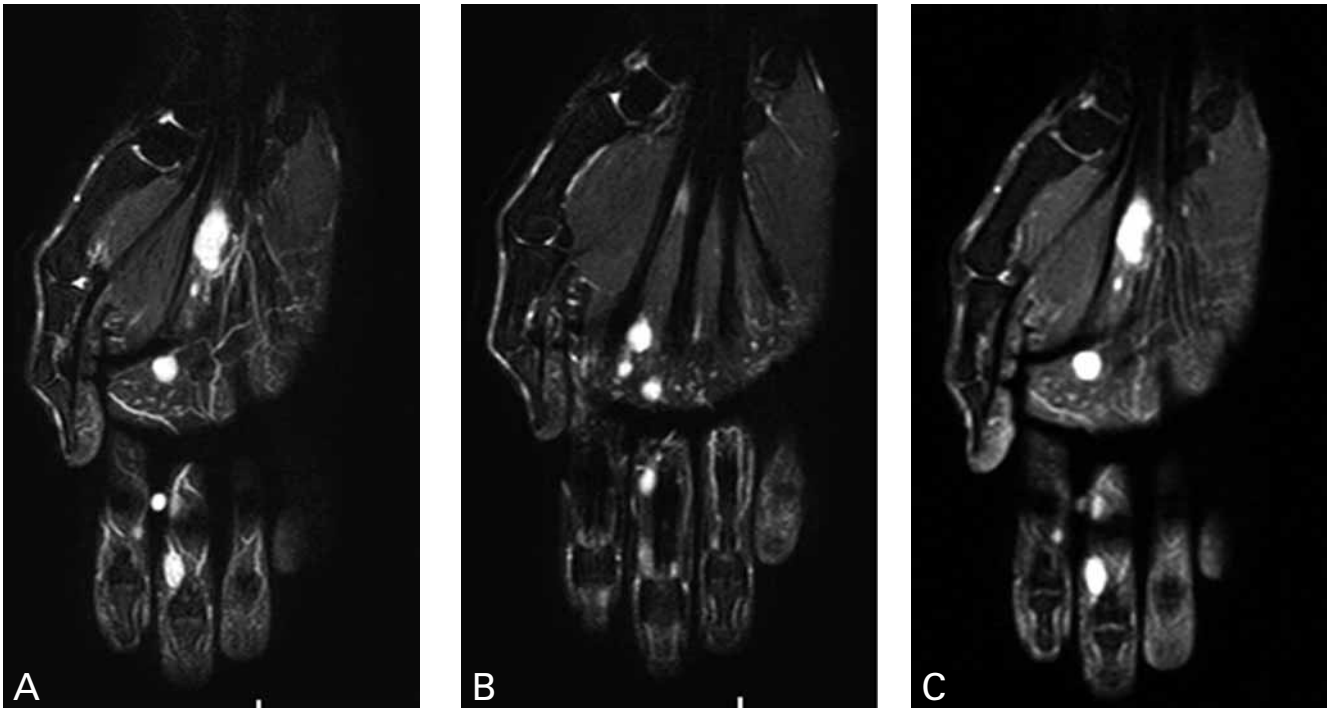

Histological examination after resection of one of the nodules revealed typical features of a schwannoma. As a consequence the diagnosis of **Schwannomatosis** was made. It is a rare condition characterized by the presence of multiple schwannomas, without clinical or radiological evidence of neurofibromatosis Type 1 or 2.

JBR–BTR, 2007, 90: 403.

Case 8
A 20-year-old woman had a swelling at the volar aspect of the tuft of the thumb.
Plain radiography revealed a well defined area of compact bone arising from the periost (Fig. A).
Surgical resection was 5 months later followed by a recurrence (Fig. B).

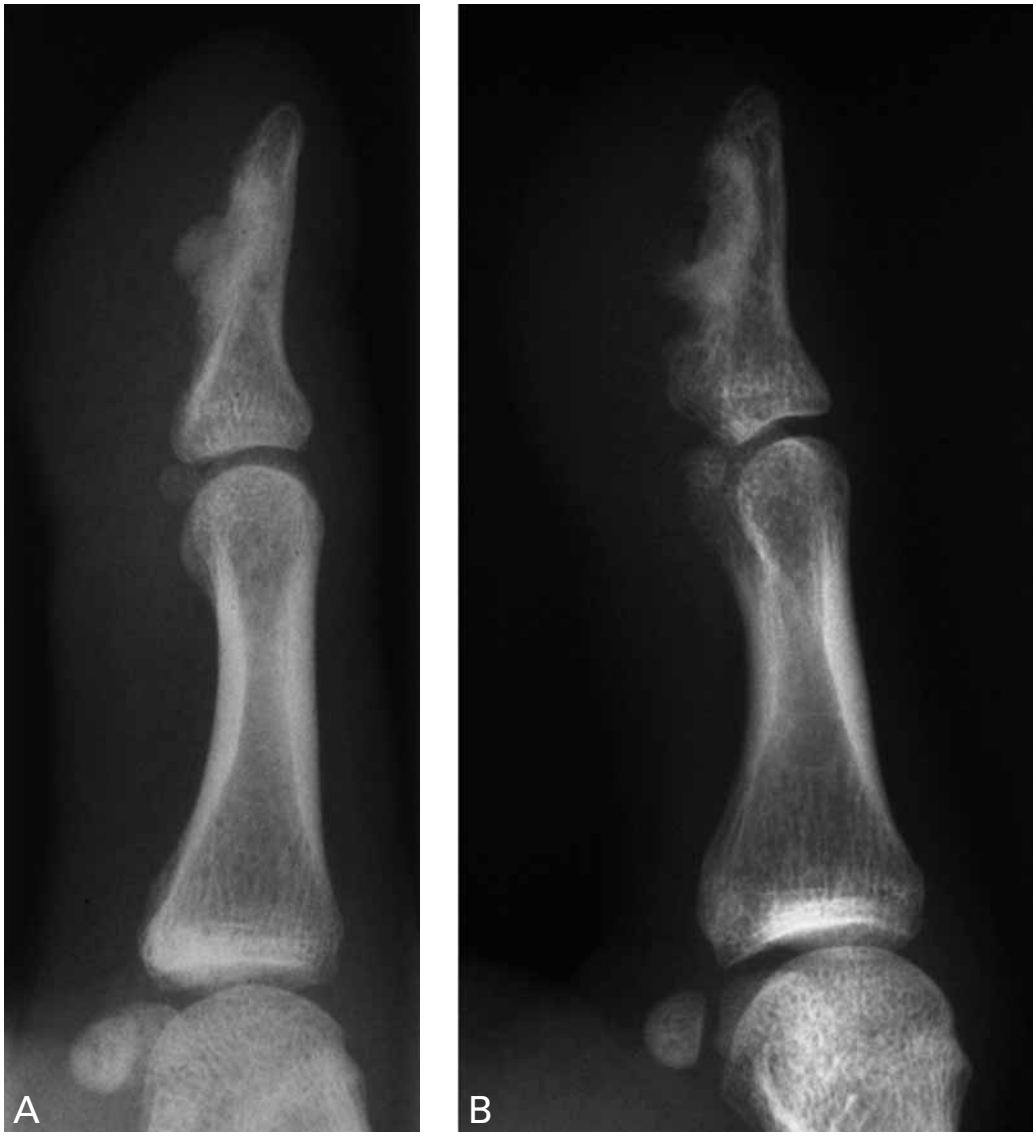

This is a **turret exostosis**, also known as an acquired osteochondroma. It is the end stage of a spectrum of reactive lesions, which are florid periostitis, Nora's lesion and turret exostosis.
It is considered as a non-touch lesion.

JBR–BTR, 2007, 90: 404.

Case 9
A 42-year-old male presented with pain and swelling of his feet. He also had a non-healing ulcer on the first toe of the right foot. Two months later he complained of pain in both hands, located at the level of the PIP-joints. There were no signs of Raynaud's phenomenon, skin abnormalities or Sjögren syndrome. Patient had a history of 30 pack years of smoking. A CT-angiography revealed no abnormalities of the large and middle large arteries. Angiogram of the right hand (Fig. A and B) shows multiple occlusions of digital arteries in the fingers and collateral vessels in the first en second digit with a corkscrew appearance in the index finger.

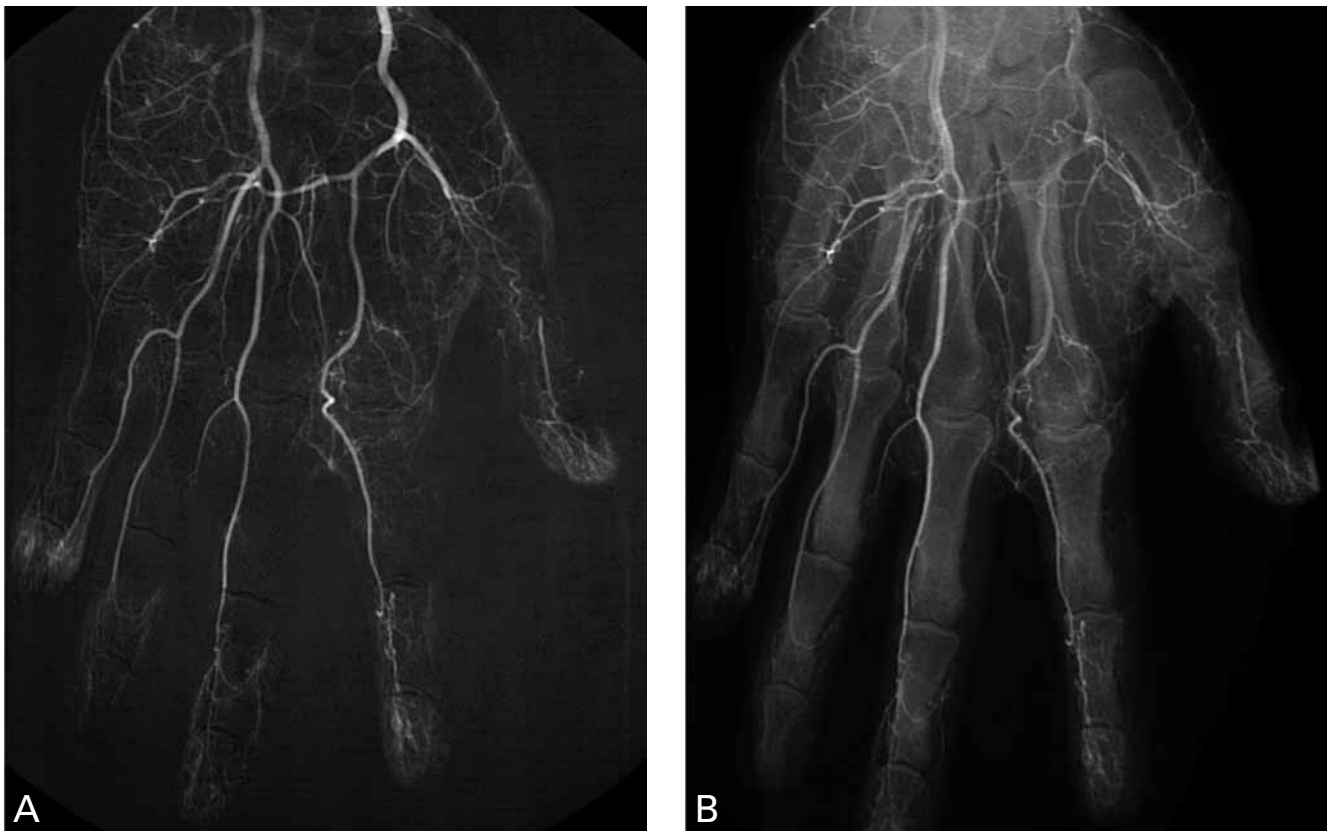

Angiographic abnormalities are typical for **Buerger's disease (thrombangiitis obliterans**). The diagnosis was confirmed by histopathology, after amputation of the first toe of the right foot. Tobacco abuse is a risk factor.

JBR–BTR, 2007, 90: 405.

Case 10
Conventional radiography (PA view) (Fig. A) of the left hand demonstrates shortening of the first, fourth and fifth metacarpal (positive metacarpal sign) with soft tissue calcifications along the fourth and fifth digits. Conventional radiography of the thumb (magnified PA view) (Fig. B) in another patient shows shortening of the first metacarpal with soft tissue calcifications along the phalanx.

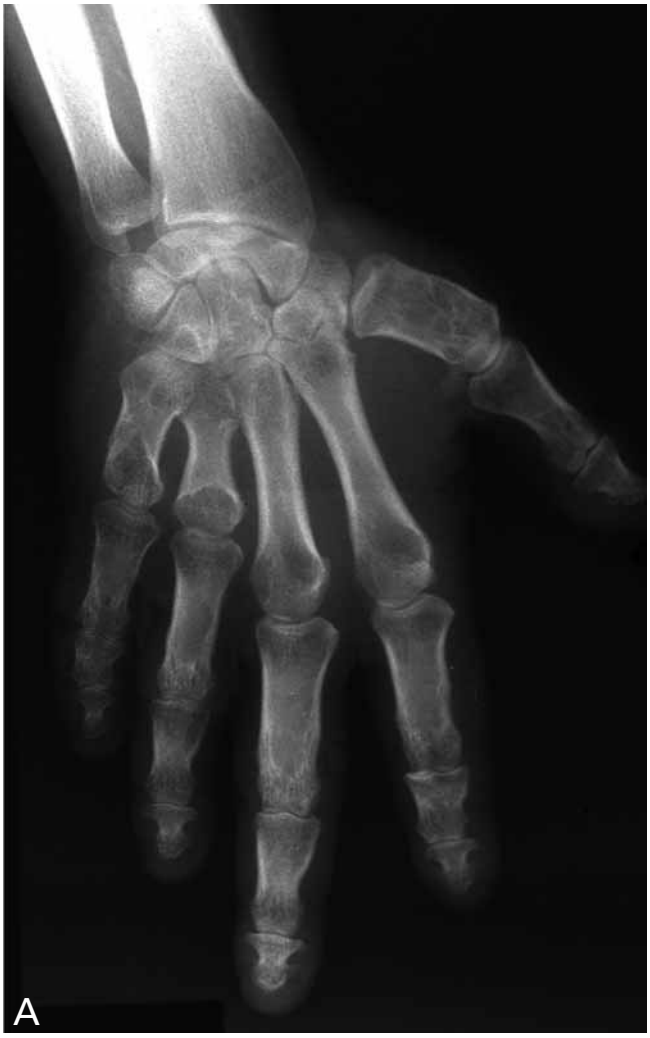

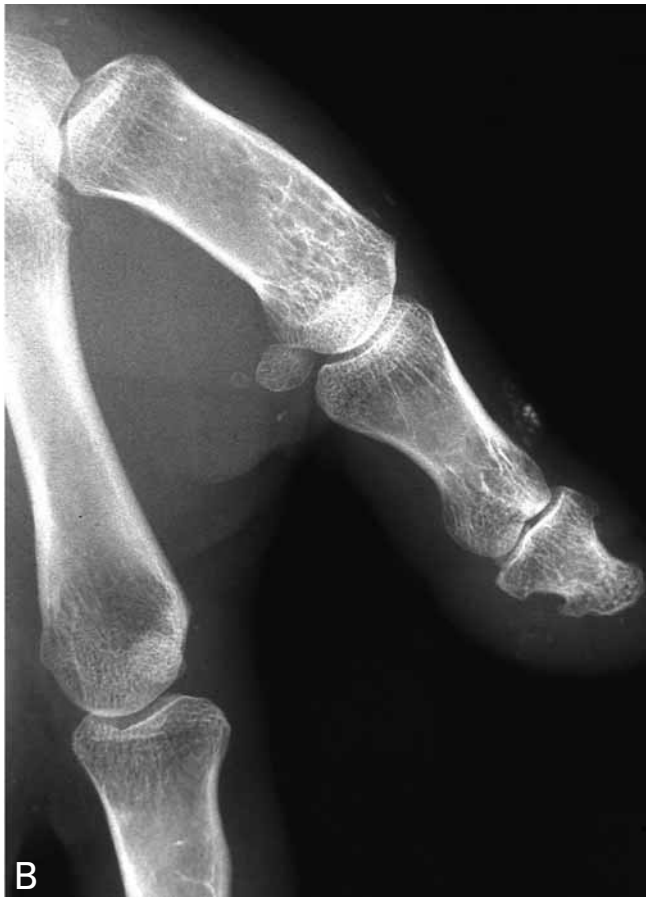

Pseudohypoparathyroidism was diagnosed. Pseudohypoparathyroidism (PHP), first described by Fuller Albright in 1942, is a congenital X-linked dominant genetic disorder characterized by hypocalcemia, hyperphosphatemia, normal or increased serum levels of parathyroid hormone (PTH) and resistance to the biological activity of PTH due to end organ resistance, presence of antienzymes or defective hormone. These abnormalities typically go along with an unusual constellation of developmental and skeletal defects such as short obese stature, round face, brachydactyly (usually fourth and fifth metacarpals), dental hypoplasia and soft tissue calcifications.

JBR–BTR, 2007, 90: 406.

Case 11
Conventional radiography of the left hand (oblique and PA view and detail of MCP joint 3) (Fig. A) shows destruction with fragmentation of the third metacarpal head. Mild erosive lining at the base of the proximal phalanx with some periosteal reaction and thickening of the surrounding soft tissues. Also note cartilage loss at the radiocarpal joint with heterotopic calcified debris at the distal ulna and an old fracture of the distal radius. Lateral radiograph of the ankle in the same patient (Fig. B) demonstrates hindfoot destructive arthropathy in a hypertrophic reparative sclerotic phase.

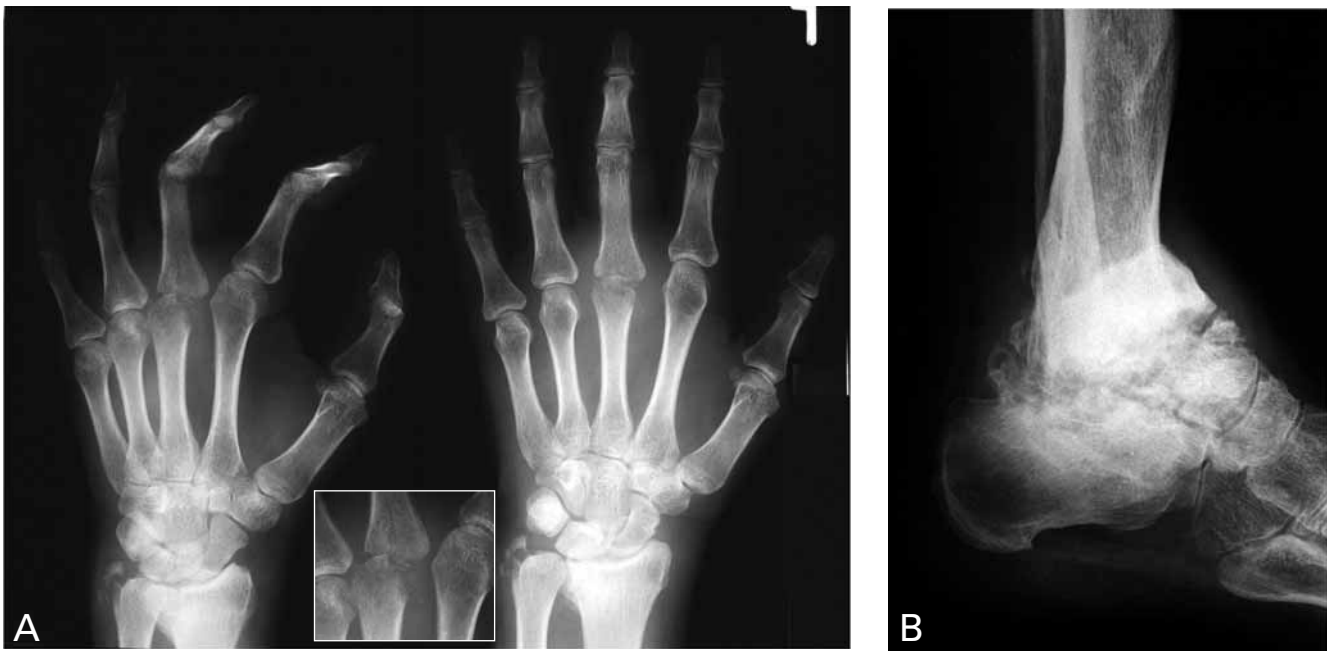

Acute eruption of **neuropathic osteo-arthropathy** (Charcot arthropathy) of the MCP joint in a diabetic patient with known chronic Charcot joint of the ankle and wrist was diagnosed. Neuropathic osteo-arthropathy represents a traumatic arthropathy due to loss of pain sensation and proprioception of the affected limb associated with sympathetic dysfunction resulting in local hyperemia and bone resorption. Nowadays, it is seen most frequently in patients with diabetes mellitus. The ankle and foot are most commonly affected, hand involvement is much less frequent.

JBR–BTR, 2007, 90: 407.

Case 12
Radiography (Fig. A) shows an erosion at the base of the second metacarpal bone (arrows) without other pathological findings. There is a marked thickening and contrast enhancement of the radiocarpal and mid-carpal joint capsule on MRI (sagittal T1-weighted, axial T1-weighted after administration of Gadolinium chelates and with fat suppression) with an additional erosion at the volar aspect of the capitate (Fig. B and C).

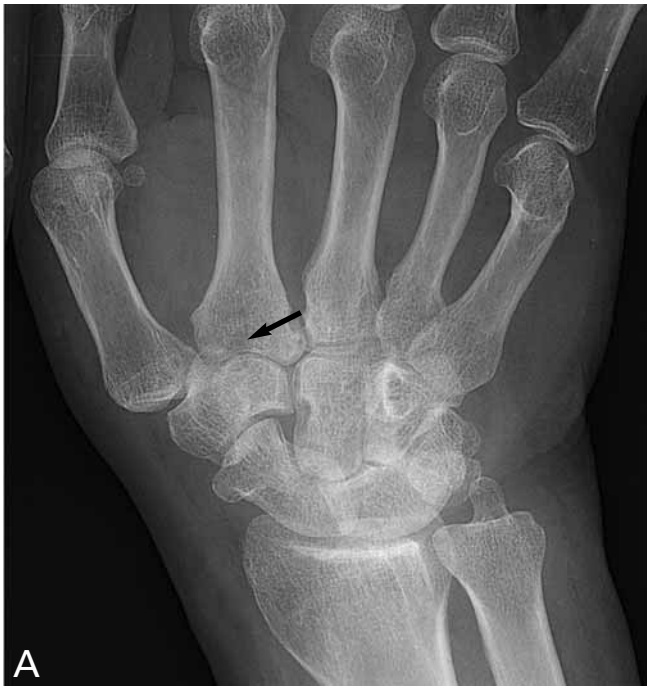

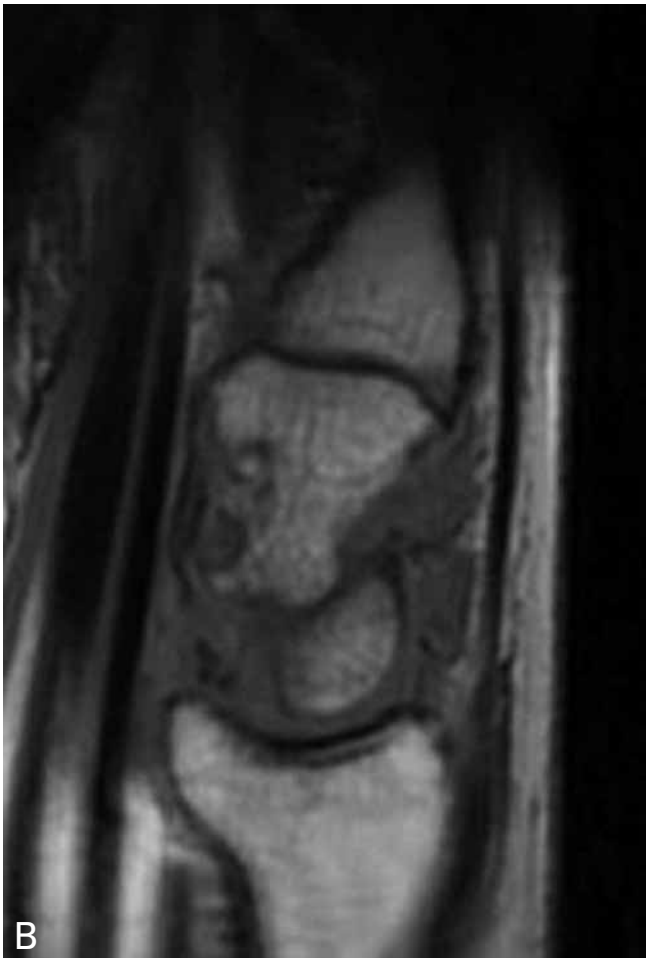

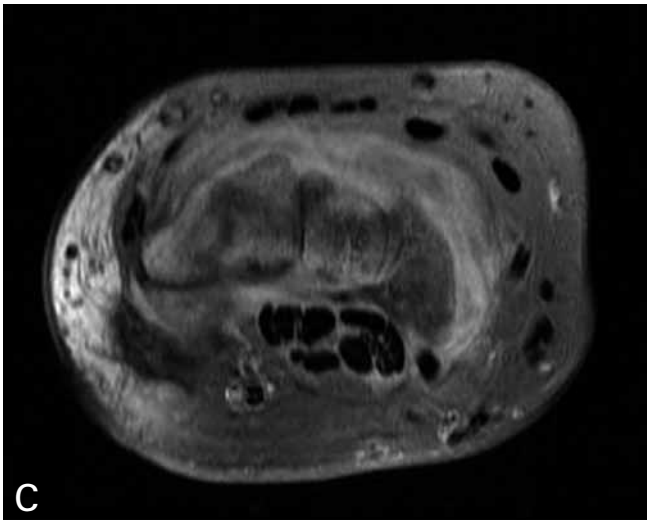

Although findings on radiography are not characteristic, MR features of an erosive, inflammatory joint disease, together with a positive serology (increased rheumatoid factor) are diagnostic for **rheumatoid arthritis**.

JBR–BTR, 2007, 90: 408.

Case 13
Conventional radiography of the right wrist (PA and lateral view) (Fig. A) shows widened physes and flaring and cupping of the metaphyses in distal radius and ulna. Diffuse osteopenia and coarsened trabecular bone.
Conventional radiography of both hands (PA view) of an other patient (Fig. B) shows the advanced demineralization and disorganization of the metaphysis. The provisional calcification zone of the metaphysis is much more distant from the calcification center of the epiphysis than is normal for age.

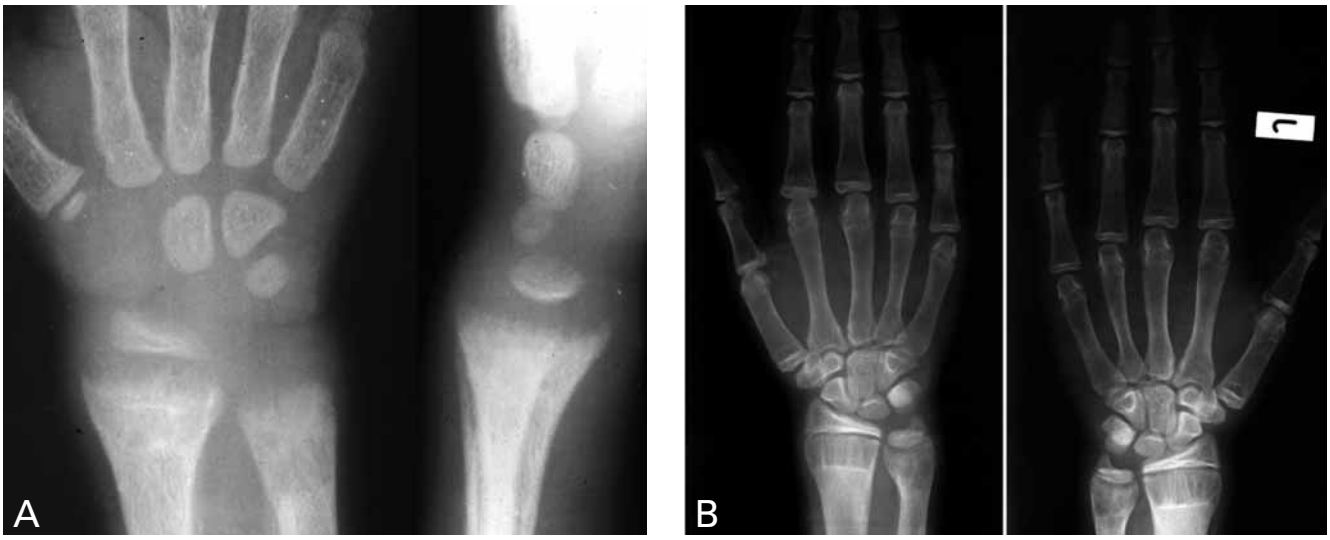

The diagnosis of **Rickets** (Phenytoin-induced in Fig. A and Dietary and lack of sunlight due to clothing-induced in Fig. B) was made. Rickets is defined as the failure of osteoid to calcify in a growing person. Failure of osteoid to calcify in the adult is called osteomalacia. Rickets occurs when the metabolites of vitamin D are deficient. Less commonly, dietary deficiency of calcium or phosphorus may produce rickets. Vitamin D (cholecalciferol [vitamin D-3], a steroid compound) is formed in the skin under the stimulus of ultraviolet light. Ultraviolet light was the only significant source of vitamin D until early in the 20th century when ergosterol (vitamin D-2), contained in fish liver oil or as an irradiated plant steroid, was discovered.
The anticonvulsant drugs phenobarbital and phenytoin accelerate metabolism of a vitamin D metabolite (calcidiol), which may lead to insufficiency and rickets, particularly in children who are kept indoors in institutions.

JBR–BTR, 2007, 90: 409.

Case 14
Patient presenting with a painful mass lesion at the hypothenar. On T1-weighted MR image (Fig. A) there is a large mass within the hypothenar muscles (abductor digiti minimi), inhomogeneous and slightly hyperintense to adjacent normal muscle. Infiltration is seen toward the muscle belly. On T2-weighted MR image with fat suppression (Fig. B) the lesion is ill defined and of very high signal intensity, with a scar-like central component of lower signal intensity. On T1-weighted MR image after administration of Gadolinium chelates (Fig. C), there is a septal and peripheral enhancement.

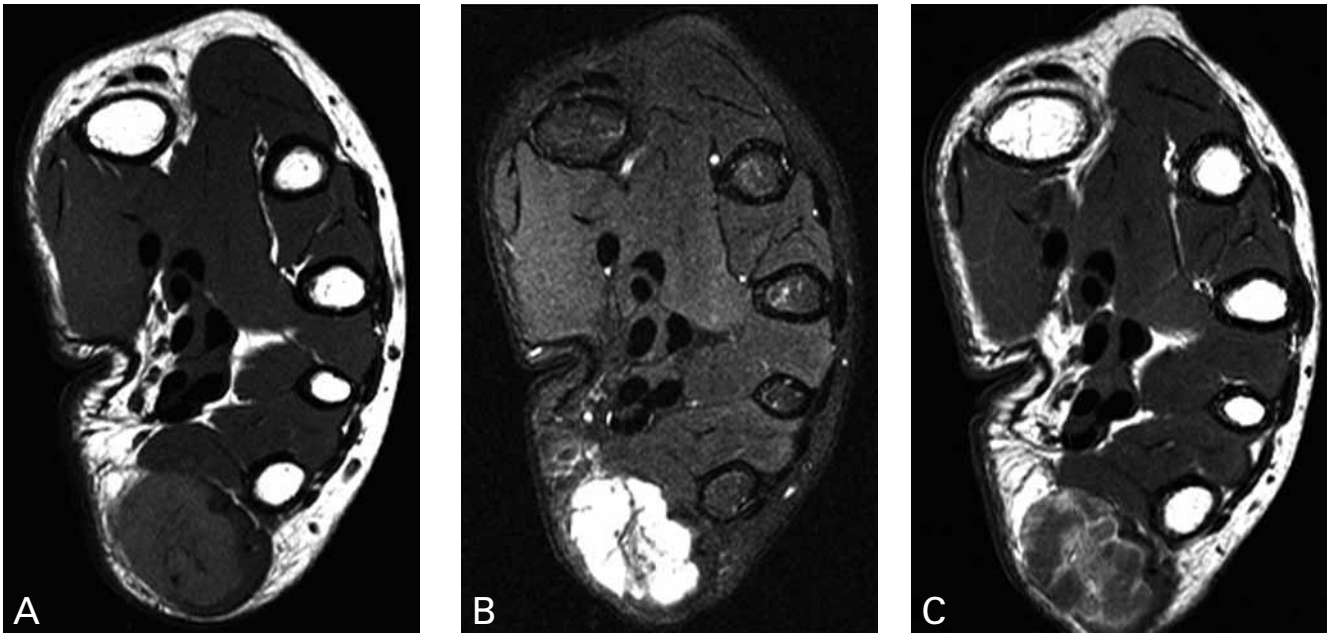

After biopsy and histological examination, the lesion proved to be an **alveolar rhabdomyosarcoma** of the hypothenar.
Although features are in favor of a malignant soft tissue tumor, MR doesn't allow to make a more tissue specific oriented diagnosis in this case.

JBR–BTR, 2007, 90: 410.

Case 15
Twenty five-year-old patient. Painless swelling, 10 years after a severe crush trauma. On radiography (Fig. A and B) an expansile, lytic lesion with cortical disruption of its volar half is shown at the tuft of a distal phalanx. The lesion is partially surrounded by a thin sclerotic rim. Also notice a small pathologic fracture at the proximal site. On color Doppler ultrasound (not shown) no intralesional vascularization could be demonstrated.

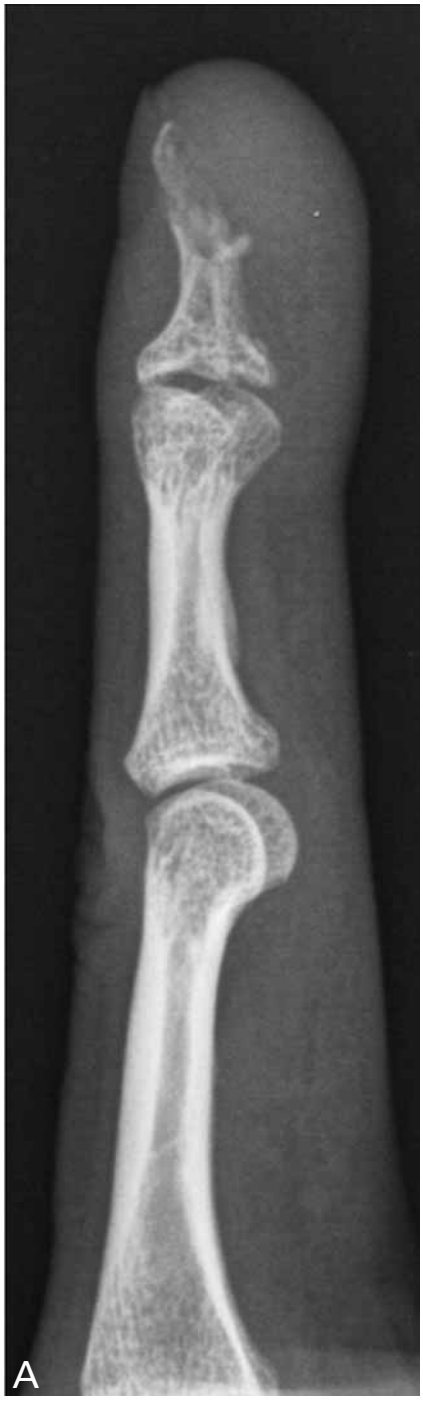

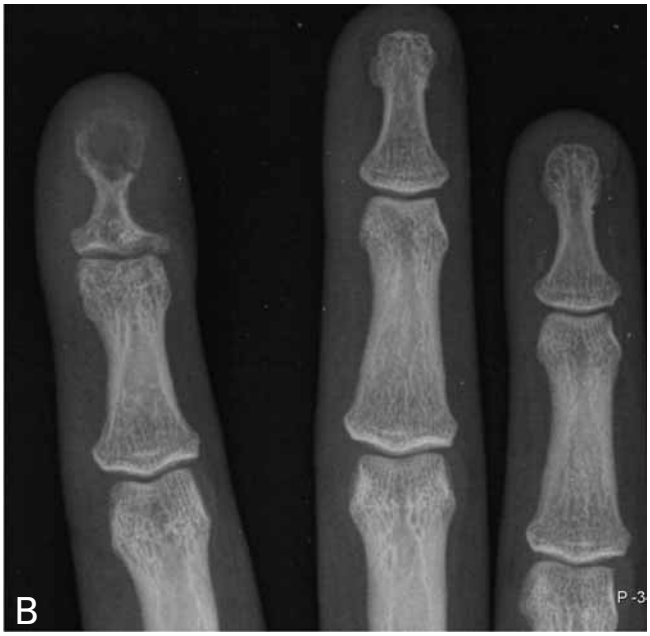

The differential diagnosis of this lesion is an epidermal cyst or a glomus tumor. The clinical presentation and the absence of intralesional vascularisation are in favor of an **epidermal cyst,** which was proven by the histological examination after curettage.

JBR–BTR, 2007, 90: 411.

Case 16

A 40-year-old man with pain and swelling at the dorsum of the right wrist had a MR examination 7 months after a wrist injury.

There was no significant scapholunate dissociation on radiographs. The arthrogram was negative as well. STIR and 2D gradient echo MR images were obtained in the coronal plane as well as proton density (PD) and T2-weighted spin echo images in the transverse plane (with 2 mm thick slices).

The ventral portion of the scapholunate (SL) ligament is thickened and amorphous with a low signal intensity on T2 (arrow) probably due to fibrous infiltration (Fig. A). The presence of fibrous scar tissue in injured SL ligaments might partially explain the absence of contrast penetration at arthrography.

The ligament has an intermediate signal intensity on T2*-weighted gradient echo image (arrow), increased in comparison with the low signal triangular fibrocartilage (Fig. B).

The thickening of the ventral portion of the scapholunate (SL) ligament should also be recognized on the axial PD and T2-weighted images (Fig. C and D, arrow).

On the coronal T2-weighted image (Fig. E), high signal fluid is demonstrated in the adjacent scapholunate space as well as low signal subchondral sclerosis (as a sequel of subchondral bone impaction) (arrow).

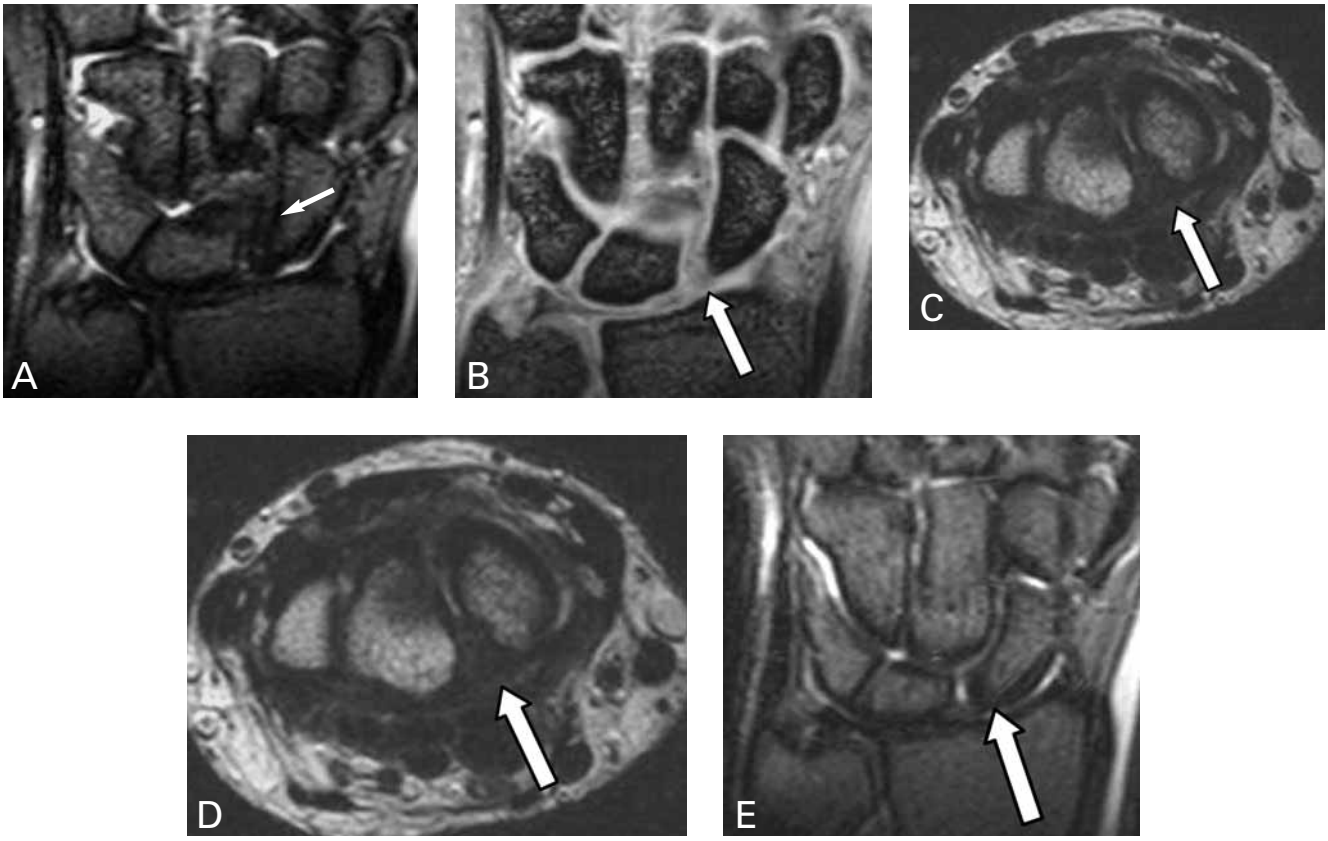

Fibrous thickening of the volar part of the **SL ligament** is indicative of a **sequel of partial traumatic rupture or elongation (stretching).**

The area of bone sclerosis at the proximal pole of the scaphoid might be in this case a sequel of **subchondral bone impaction.**

JBR–BTR, 2007, 90: 412.

Case 17
Seventy four-year-old patient. Radiography (Fig. A) shows diffuse involvement of the proximal phalanx of the middle finger with an increased diameter and length, thickening and tunneling of the cortex and a coarse trabecular pattern.

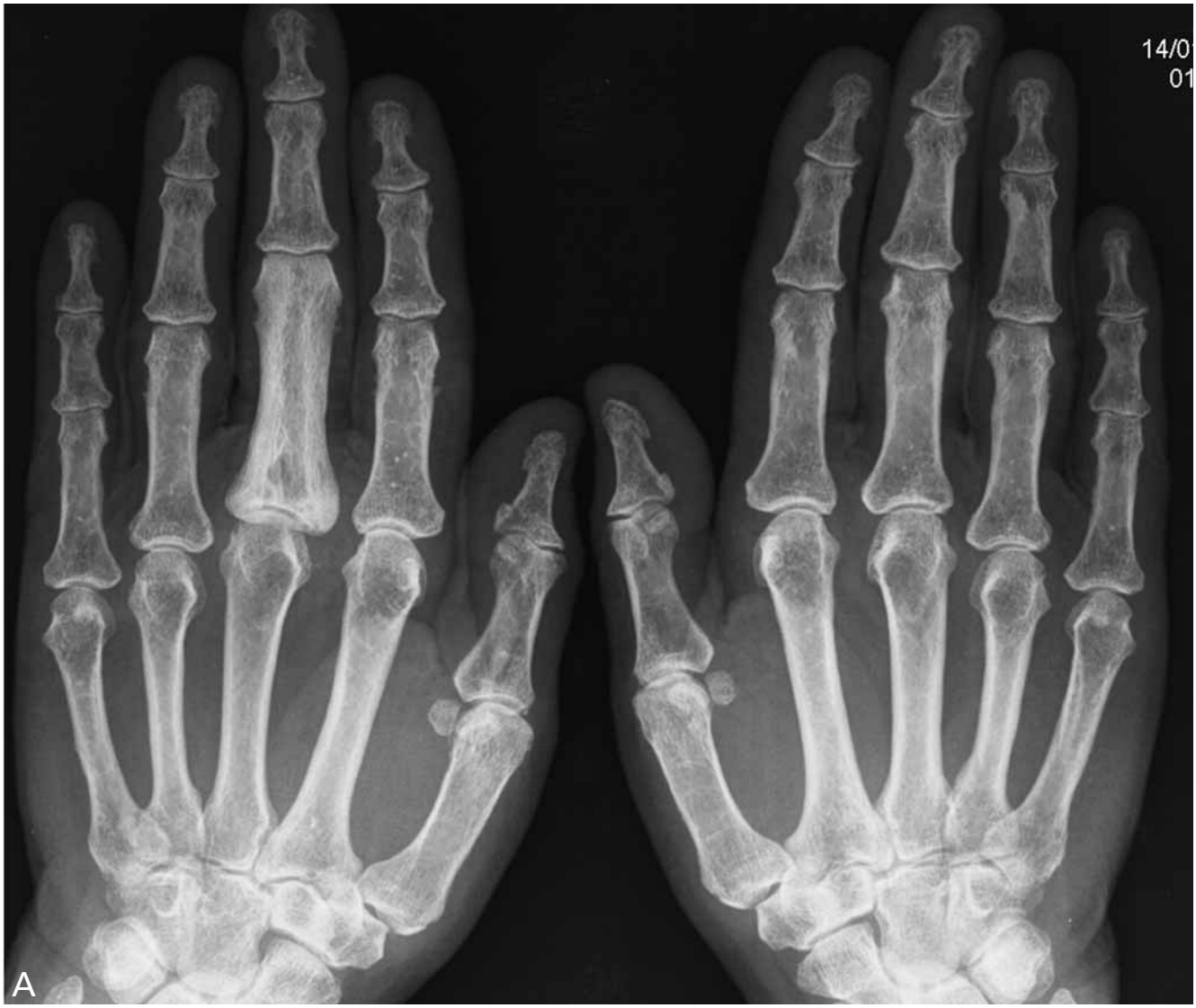

Typical case of **Paget's disease**. Paget's disease of the hand may present as monostotic disease or be part of poly-ostotic involvement.

JBR–BTR, 2007, 90: 413.

Case 18
A 53-year-old man had a soft tissue swelling on the radial aspect of the proximal phalanx of the second finger of the right hand. The swelling gradually became firmer.
Serial plain radiographs showed a parosteal soft tissue lesion (Fig. A) developing primarily to a calcified lesion (arrows) (Fig. B) and finally to a bony lesion (Fig. C).

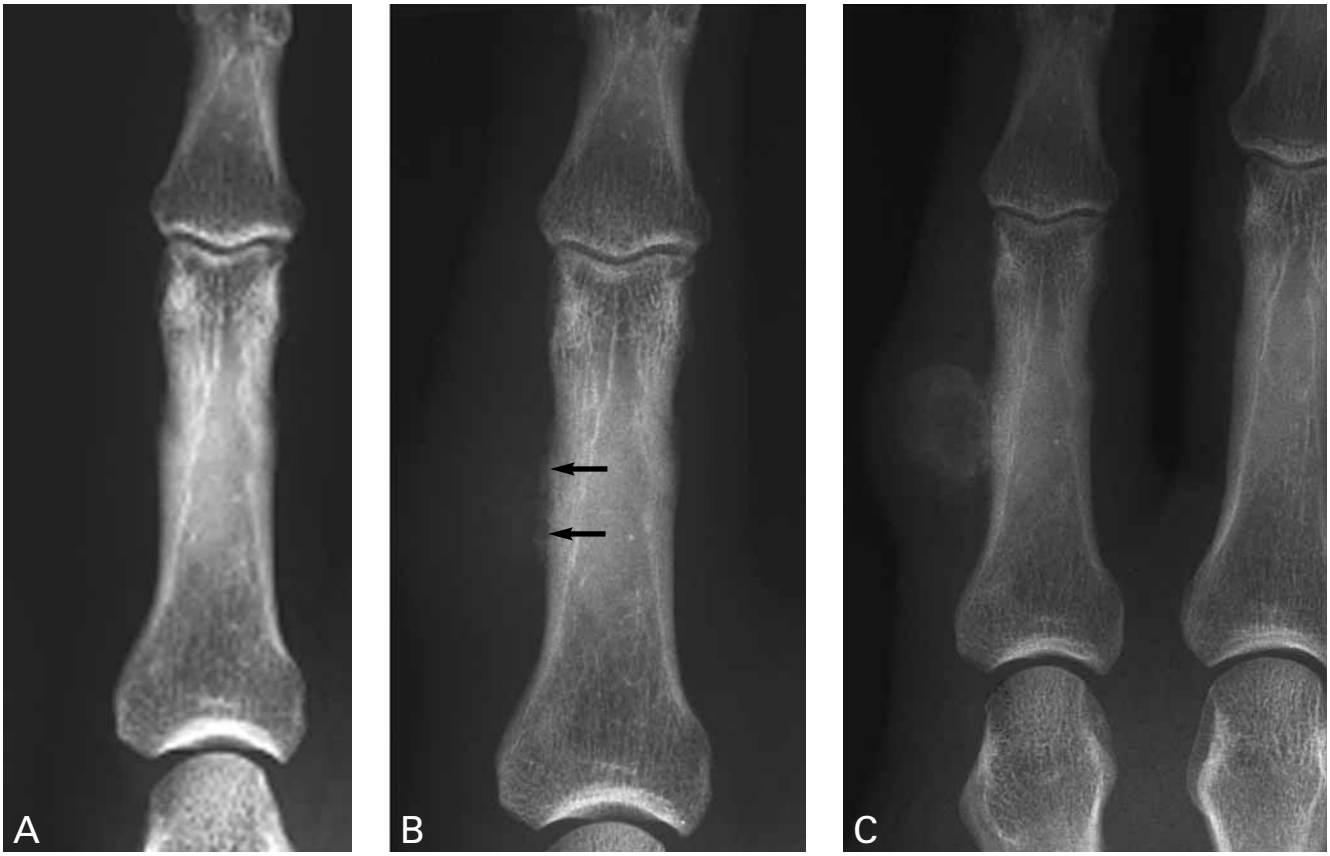

This is an illustration of the spectrum of reactive lesions, as described by Dorfman, with **florid reactive periostitis as stage 1, Nora's lesion as stage 2 and turret exostosis as the final stage**.

JBR–BTR, 2007, 90: 414.

Case 19

MRI shows a polylobular lesion of low signal intensity on T1-weighted image (Fig. A), of high signal intensity on T2-weighted image (Fig. B) and enhancing markedly after administration of Gadolinium chelates (Fig. C), which is located deep to the flexor compartment of the hand. Presence of a few signal voids within the lesion.

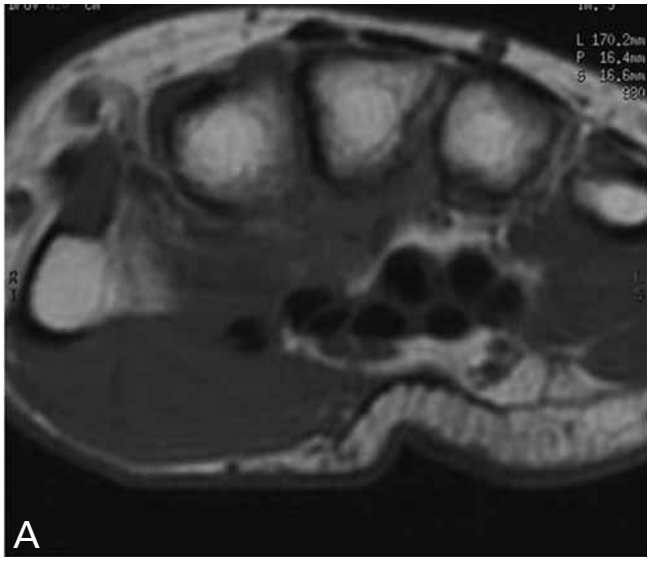

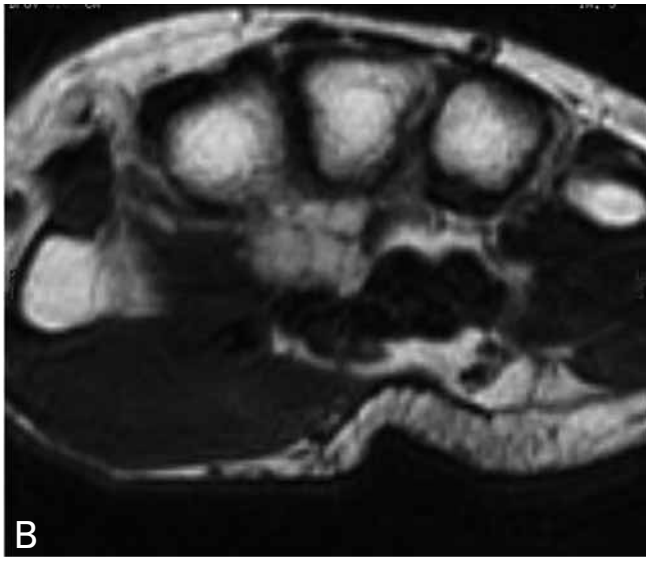

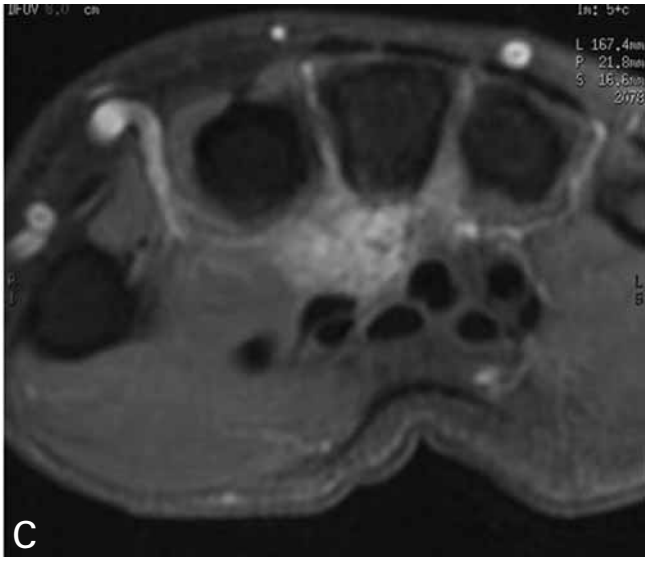

The lesion proved to be an **hemangioma**, the signal voids correspond to intralesional phleboliths.

JBR–BTR, 2007, 90: 415.

Case 20
A 27-year-old man complained of a swelling on the dorsal side of the proximal phalanx of the first digit.
Conventional radiography showed a sharply marginated sessile bony lesion, periosteally located (Fig. A).
T1-weighted MR images showed a low to intermediate signal of the lesion (Fig. B).
T1-weighted MR images after administration of Gadolinium chelates showed enhancement of the peripheral side of the lesion, a zonal phenomenon (Fig. C).

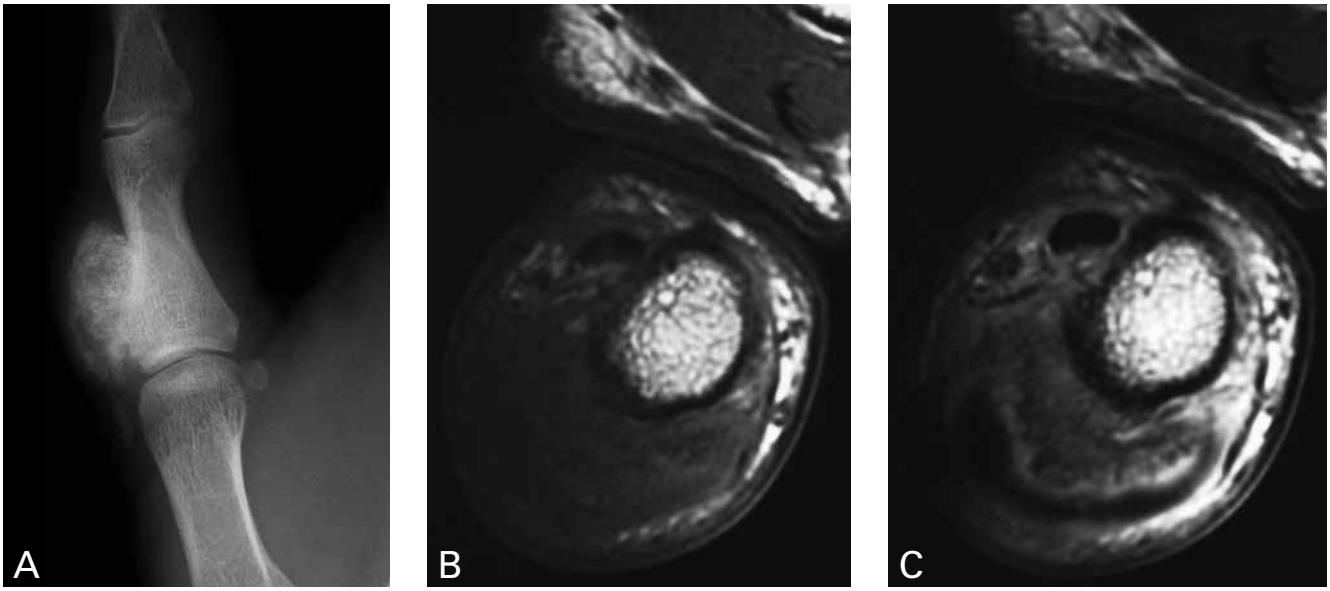

This is an example of a **turret exostosis** with distinct appearances on conventional radiography.
On MRI the lesion has a non specific presentation, which is also the case for florid reactive periostitis and Nora's lesion.

JBR–BTR, 2007, 90: 416.

Case 21
Patient presents with arthritis of the left wrist and subtle erosions on plain radiography.
3T coronal TSE T1-weighted image of the left wrist (Fig. A) demonstrates radiocarpal and ulnocarpal joint space narrowing and significant synovial proliferation at the radiocarpal, ulnocarpal and radioulnar joints with marked erosions at the radius, scaphoid, lunate and triquetral bones. On 3T coronal T1–weighted SPIR image after administration of Gadolinium chelates (Fig. B) there is enhancement of the synovium at the distal radius and ulna and proximal carpal bones. Axial T1-weighted SPIR image after administration of Gadolinium chelates (Fig. C) confirms the significant synovial enhancement of the radio-ulnar joint and deep to the extensor tendons.

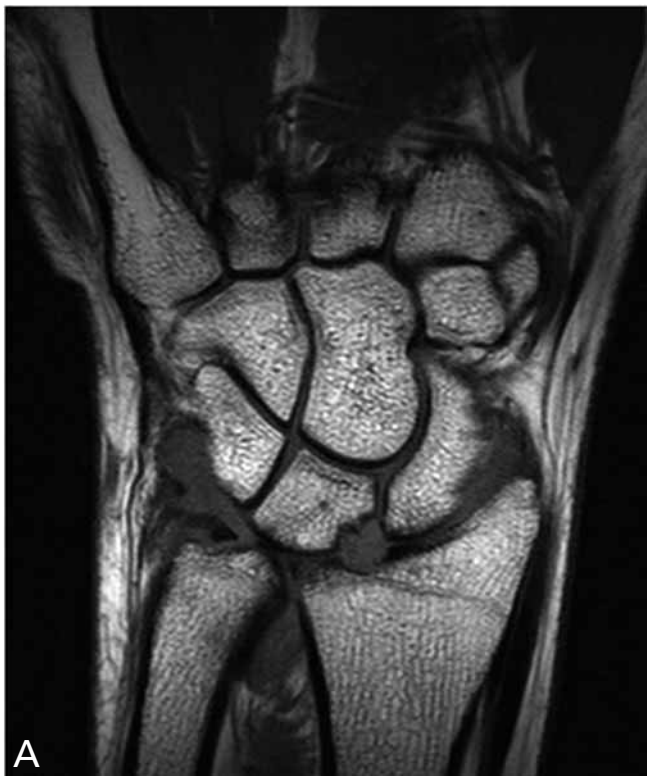

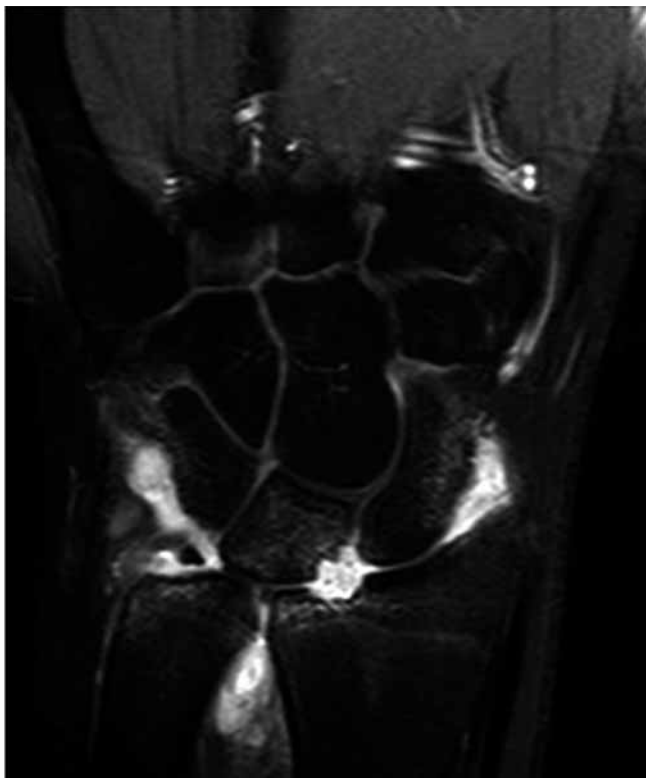

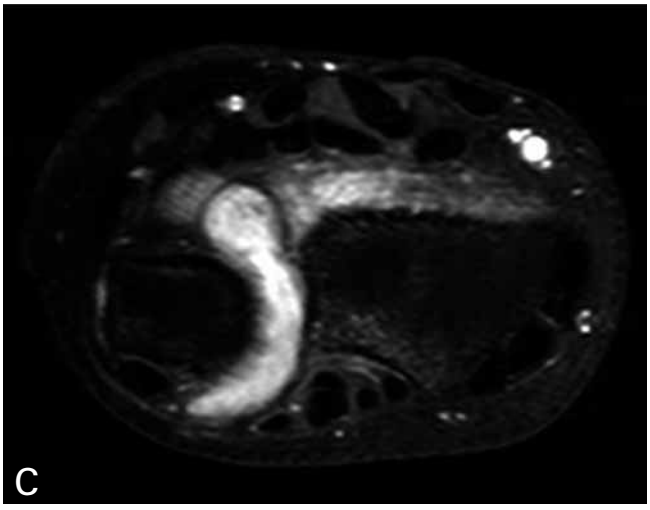

Characteristic findings of **rheumatoid arthritis on MRI**.

JBR–BTR, 2007, 90: 417.

Case 22

Patient presents with radiocarpal pain 15 years after an intra-articular fracture of the radius. 3T coronal T2-weighted image of the left wrist (Fig. A) shows a slight ulna minus variance, sequela of a healed intra-articular fracture of the ulnar aspect of the distal radius and a slightly increased signal intensity of the lunate bone. Coronal TSE T2 (SPAIR)-weighted image (Fig. B) demonstrates joint space narrowing between the distal radius and lunate with edema of the lunate and ulnar aspect of the distal radius associated with joint space effusion. Coronal T1 (SPIR)-weighted image after administration of Gadolinium chelates (Fig. C) shows enhancing synovium, enhancement of the lunate bone and distal radius and enhancement within a tear of the triangular fibrocartilage complex.

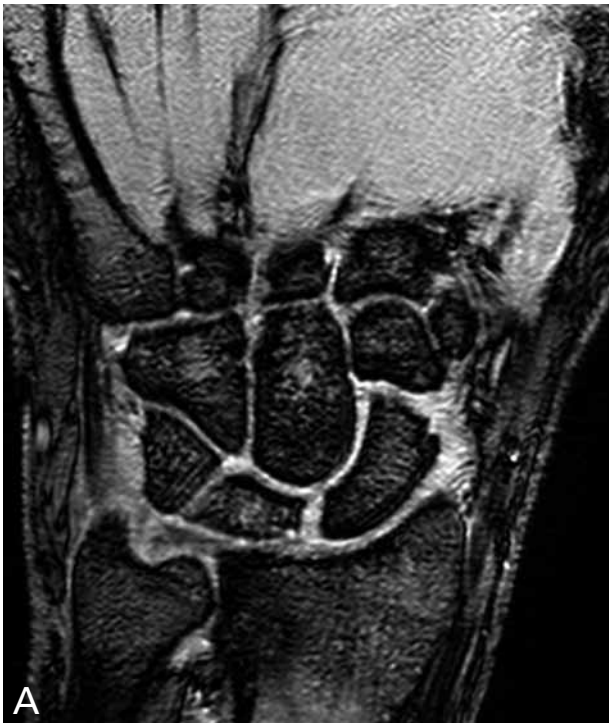

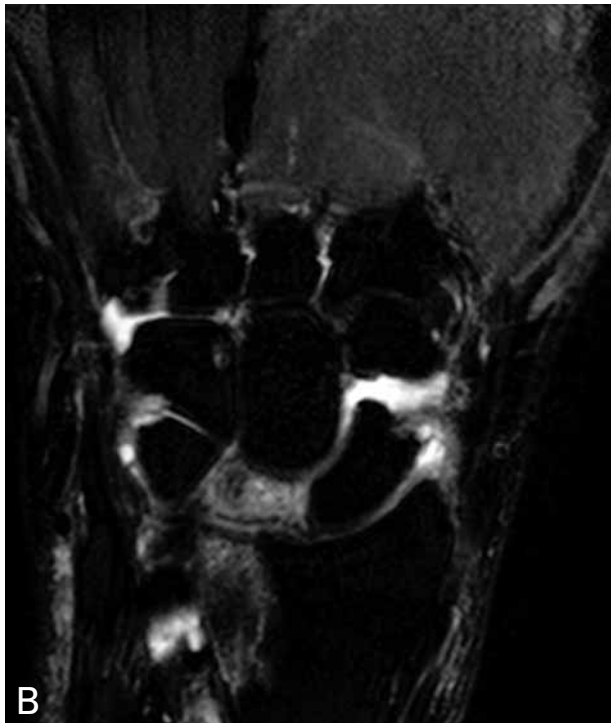

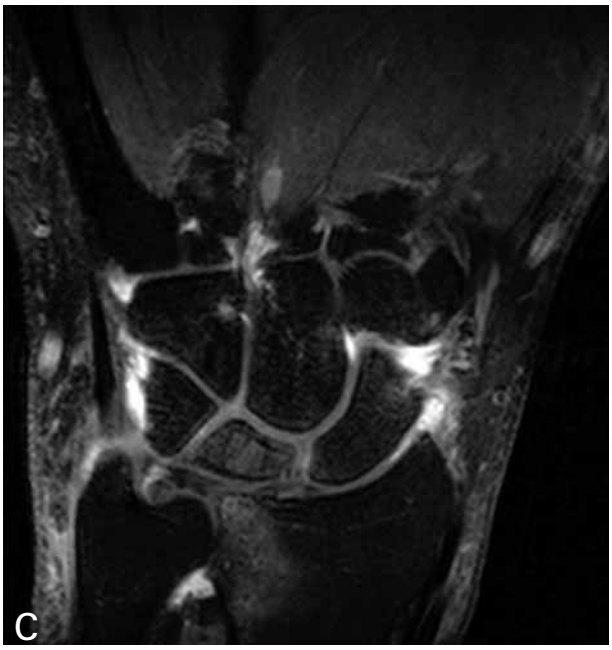

Osteonecrosis of the lunate bone, most likely resulting from previous trauma with an intra-articular fracture of the radius and slight ulna minus variance.

JBR–BTR, 2007, 90: 418.

Case 23
14.5-year-old boy with Crohn's disease since october 2003, treated with Imuran® 50 mg and 3 times Pentasa® 1 g a day. He frequently suffers of diarrhea and abdominal pain. Puberty has not started yet. Therefore the pediatrician requests an evaluation of the bony age of this patient.
PA radiography of left wrist and hand (Fig. A) shows no fusion of the epiphysis of fingers and distal radius. The hamulus of the os hamatum and the processus styloideus ulnae is not fully developed. The os pisiform is still very small.

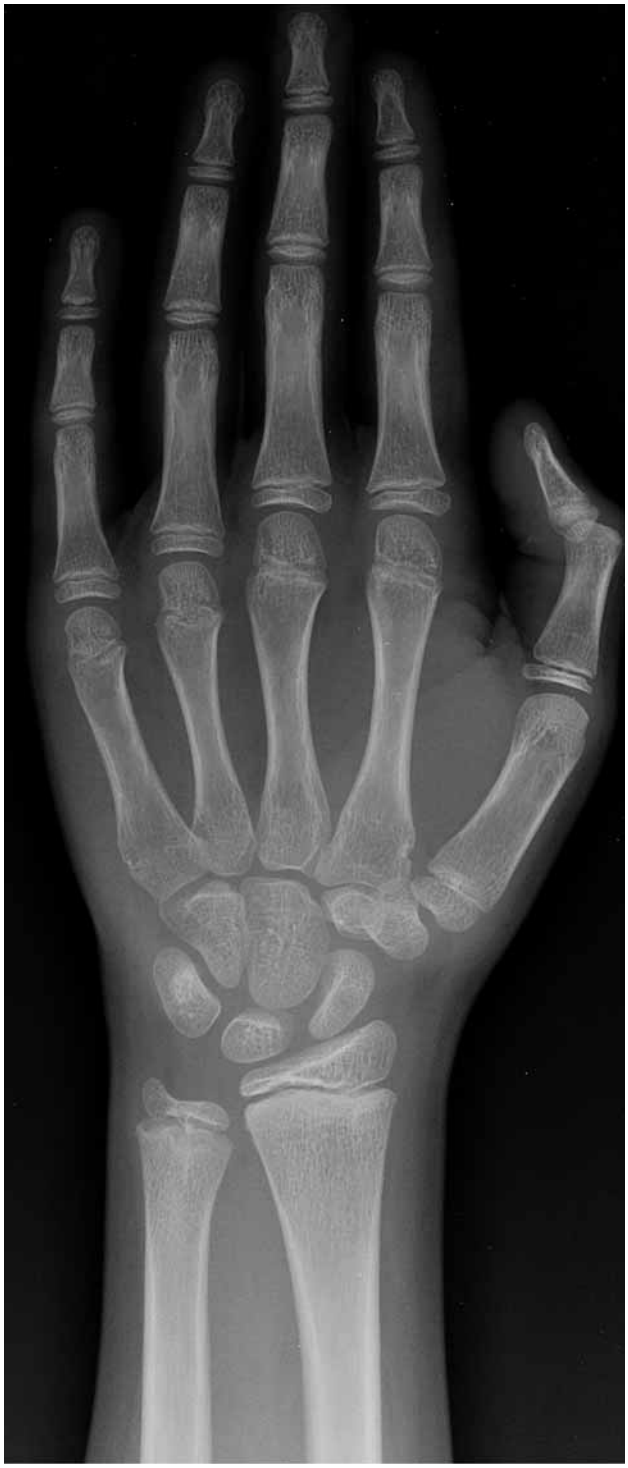

Based upon the Greulich and Pyle atlas, bone age of this young boy is between 12 years and 6 months and 13 years for a calendar age of 14 years and 6 months.
Growth is retarded by a combination of chronic medication and chronic malnutrition.

JBR–BTR, 2007, 90: 419.

Case 24
3T coronal T1-weighted MR images (Fig. A and B) of the right wrist in a child demonstrate a decreased carpal angle as well as a thickened radiotriquetral ligament.

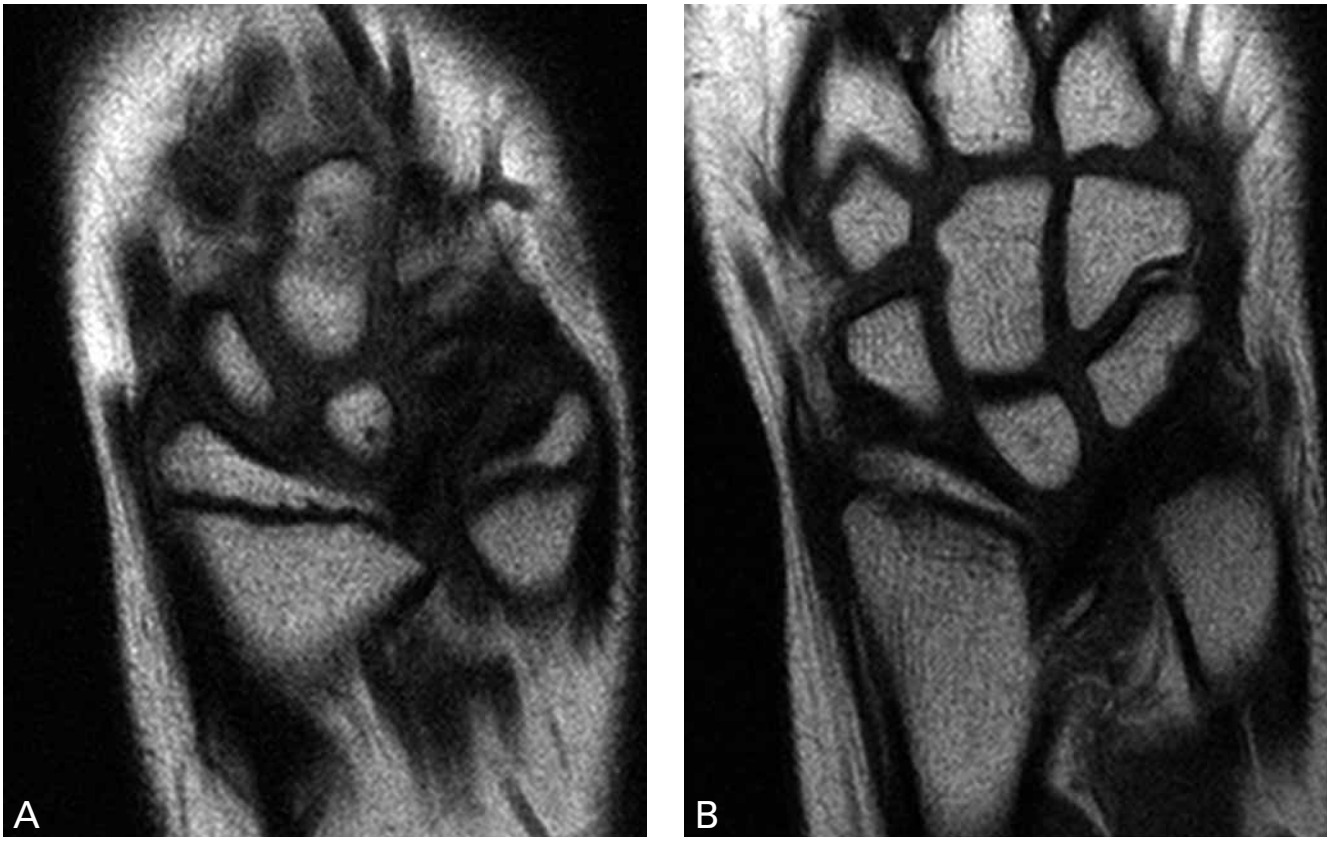

The imaging findings are characteristic for **Madelung's deformity**.
Although various forms of Madelung's deformity exist, the two main types are the isolated primary type and the one associated with dyschondrosteosis (Leri-Weill syndrome). Morphological similarities and differences between these two types have been described. High resolution MRI is capable to differentiate these two main types by demonstrating an anomalous volar extrinsic ligament (radiotriquetral) in the primary type.

JBR–BTR, 2007, 90: 420.

Case 25

An expansile, osteolytic, subarticular tumor is seen at the distal end of the third metacarpal, involving both the epiphysis and metaphysis. The whole width of the host bone is involved and cortical destruction is noted. There are no internal calcifications seen on plain radiography (Fig. A). Coarse trabeculations are found, most prominent in the periphery of the lesion.

On MRI, the lesion has intermediate SI on coronal T1-weighted images (Fig. B), and characteristic predominantly low SI on coronal T2-weighted images without fat saturation (Fig. C). A biopsy of the lesion was performed.

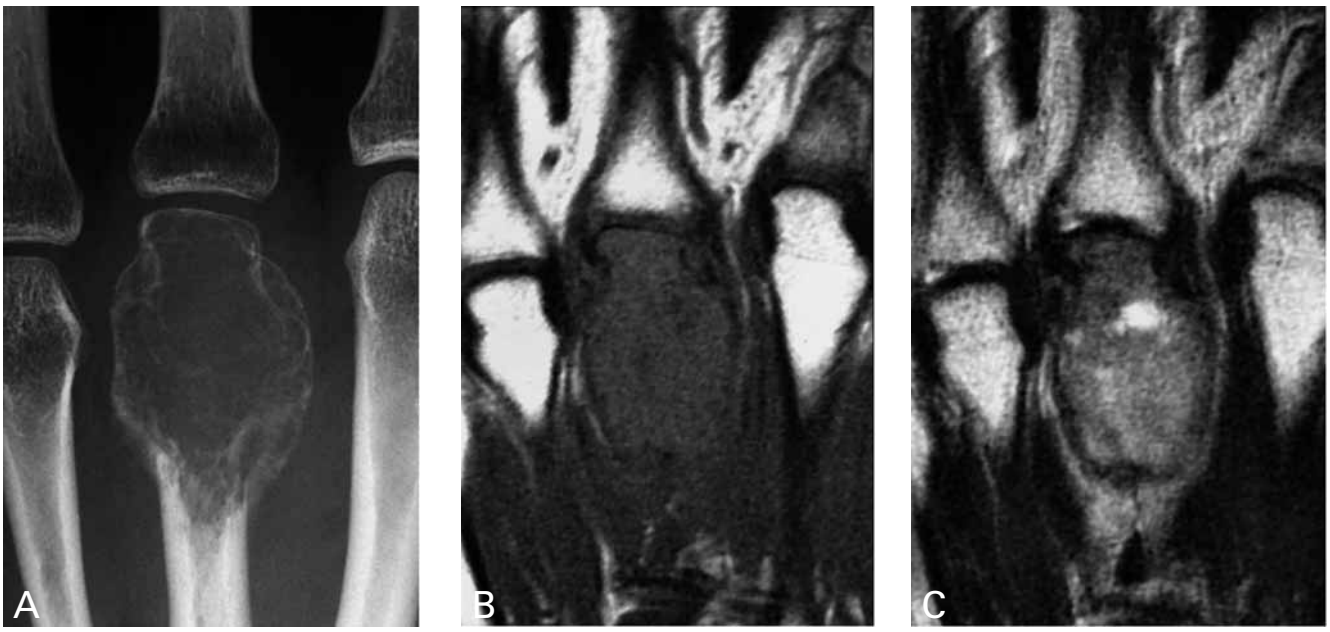

The combined findings on plain film and MRI, as well as the location of the lesion, are in favor of a **giant cell tumor of bone**. But even if imaging findings are suggestive for giant cell tumor of bone, a biopsy prior to surgical treatment is essential, since many mimickers (such as enchondroma, aneurysmal bone cyst, giant cell reparative granuloma, metastasis, and osteomyelitis) may be found at examination of the curettage specimen of initially so-called «typical» giant cell tumor of bone on plain film and/or MR imaging.

At histological examination, diagnosis of giant cell tumor of bone is confirmed. Numerous multinucleated giant cells are seen. The nuclei of the stromal cells are identical to the nuclei in the giant cells, a feature that distinguishes giant cell tumors from other lesions that also contain giant cells.

JBR–BTR, 2007, 90: 421.

Case 26

40-year-old female patient with lucent lesion within proximal phalanx of the 5th digit.

Plain radiography (Fig. A) demonstrates eccentric, well-demarcated, slightly lobulated lytic lesion. The lesion has a sharp sclerotic margin on one side and cortical thinning with expansion on the other side. There is no cortical destruction, there are no soft tissue abnormalities. There are some subtle internal ridges, no calcifications are seen.

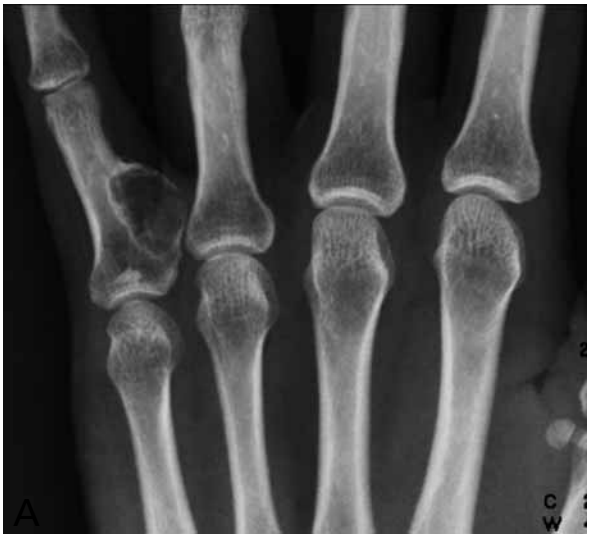

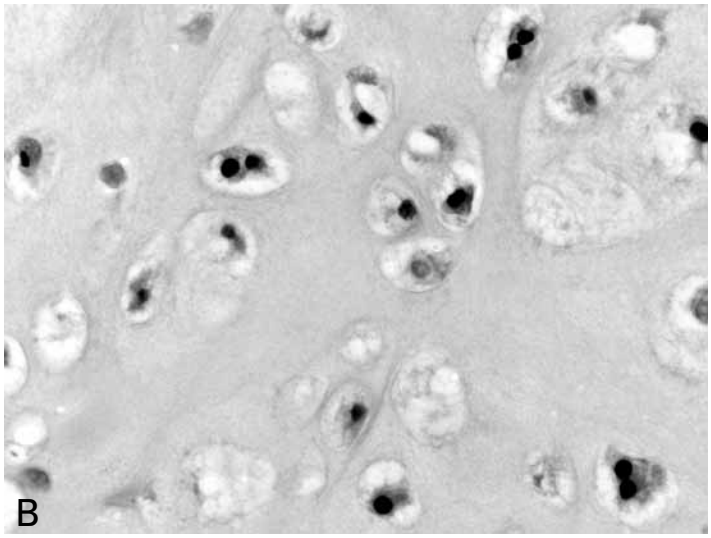

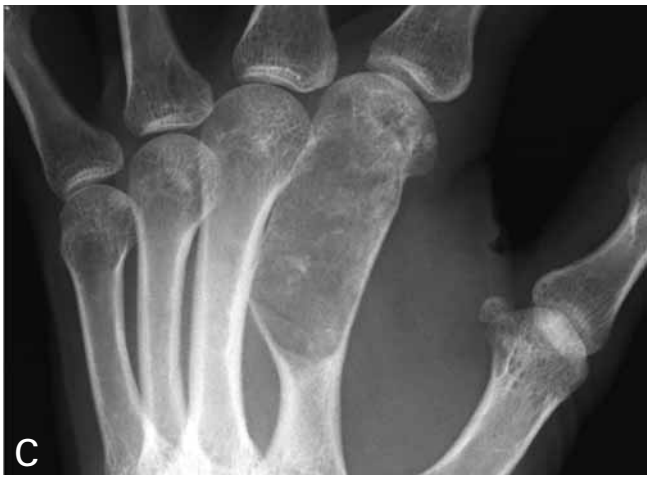

Radiologic diagnosis is consistent with **eccentric enchondroma**.

Histopathologic analysis of the curetted lesion demonstrated **cellular enchondroma** (Fig. B). The tumor has histologic characteristics (mucomyoid matrix, cellularity, double nuclei) that would make a diagnosis of low-grade chondrosarcoma when appreciated within a long bone. These criteria, however, are considered benign when encountered within a phalanx.

In another 43-year-old male patient, a lytic lesion is shown in the second metacarpal bone (Fig. C). There is expansion and cortical thinning, but no destruction. There are some focal internal calcifications. Radiologic diagnosis is consistent with **enchondroma**. Statistically, however, low-grade chondrosarcoma is not unlikely. Histopathologic analysis of curetted specimen demonstrated a similar pattern as was shown in Fig. B, now consistent with **low-grade central chondrosarcoma**. In this case of a lesion within metacarpal bone, findings of relative high cellularity, atypia and double nuclei are not compatible with diagnosis of enchondroma.

JBR–BTR, 2007, 90: 422.

Case 27

A 38-year-old woman had chronic painful swelling at the dorsal aspect of the proximal interphalangeal (PIP) joint of the middle finger, since 2 years. Radiographs were normal.

Sagittal STIR (Fig. A) and T1-weighted spin echo (Fig. B) MR images were performed as well as transverse and coronal T1-weighted spin echo images before (Fig. C and E) and after administration of Gadolinium chelates (Fig. D and F).

The sagittal and transverse images show hypointense infiltration at the dorsolateral subcutaneous soft tissues on T1-weighted images (B, C) that also shows enhancement after contrast injection (D).

Transverse and coronal images show a thickening at the proximal attachment of the ulnar collateral ligament (C and E, long arrow). This area also shows contrast enhancement (F). Compare to the intact radial collateral ligament (F, short arrow).

An associated discontinuity of the sagittal band is suspected at the same level on the transverse views (C, D; dorsolateral side).

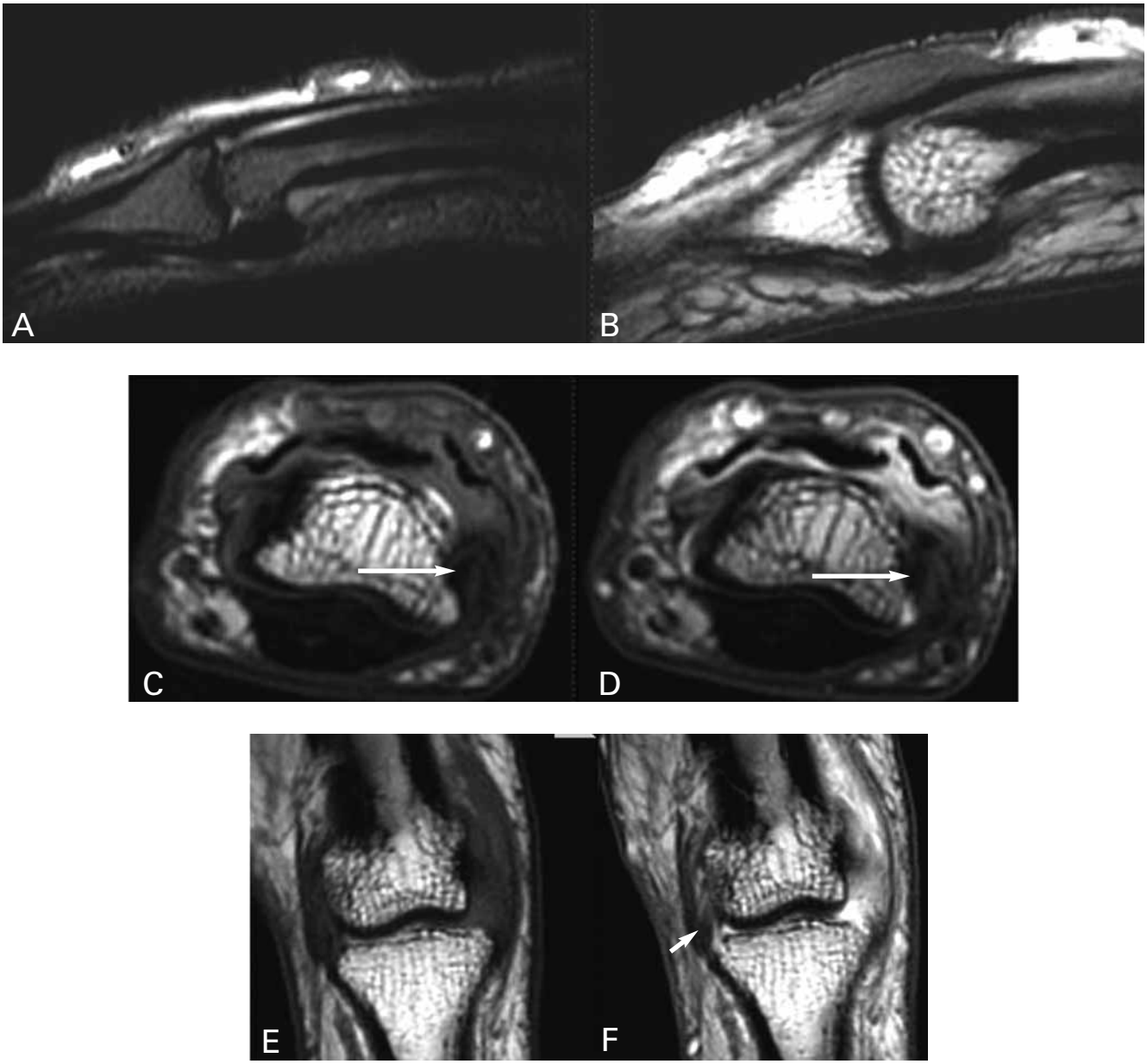

Rupture of the ulnar collateral ligament of the PIP joint of the middle finger and suspicion of discontinuity of the overlying sagittal band.

Fibrous scar tissue is present in the dorsolateral subcutaneous soft tissues (corresponding to the clinically detected painful swelling).

JBR–BTR, 2007, 90: 423.

Case 28

A 47-year-old male biker is hospitalized for a pulsatile mass in the palm of his left hand with ischemic lesions on fingers 2 and 3. A sonography reveals a partially trombosed palmar arc aneurysm confirmed on selective arteriography. Early arterial phase (Fig. A) reveals an aneurysmal dilatation of the ulnar part of the palmar arc with delayed filling of digital arteries of finger 1 and 2 and multiple filling defects in the digital arteries of finger 3 and 4. Peak opacification (Fig. B) shows good (late) peripheral filling with residual hypovascular areas at the base of finger 2 and tip of finger 3. A similar case is shown in Fig. C presenting with an aneurysmal lesion at the distal part of the ulnar artery.

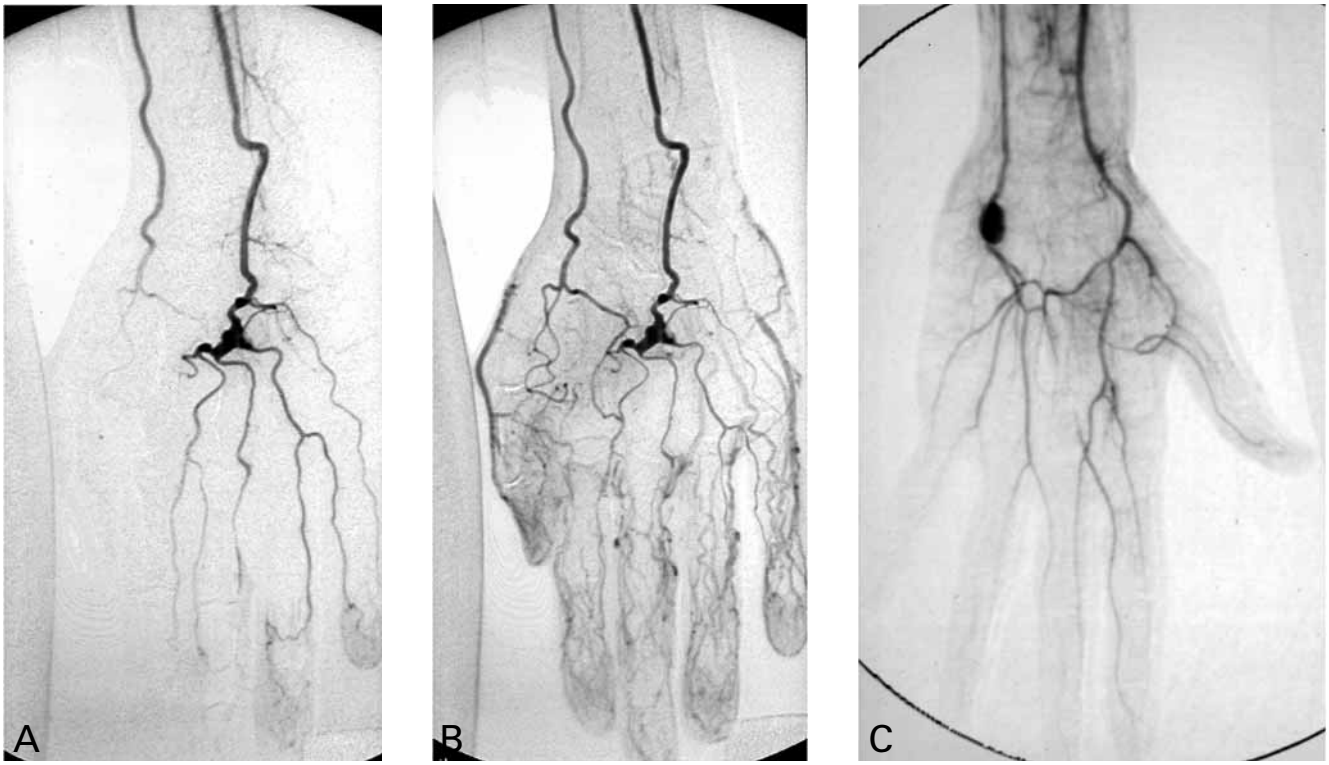

The clinical and angiographic findings are suggestive of a **hypothenar hammer syndrome** although the aneurysmal lesion is usually found in the distal part of the ulnar artery (Fig. C). In this case, the therapy was conservative.The patient was put on an antiplatelet regimen and biking stop was suggested. In some cases, surgical therapy (excision) of the aneurysm and vascular reconstruction is necessary.

JBR–BTR, 2007, 90: 424.

Case 29

A 47-year-old man presented with a history of previous left wrist trauma (fall in hyperextension). The initial radiographies were normal. Conservative therapy (immobilization in a brace) had failed and pain persisted after two months, especially in ulnar deviation and dorsal flexion. Control radiographs were normal as well.

MRI showed a clearly defined low signal area corresponding to subchondral erosion on both sides of the attachment site of the lunotriquetral (LT) ligament on a T1-weighted image (arrows) (Fig. A). The tip of the triangular hypointensity of the LT ligament was split on 3D-gradient echo imaging (Fig. B). There was not yet a step-off sign between the carpal bones.

As a LT-arthrodesis was considered, the surgeon asked for confirmation of the lesion. Triple wrist arthrography was performed and illustrated a clear leak through the LT ligament (Fig. C midcarpal injection).

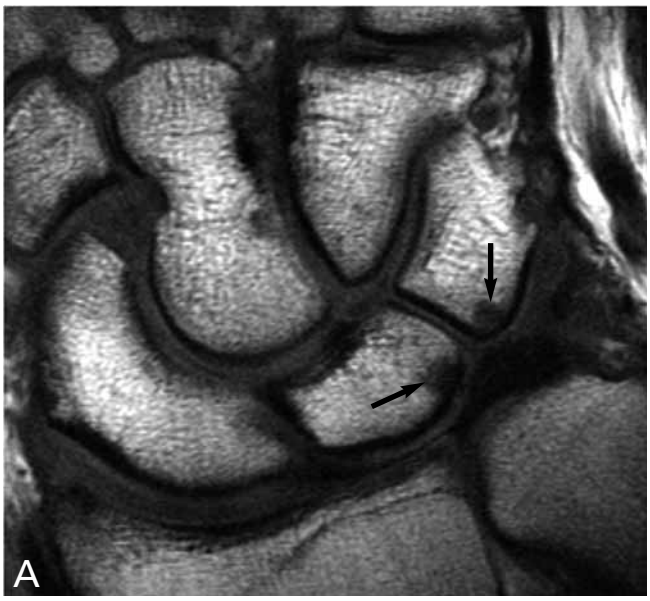

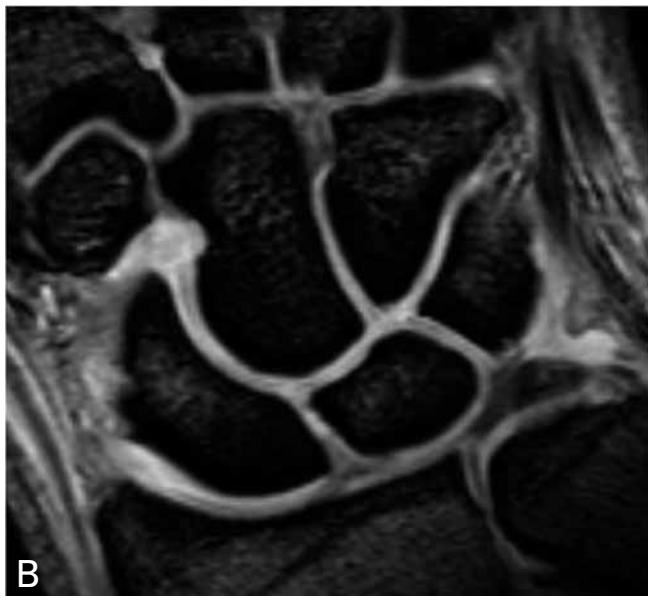

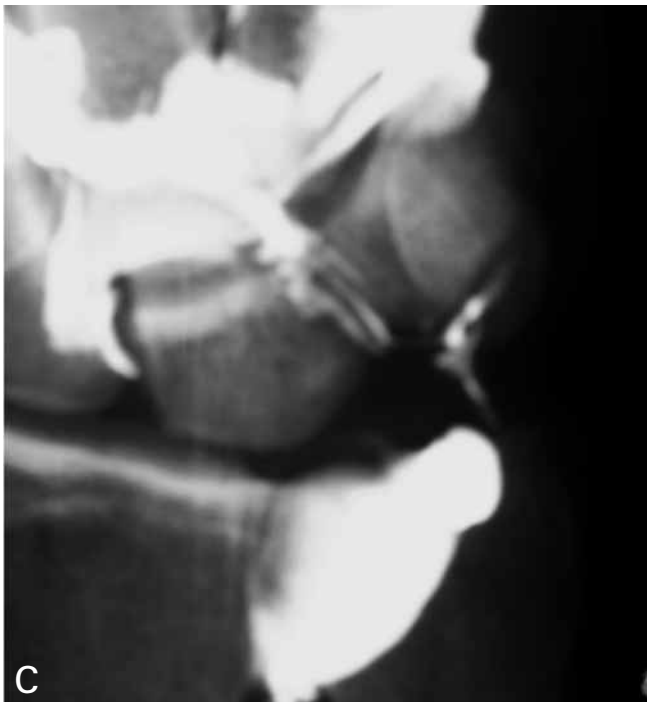

Diagnosis: **Lunotriquetral ligament tear**.

JBR–BTR, 2007, 90: 425.

Case 30
Eighteen-year-old patient. Radiography (Fig. A and B) shows multiple bone lesions confined to the fourth and fifth ray of the hand involving the metacarpals as well as the proximal and middle phalanx. The aspect of the lesions is variable: some are expansile, while others are not. There are non-homogeneous, lytic lesions, while the fourth middle phalanx and especially the fifth metacarpal present with an increased density.

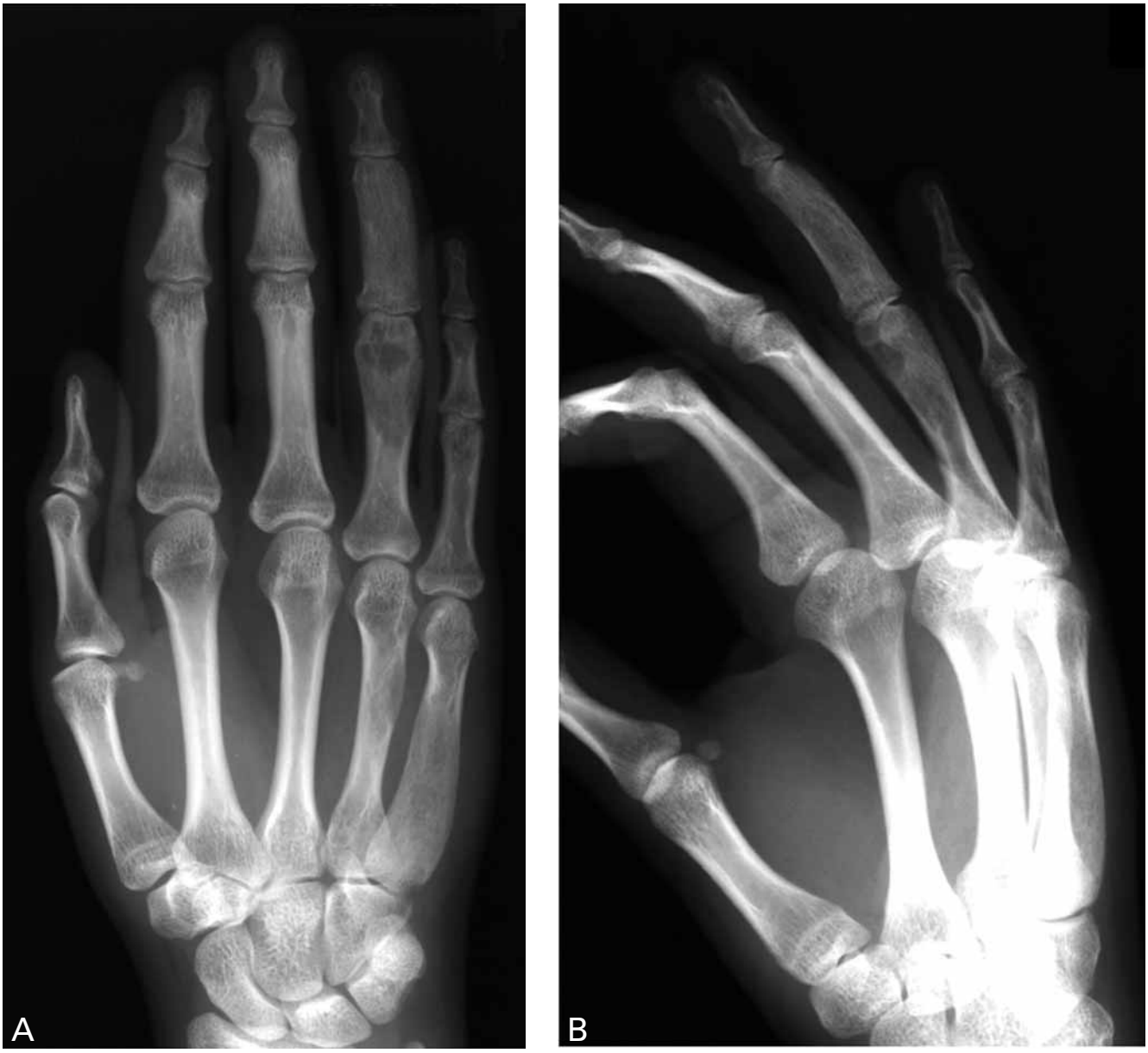

In case of multiple lytic lesions in a hand, one could think of enchondromatosis (Ollier's disease). However, especially the ground-glass appearance of the fifth metacarpal is characteristic of **fibrous dysplasia**. Fibrous dysplasia of the hand is almost exclusively seen with poly-ostotic involvement of at least the ipsilateral upper limb.

JBR–BTR, 2007, 90: 426.

Case 31

A 42-year-old woman experienced 3 weeks ago a sudden episode of swelling at the dorsoradial aspect of the interphalangeal (IP) joint of the right thumb.

Standard radiographs of the right and left thumbs are shown. MRI includes bilateral coronal 2 mm thick images in T1 and STIR sequences, bilateral sagittal T2-weighted images with fat saturation and 1 mm thick slices obtained with a 3D sequence acquisition. Coronal (Fig. C and D) and sagittal (Fig. E) MR images depict an area of subchondral bone impaction with bone marrow edema at the dorsal-lateral aspect of the distal epiphysis of the first proximal phalanx, which, in retrospect, is already visible on the radiographs (Fig. A and B). The signal intensity of the lesion is low on T1-, high on fat saturated T2-weighted images.

A small low signal intensity fragment is detected in a distended dorsoradial joint recess (Fig. F, arrow).

MRI demonstrates the normal appearance of the ulnar and radial collateral ligaments (Fig. C and D).

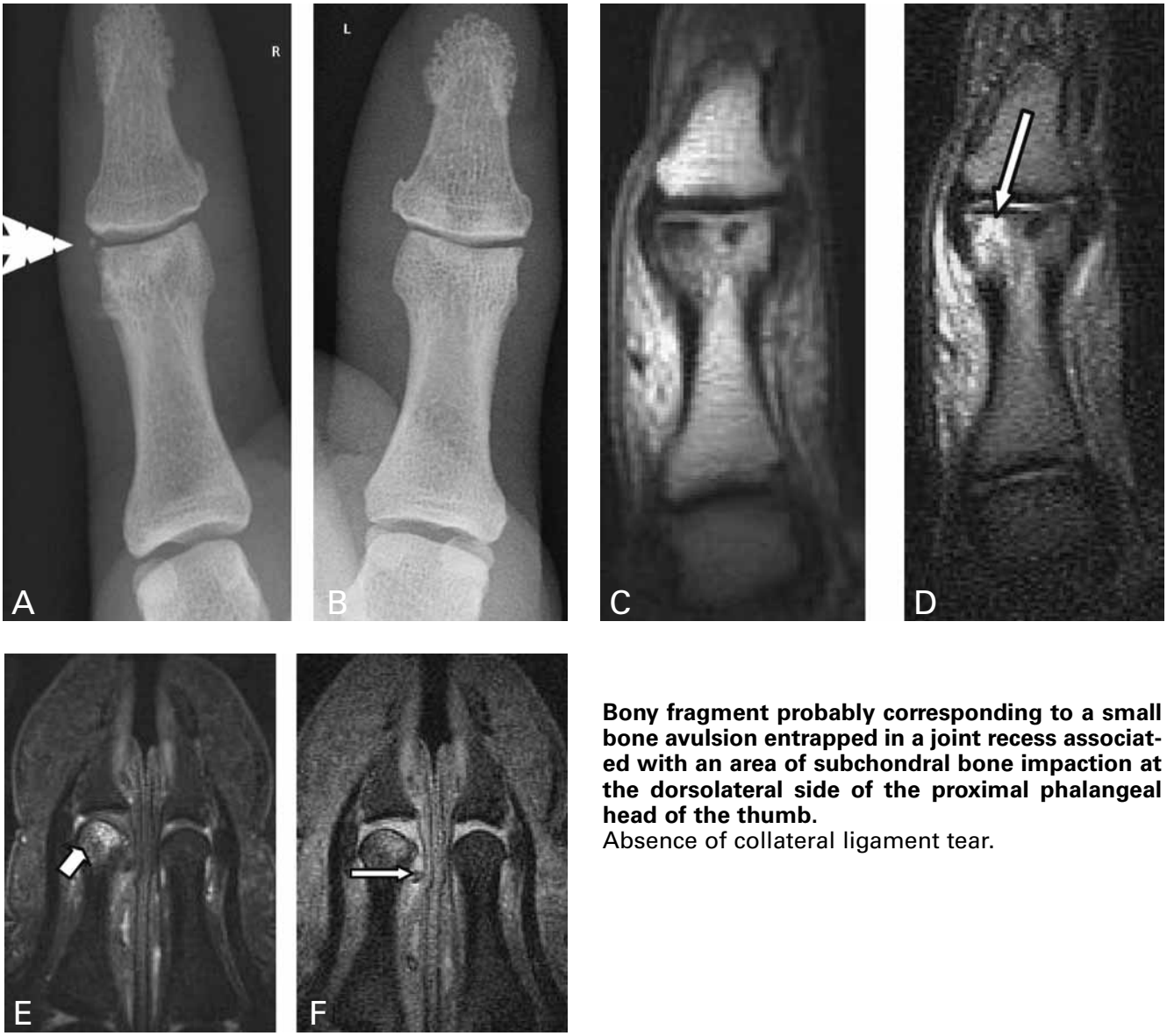

Bony fragment probably corresponding to a small bone avulsion entrapped in a joint recess associated with an area of subchondral bone impaction at the dorsolateral side of the proximal phalangeal head of the thumb.

Absence of collateral ligament tear.

JBR–BTR, 2007, 90: 427.

Case 32
Sonogram of the right hand palm in a 25-year-old woman.
Longitudinal section (Fig. A): linear hyperechoic structure in the subcutis with length of 8 mm surrounded by hypoechoic area, paralleling the hyperechoic structure.
Transverse section(Fig. B): the central structure appears as a very hyperechoic dot with acoustic shadowing. The surrounding hyopechoic rim is also well appreciated on this section.

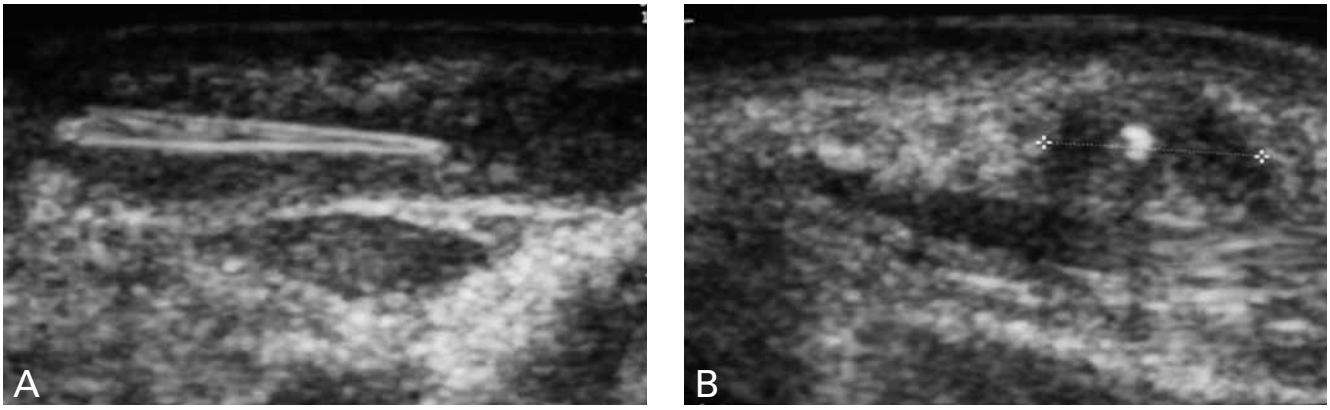

The imaging findings, together with a history of recent puncture of the skin by wood, are pathognostic of **wood splinter** in the superficial tissues of the hand, **surrounded by inflammatory reaction.**

JBR–BTR, 2007, 90: 428.

Case 33

A 24-year-old angler presented with a perforating lesion caused by a stab injury of the left index finger at the ulnar-volar aspect. Surgical exploration revealed no abnormality, the wound was sutured. Two months later he still presents with flexion deficit of his index finger at the DIP joint.

Ultrasound of the flexor compartment of the left index at the level of the PIP joint (Fig. A): thickening of the flexor tendon sheath and pulley system at the ulnar aspect is demonstrated on longitudinal and axial images (respectively top and bottom left). Distally to the crossing of the flexor digitorum tendon the profundus tendon is located volar to the superficialis tendon slips on longitudinal and axial images (respectively top middle and right). Distally adjacent to the crossing of both tendons a perforation of the ulnar half of the profundus tendon is seen on longitudinal and axial images (respectively bottom middle and right).

On sagittal MR images of the left index (Fig. B) the perforation of the ulnar slip of the flexor digitorum profundus is confirmed. (white arrows).

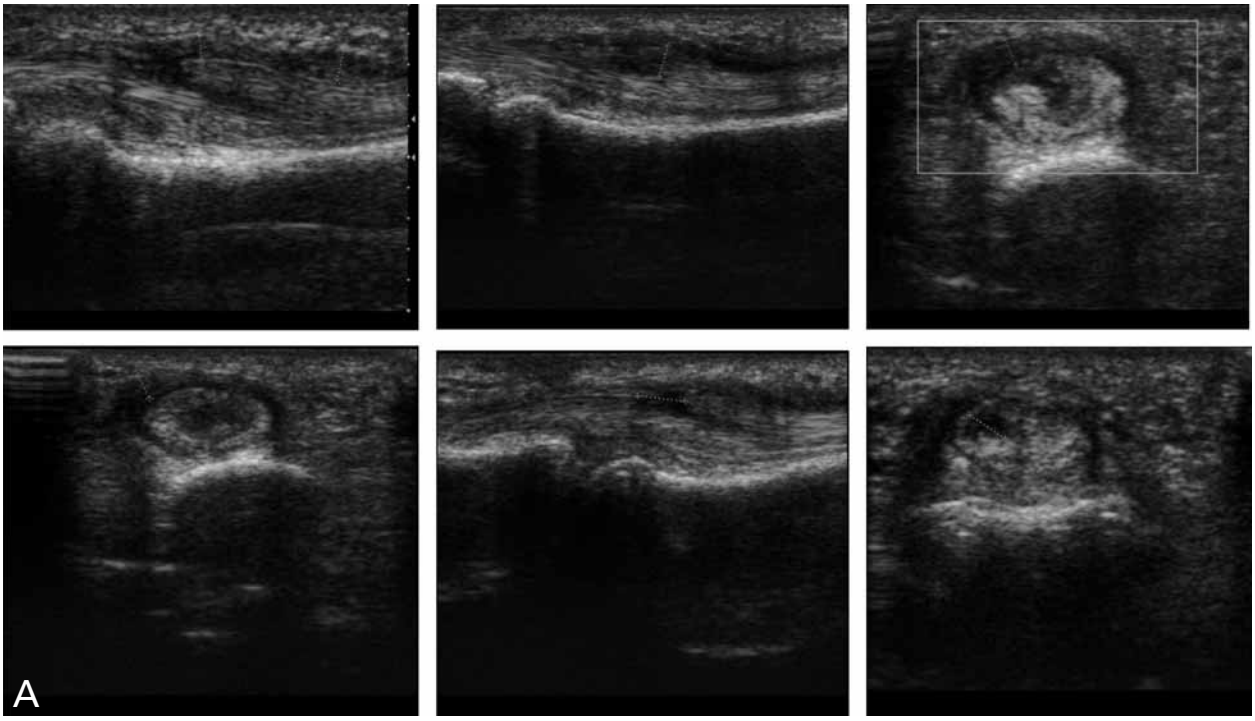

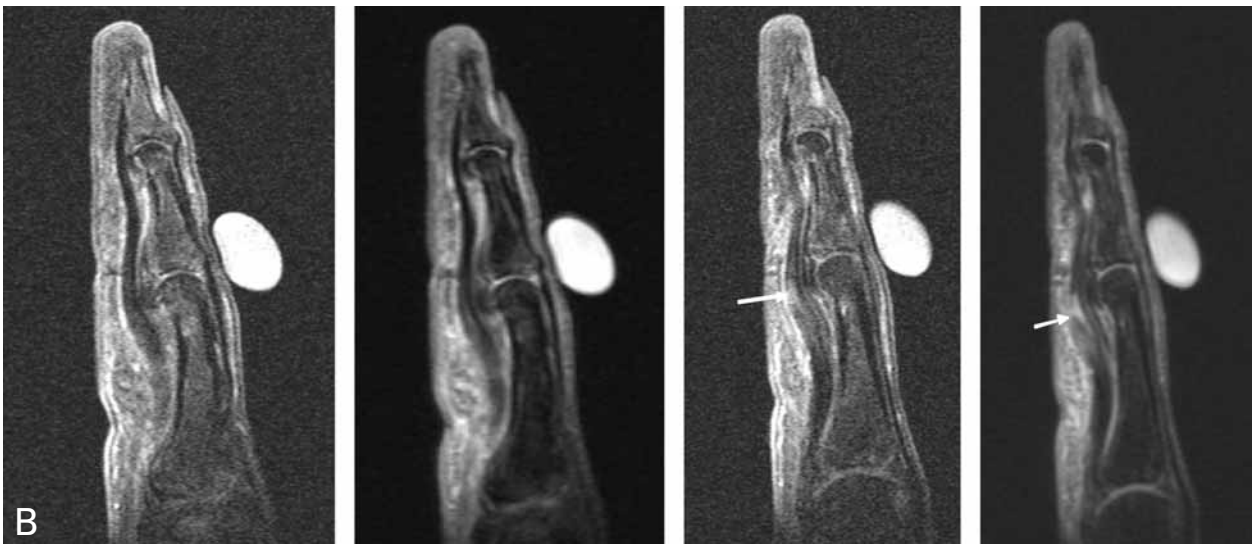

Diagnosis: **partial tear of the flexor digitorum profundus tendon, tear at the ulnar part due to perforating trauma.**

JBR–BTR, 2007, 90: 429.

Case 34

Six-year-old boy complaining of swelling and pain on the radial side of the hand palm. A focal area of hyperdensity is seen adjacent to the first metacarpal on the radiography (Fig. A). On T1-weighted MR images after administration of Gadolinium chelates, a large and strongly enhancing area is seen in the soft tissues of the thenar (Fig. B). Bone scintigraphy showed a hot spot in the same area (not shown). The unenhanced coronal T1-weighted MR image taken 9 months later demonstrates broad band-like areas of high signal intensity (suggestive of fat) arranged in a circle (Fig. C). At this time, only little enhancement is seen centrally in the lesion (not shown).

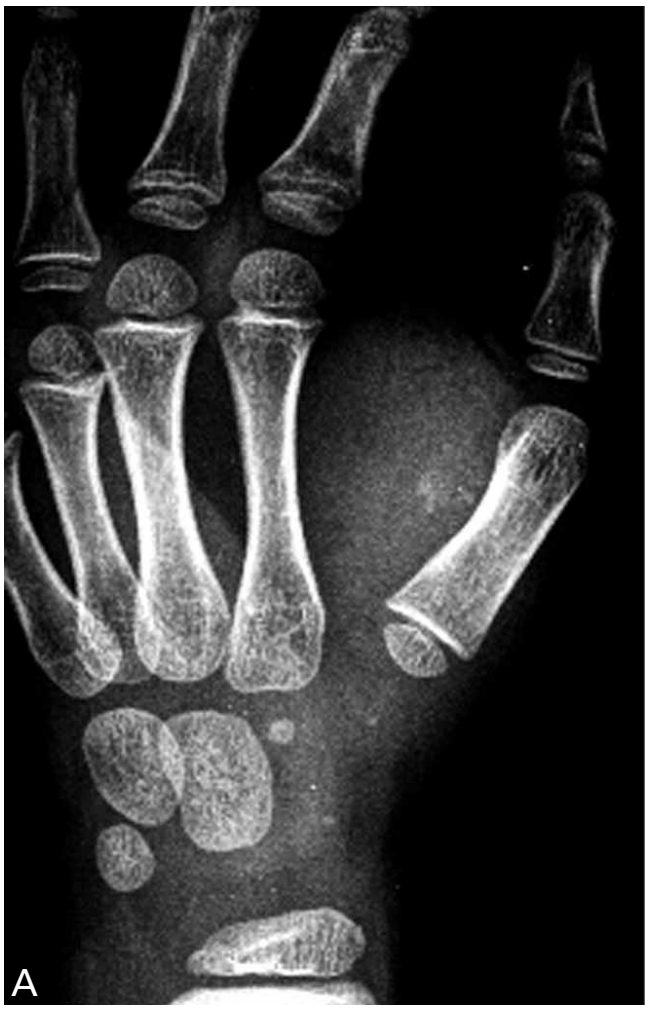

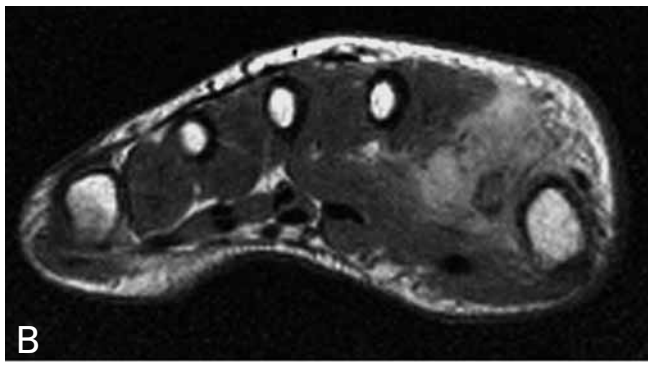

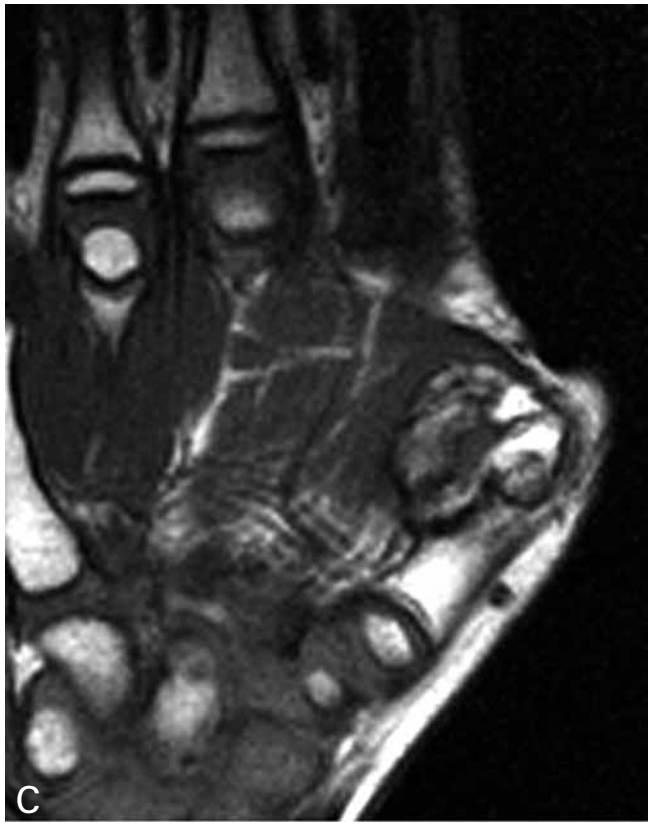

Based on the evolution of the inflammatory soft tissue lesion with small calcifications to a less inflammatory lesion with peripheral band-like ossification (fatty bone marrow, centripetal ossification), the presumed diagnosis of **myositis ossificans** was confirmed.

JBR–BTR, 2007, 90: 430.

Case 35

Forty-one-year old construction worker used to drilling concrete complaining of small soft tissue nodule on the ulnar side of the wrist. MR imaging reveals an oval soft tissue mass superficial to the flexor tendons and immediately distal to the hamulus of the hamate. This mass is of spontaneous high signal on T1-weighted MR image with a central area of lower signal intensity (Fig. A). Comparable signal intensities are seen on T2-weighted gradient echo image with a more pronounced low signal area centrally (Fig. B). The contrast-enhanced MR angiography demonstrates occlusion of the superficial palmar arc (no longer visible) and a partially thrombosed aneurysm at the junction of the superficial to the deep palmar arc (Fig. C).

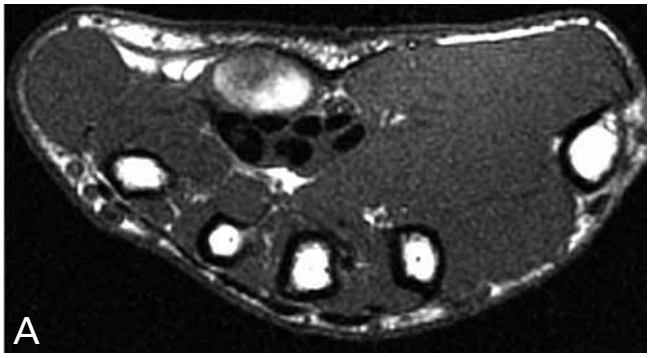

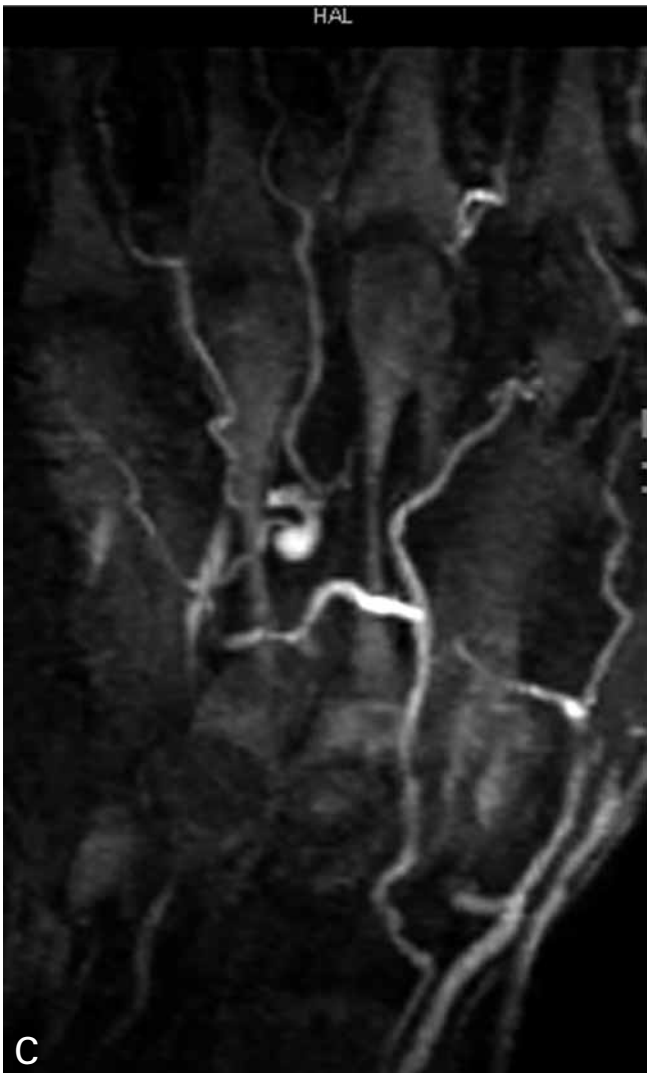

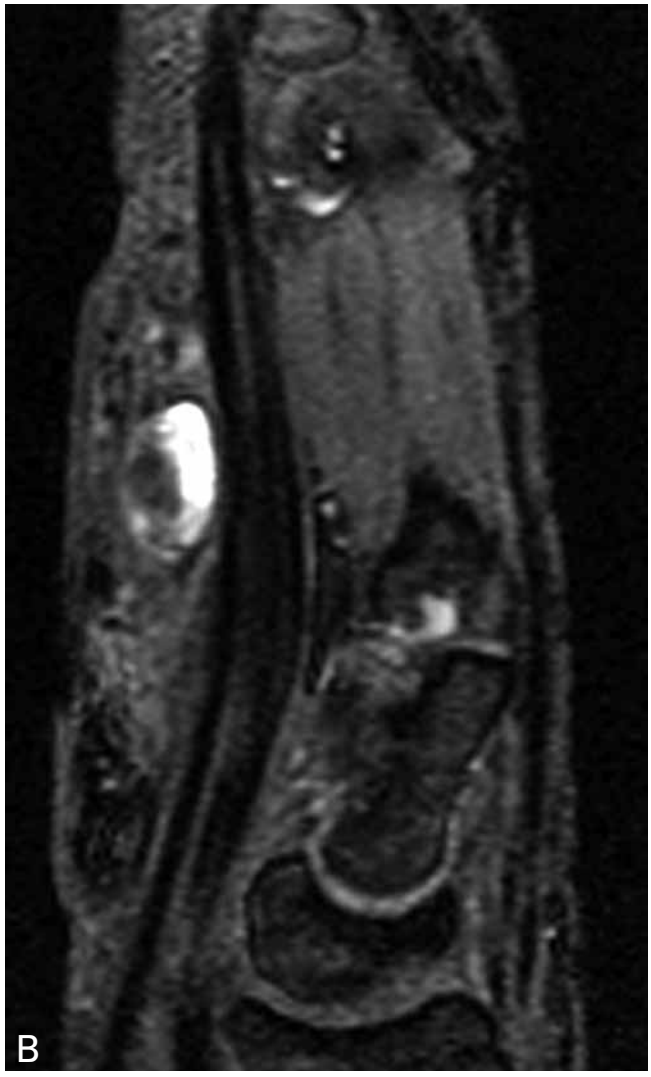

The soft tissue mass was diagnosed to be a posttraumatic aneurysm resulting from repeated trauma to the wrist due to drilling activities, known as **hypothenar hammer syndrome**. In this case, the well-perfused deep palmar arc prevented ischemic changes of the digits.

JBR–BTR, 2007, 90: 431.

Case 36

On plain film, periosteal new bone formation is seen at the radial side of the diaphysis of the first metacarpal (Fig. A). Prominent sclerotic changes are noted at the diaphysis, and at the distal metaphysis and epiphysis. Within the distal epiphysis, a small osteolytic area is present, with a focal calcification in the centre, corresponding to a «nidus» (white arrow). This nidus is located in a subperiosteal location.

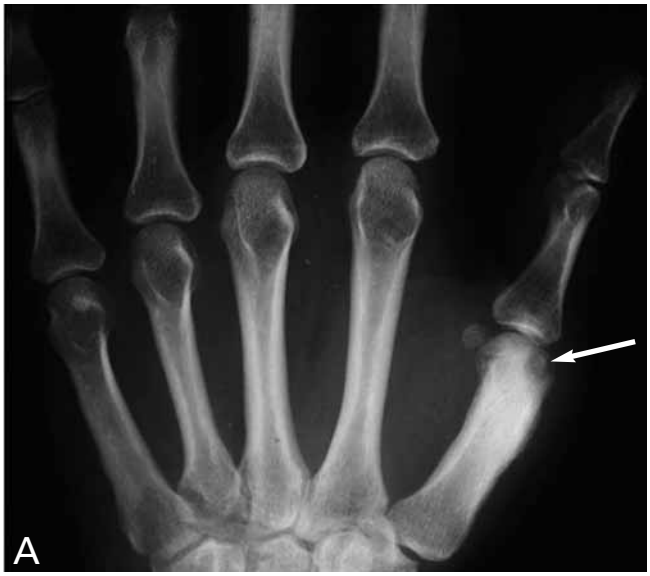

Imaging findings are highly suggestive for **subperiosteal osteoid osteoma**.

Only a small percentage of cases of osteoid osteoma arise in the hand, most of them being located within the medulla or in the cortex. Subperiosteal osteoid osteoma of the hand is extremely rare. In contradistinction with other skeletal locations, osteoid osteoma in the hand is more often painless.

JBR–BTR, 2007, 90: 432.

Case 37

80-year-old male patient with lytic lesion of the middle phalanx of 2nd digit.

Initial plain radiography shows relatively well-defined lesion with internal ridges (Fig. A). Cortical bone on one side appears to be thinned without breakthrough. On the other side, there is subtle cortical permeation and probably some soft tissue swelling. Nine months later, there is progressive cortical destruction and soft-tissue extension of the lesion (Fig. B). Axial T1-weighted MR image after administration of Gadolinium chelates, with fat-selective presaturation shows clear circumferential permative cortical destruction and soft-tissue extension of tumor (Fig. C).

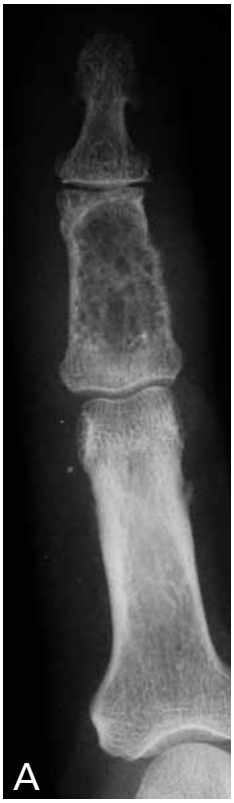

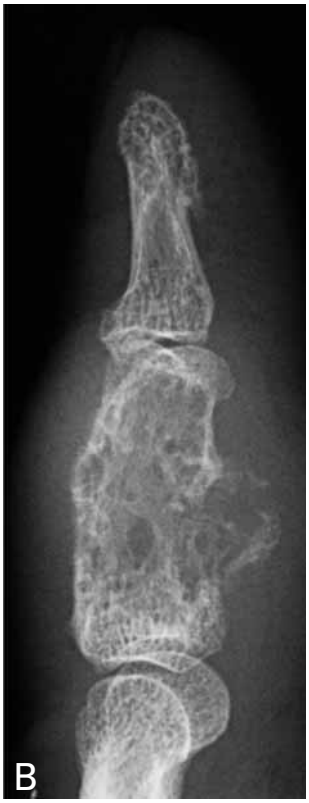

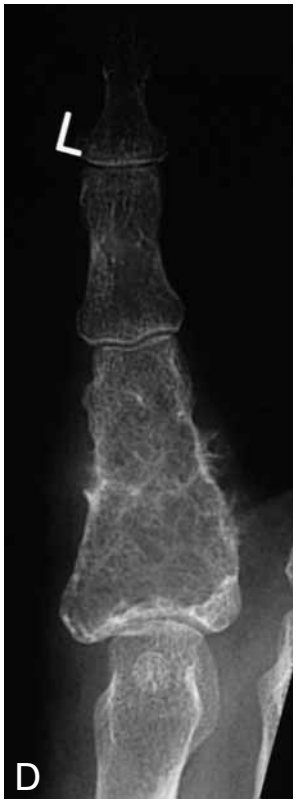

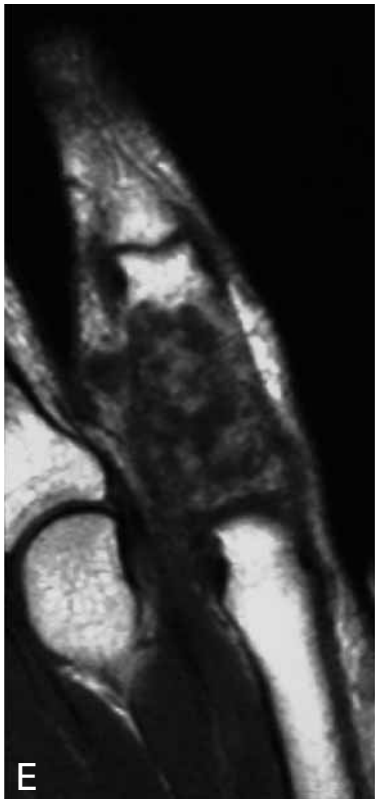

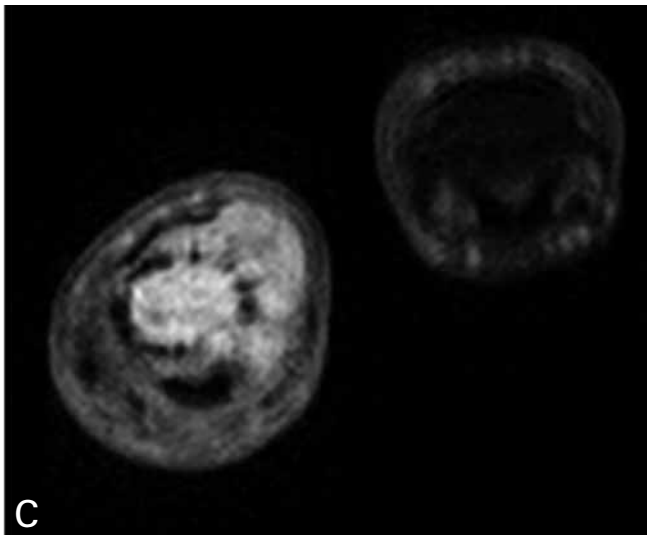

Radiologic diagnosis is **chondrosarcoma.** Histologic diagnosis was **chondrosarcoma grade 2.**

Similar radiologic characteristics of chondrosarcoma of proximal phalanx in 65-year-old male patient (Fig. D), including irregular and permeative cortical destruction, spiculation and soft-tissue swelling. MR imaging (coronal T1-weighted contrast-enhanced turbo spin-echo image) shows intra- and extraosseous tumor extension with heterogeneous nodular and septonodular enhancement (Fig. E).

JBR–BTR, 2007, 90: 433.

Case 38
Patient was imaged on a 3T MR system with a dedicated wrist coil, because of a soft tissue tumor in the hand. Coronal (Fig. A) and axial (Fig. B) T1-weighted images show a lobulated mass of high signal intensity containing thin septations. The tumor extends in several compartments rather than displacing structures. On T1-weighted images with fat suppression, after administration of Gadolinium chelates (Fig. C and D), only the thin septations enhance, signal of the tumoral tissue being homogeneously suppressed.

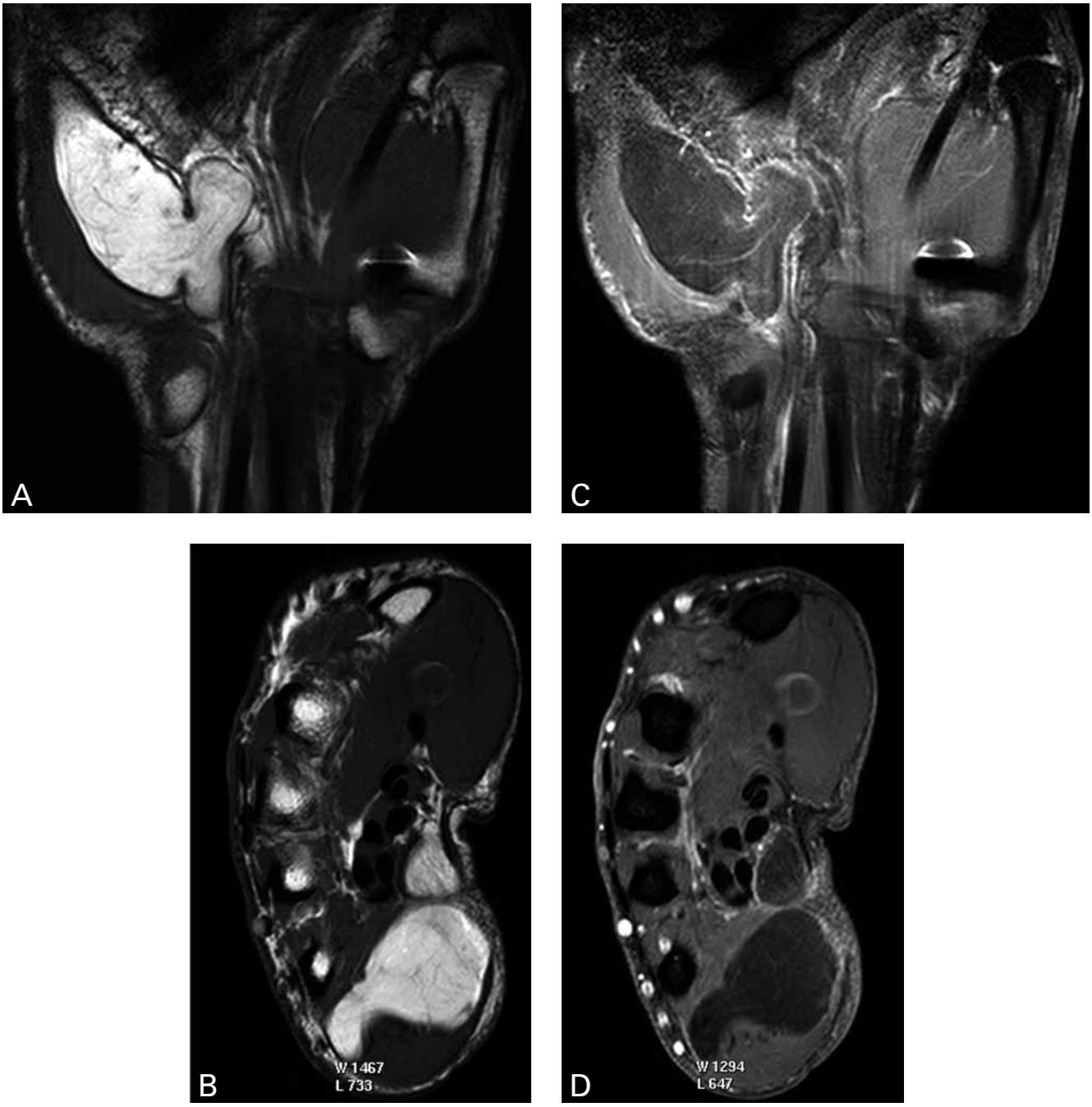

Characteristic findings of a **usual lipoma** on MRI. Although fat suppression is superior at higher field strengths, inhomogeneity in the periphery of the field is a disadvantage. Note homogeneous signal intensity despite disturbance of local field caused by metal foreign body.

JBR–BTR, 2007, 90: 434.

Case 39
A boy of 14 years and 3 months old consults a pediatrician for prediction of adult stature. The boy has always been tall for his age with onset of puberty for two years. The boy is very sportive and is training more than twenty hours a week. His present length is 1.73 m (P75) and his weight is 68 kg (P75-P90). The father of the boy is about 1.7m and his mother 1.56 m.

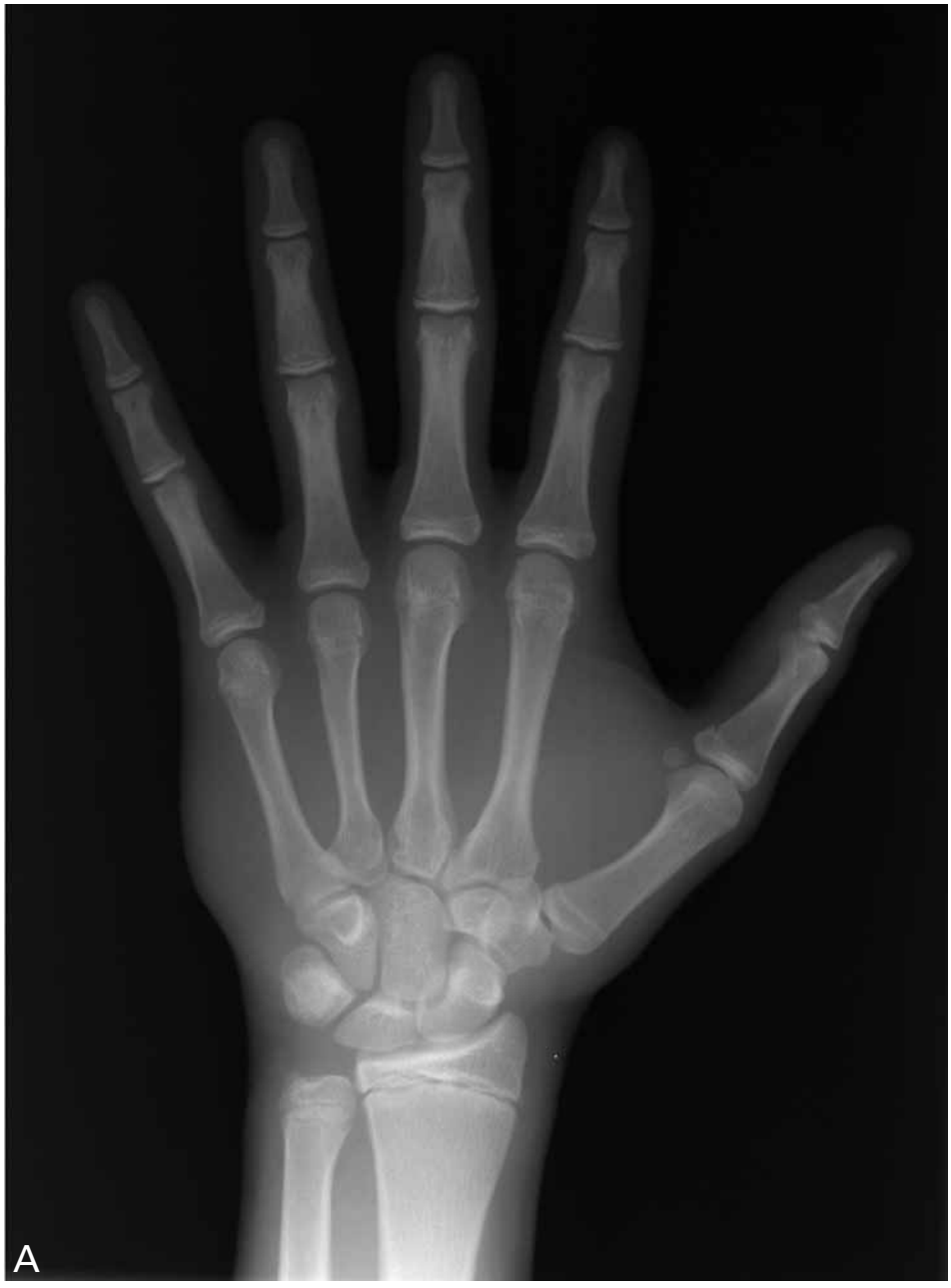

The bone age of the patient is 15 years and 6 months to 16 years for a calendar age of 14 years and 3 months. Note on the AP radiography of the left hand and wrist (Fig. A) that the epiphysis of the first metacarpal is already closed. There is already narrowing of the epiphysis of the distal end of the second till fifth metacarpal and the base of the phalanges.
Based on tables of Greulich and Pyle prediction of percentage of length for retarded, average and advanced bone ages can be made. According to these tables we can predict that **the patient has already achieved 97% of his end length**.

JBR–BTR, 2007, 90: 435.

Case 40
A boy of fourteen years and nine months old is referred for prediction of his adult length.
AP radiography of the left hand and wrist (Fig. A) shows that the bony age of the patient is between 14 and 15 years.

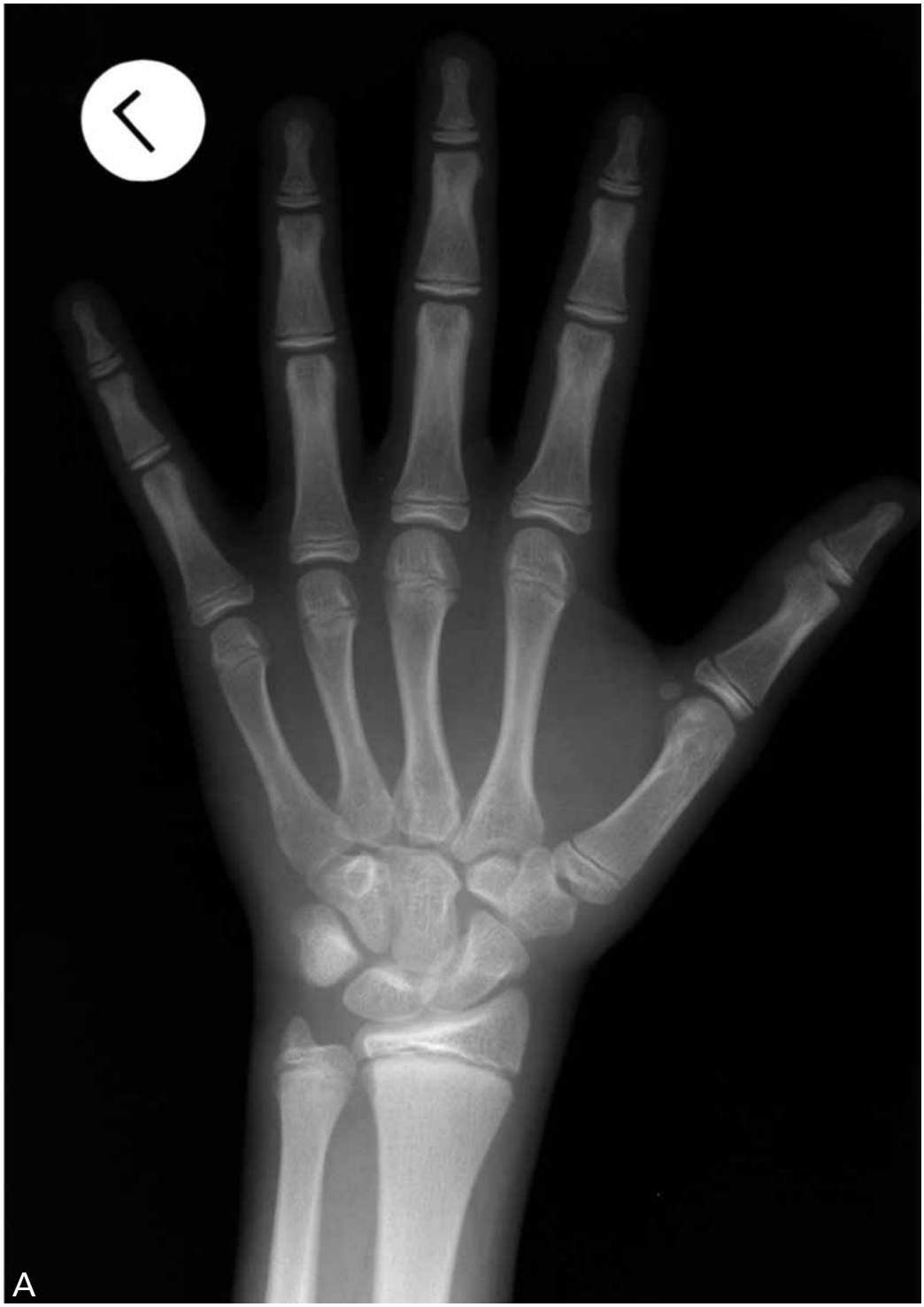

According to the atlas of Greulich and Pyle **maturation of the boy is average and his current length is 93% of his predicted adult length**.

JBR–BTR, 2007, 90: 436.

Case 41

A 46-year-old male with unremarkable medical history visited his physician because of a slow growing, intermittently painful bluish mass in the left hypothenar region. Arteriography reveals a rapidly filling vascular lesion without early venous drainage (Fig. A). Some enlarged draining veins are noticed in the late arterial phase ("peak-opacification", Fig. B) and typical "vascular lakes" are observed in the late venous phase (Fig. C).

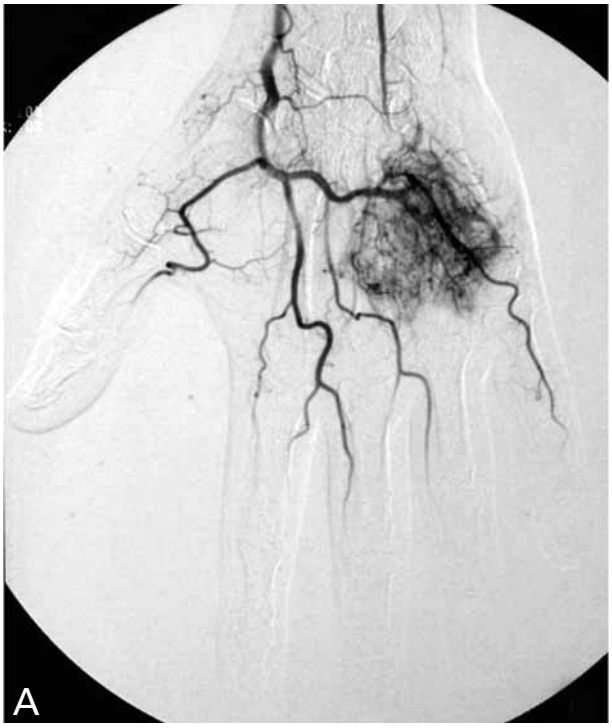

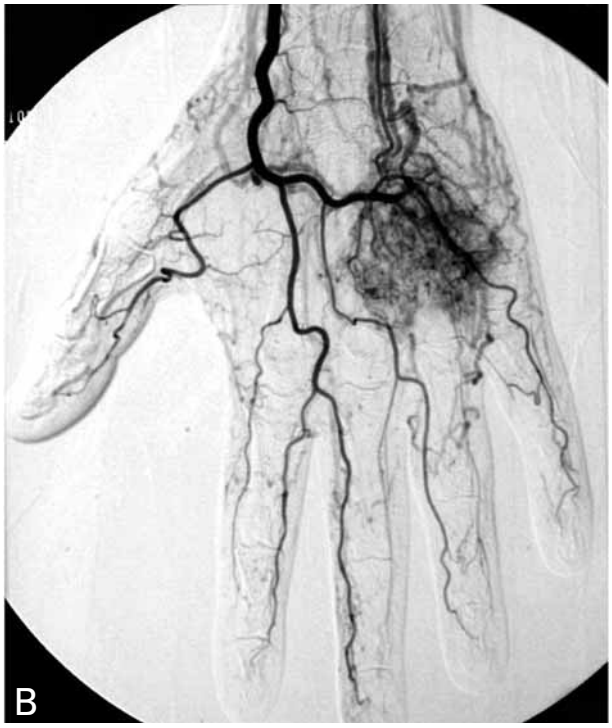

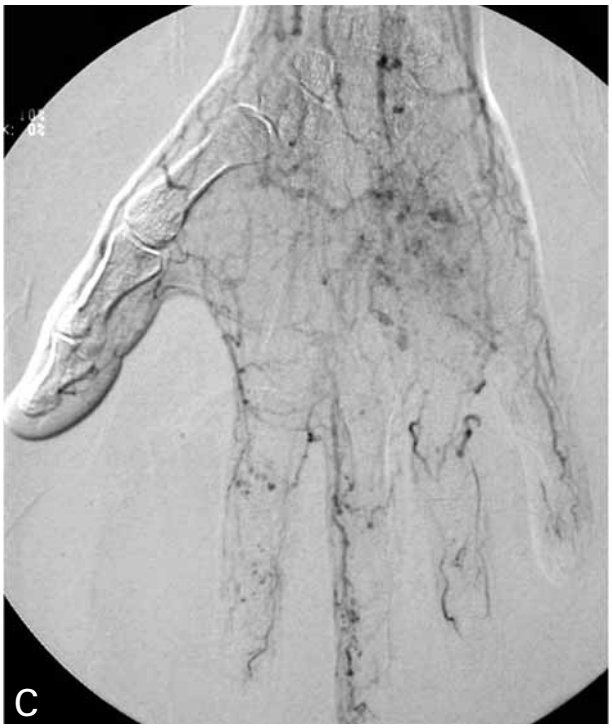

Because of impaired hand function, the mass was surgically excised, and pathologic examination revealed congeries of arterioles and venules, with prominent endothelium suggestive of a **hemangioma**. No evidence of inflammation or malignancy was found. The postoperative course was uneventful except for a slight motion deficit secondary to excision of adjacent muscle fibers.

JBR–BTR, 2007, 90: 437.

Case 42

A 61-year-old woman came in our institution two weeks after ski trauma with injury of the metacarpophalangeal joint of the left thumb in hyperabduction and hyperextension caused by the ski pole. Clinical examination showed a painful swelling at the ulnar side of the metacarpophalangeal joint.

Standard radiography and MRI of the thumb were performed.

Coronal PD-weighted image with fat saturation (Fig. A) shows a full-thickness tear of the ulnar collateral ligament (UCL) which is thickened, has an increased signal intensity with wavy outline (arrow). Compare with the lateral-sided normal radial collateral ligament.

The small and round hypointense zone within the ligament corresponds to a calcification, proximal to the metacarpal head on control radiographs (Fig. B). No asymmetric widening of the metacarpophalangeal joint is seen on the anteroposterior view.

The control coronal MR image shows an horizontal occult fracture (not seen on the radiographs) with slight persistent bone marrow edema (Fig. C).

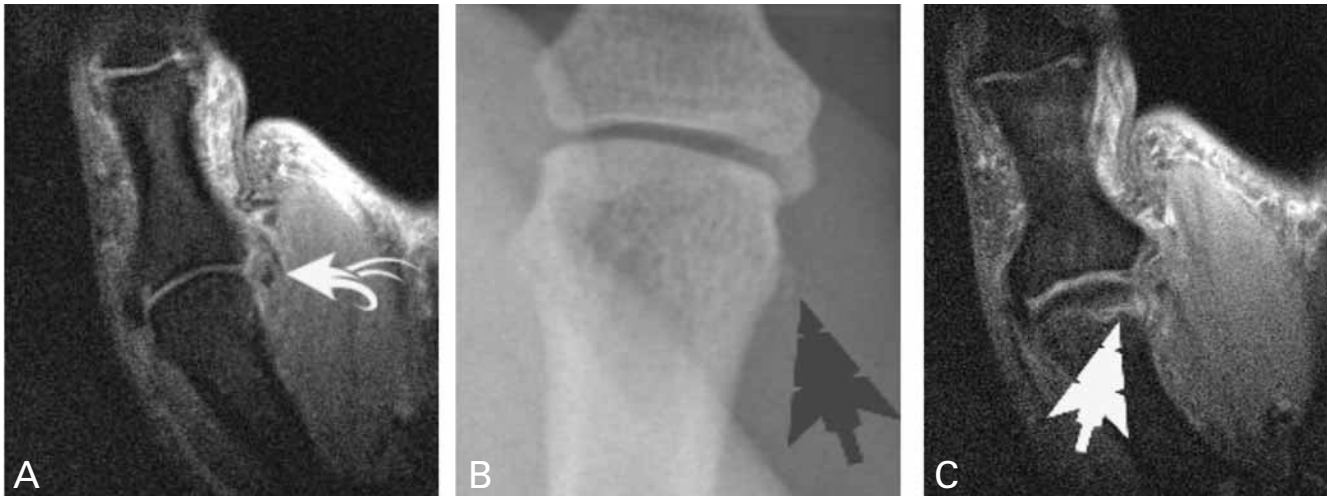

Gamekeeper's thumb or skier's thumb with a tear of the ulnar collateral ligament (UCL).

JBR–BTR, 2007, 90: 438.

Case 43
A 22-year-old male had since his birth a small soft tissue mass in the third finger of the right hand. The patient reported increased pain and swelling since one year, during his work as professional cook. MRI with dynamic series (not shown) revealed a vascular malformation, with high flow arterial component. Angiogram of the hand (Fig. A) shows a small hypervascular lesion at the level of the middle phalanx of the third finger with hypertrophy of the vessels and early venous filling. Selective angiogram of the digital artery of the third finger (Fig. B and C) shows the lesion in detail.

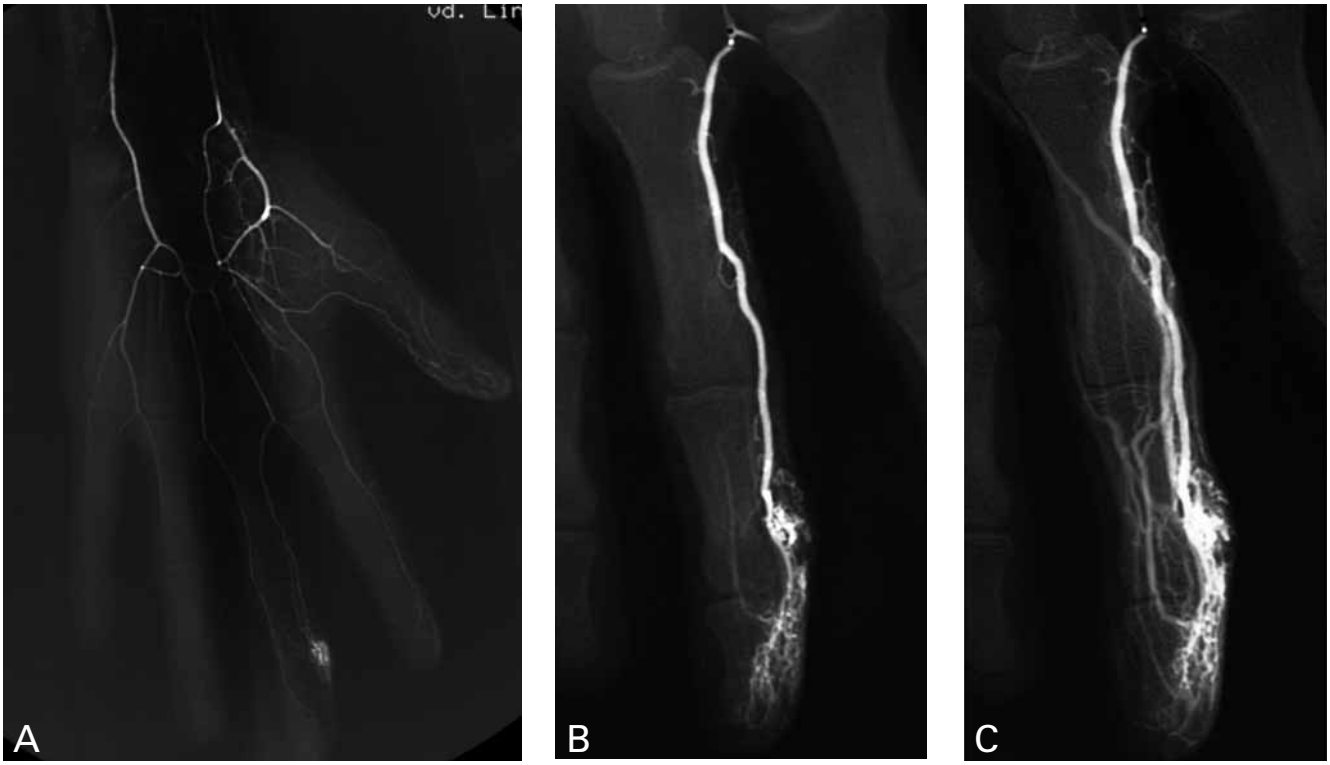

Findings are characteristic for a **congenital high flow arteriovenous malformation (AVM)**. Treatment is difficult and complete cure is hardly to achieve. Treatment options are arterial or percutaneous embolization. This patient was not treated because of high risk of ischemia.

JBR–BTR, 2007, 90: 439.

Case 44

A 52-year-old, former professional cyclist has complaints since 6 years. He presents with hypo-esthesia and paresthesia at the right fifth finger and the ulnar part of the annulary. Hand weakness is associated with hypothenar volume reduction.

Radiography of both wrists (Fig. A) shows a bilateral scapholunate dissociation and a "ring sign" due to shortening of the scaphoid at the right wrist. Soft tissue calcification is present at the volar-ulnar side of the right wrist at the level of the triangular cartilage.

Ultrasound of both wrists (Fig. B, C and D) (B: longitudinal composed images of the right side, left = distal, right = proximal; C and D: axial images of the right side). On the longitudinal images the flexor carpi ulnaris tendon is well visualized (white arrows). Calcifications are located at the distal part of the tendon with thickening of the tendon itself. On the axial images (Fig. C and D) the location of the flexor carpi ulnaris tendon at the roof of Guyon's canal is demonstrated. This tendon is located adjacent to and compressing the ulnar nerve (white arrows). At the radial aspect of the ulnar nerve the ulnar artery is blinking on the power Doppler image (Fig. D).

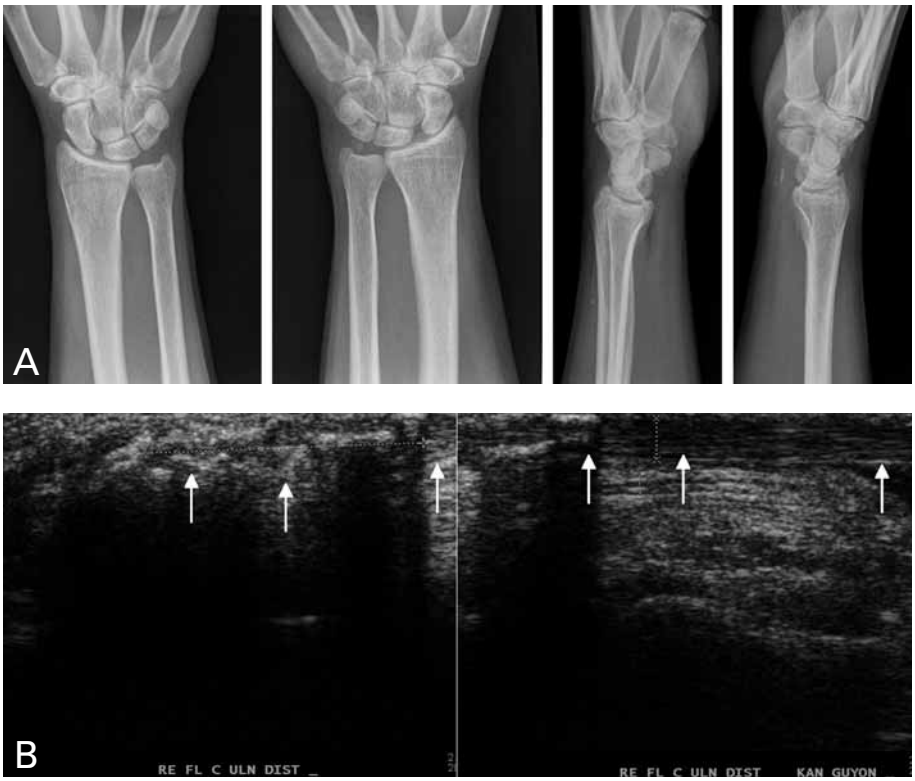

Diagnosis: **chronic ulnar nerve compression at Guyon's canal (chronic cyclist palsy)** caused by calcifying tendinosis

JBR–BTR, 2007, 90: 440.

Case 45
Sonogram at the level of the middle third of the left index in an adolescent man (arrows).
Longitudinal plane (Fig. A): Ovoid mass lesion with diameter of 6 mm *(arrow)* within the subcutis superficial to the middle phalanx of the index. The lesion is sharply demarcated and appears hypoechoic to adjacent subcutaneous fat.
Transverse plane (Fig. B): Confirmation of the mass, as described in Fig. A. Its exact location and relationship of the lesion to the adjacent flexor tendon is extremely well disclosed on this section: the lesion is located at the radial – volar aspect of the tendon and shows no contact with the latter.

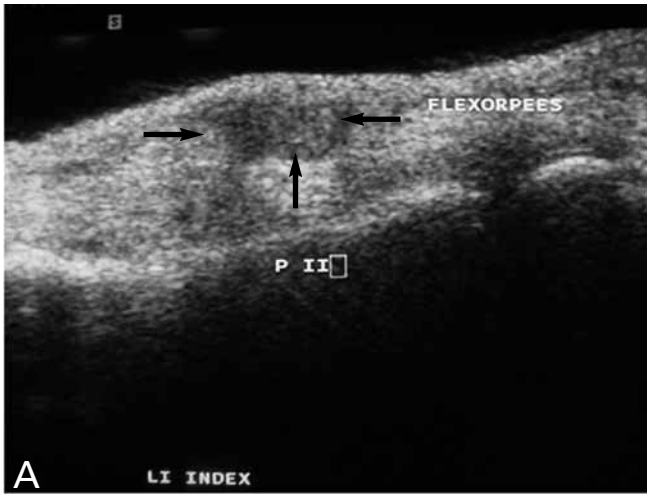

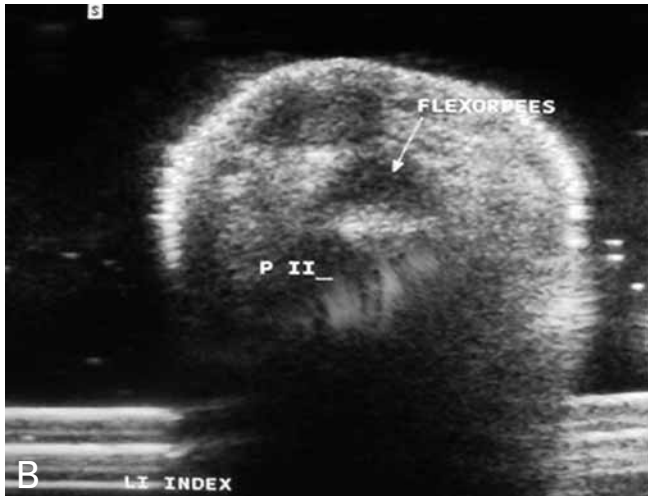

Sonographic data are suggestive for a **granuloma** within the subcutaneous tissue.

JBR–BTR, 2007, 90: 441.

Case 46
This patient had vague aches and pains and was sent up to have a radiography of his hands (Fig. A) to exclude an erosive arthropathy. What major abnormality is present, and what differential diagnosis should be considered? Histology from another patient is shown (Fig. B).

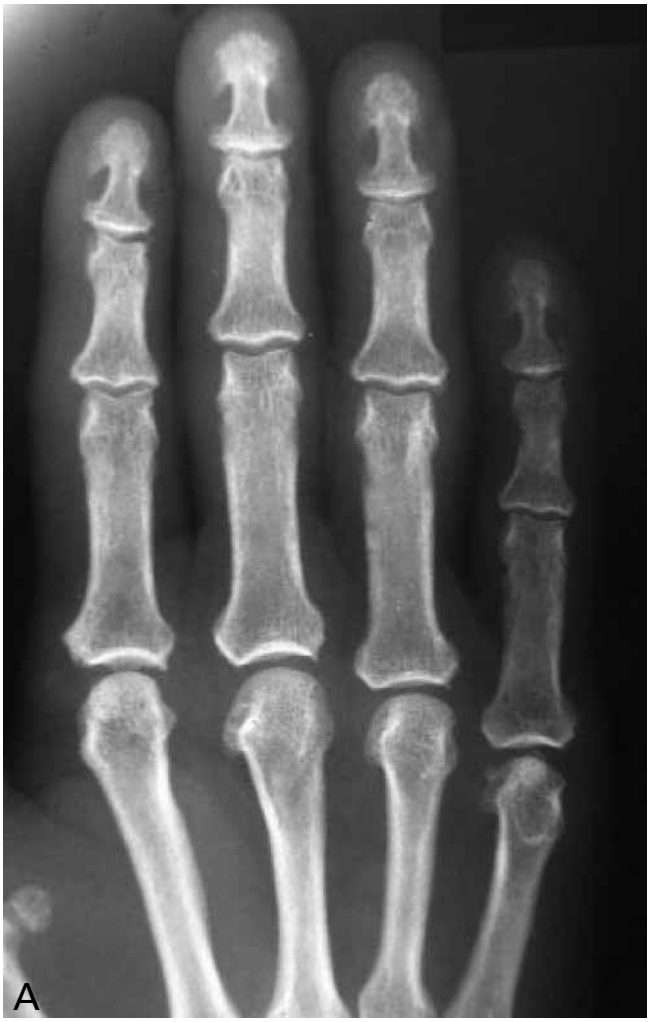

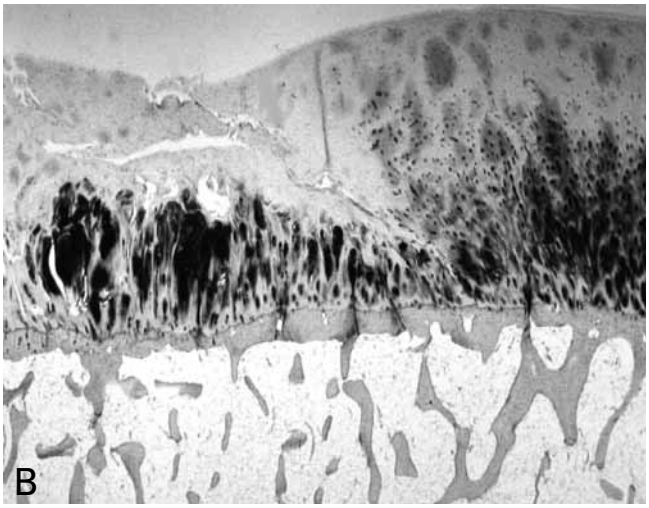

The striking feature is that the joint spaces are wider than usual – all of them, especially the MCPJs. This is the most important plain radiographic sign of **acromegaly**. Note also the arrow head – deformity of the distal tufts. The cartilage is thicker than usual, but not normal as shown in the histology. The chondrocytes hypertrophy but the thick cartilage fails quicker with secondary OA. Consider also hypothyroidism in your differential diagnosis.

JBR–BTR, 2007, 90: 442.

Case 47
Clinical information: 20-year-old man, known with an inheritable disease, presenting with slight shortening of the forearms and «bayonet-like» deformity of the wrists.
Fig. A. PA radiography of the right hand:
Multiple ring-like densities are projecting on the proximal phalanges of the second, third and fourth finger (thin black arrows). There are focal bony overgrowths (*cartilaginous exostoses*) projecting at the radial side of the fifth phalanx (white arrow) and at the distal aspect of the third metacarpal and base of the fifth metacarpal (thick black arrows). Note the continuity of the cortical and medullary bone of the overgrowth and the underlying phalanx.
Fig. B. PA radiography of the right wrist:
Ring-like densities are projecting on the distal radius (black arrows). A pedunculated *exostosis* at the distal ulna points away from the distal radiocarpal joint (white arrow). There is *shortening* of the ulna and *Madelung-like deformity* of the wrist.

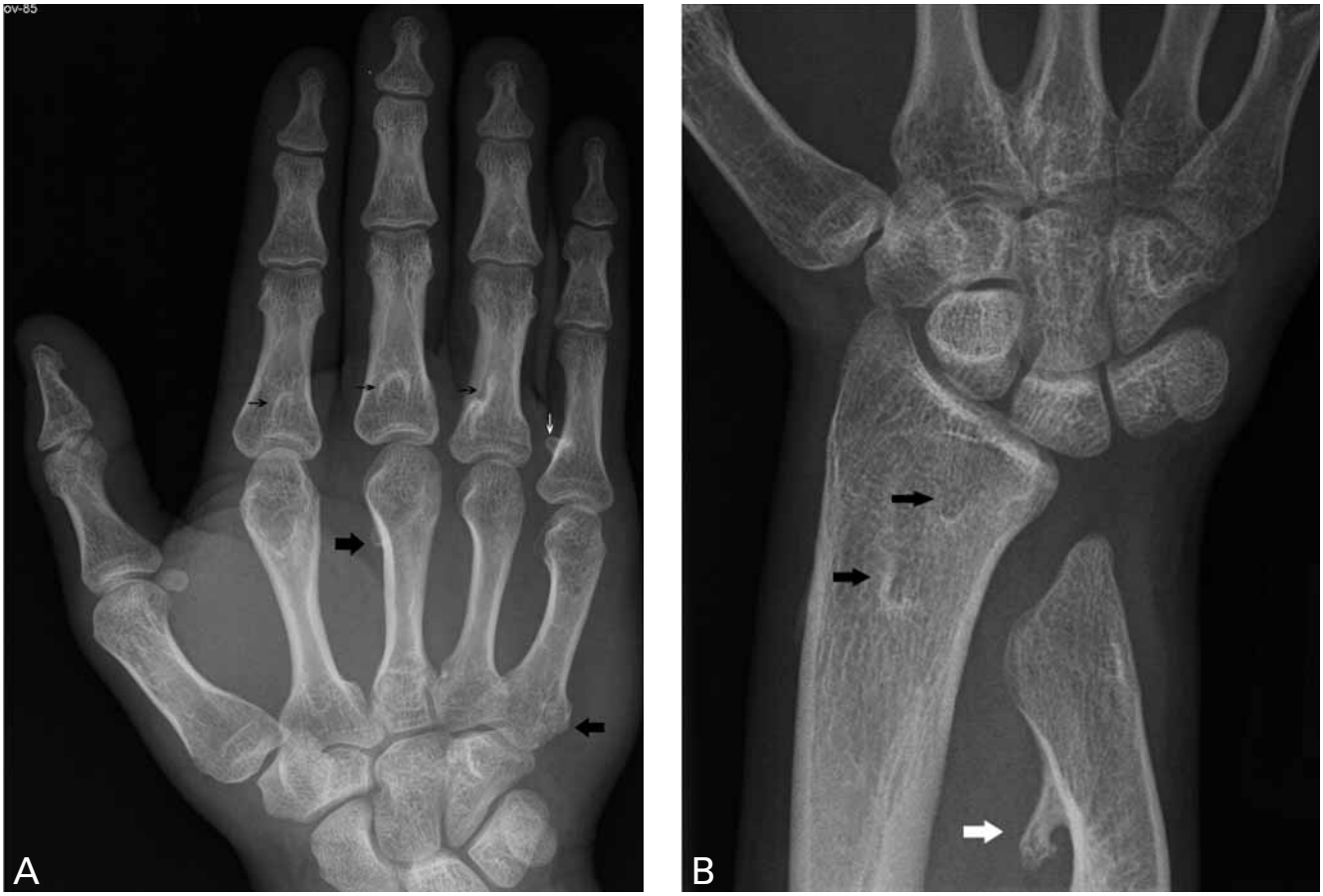

Based on the typical radiographic findings, the diagnosis of **Hereditary Multiple Exostosis (HME) Syndrome** can be made.
HME is the most common bone dysplasia, inherited on an autosomal dominant basis, with a prevalence of one to 50.000.
It is characterized by polyostotic peripheral osteochondroma formation, mainly located at the long bones of the lower and upper extremities. The long bones of the hand (metacarpals, phalanges) may be involved as well, but the carpal bones are typically spared.
At the forearm, shortening of the ulna with secondary bowing of the radius results in development of pseudo-Madelung deformity.

JBR–BTR, 2007, 90: 443.

Case 48
Clinical information: 13-year-old female with a family history of congenital heart disease, dysplastic nails and supranumerary fingers.
Fig. A. PA radiography of the right hand:
There is an extra finger (arrow) on the ulnar side of the hand (*postaxial polydactyly* or *hexadactyly*).
Note also partial bony *fusion* of the fifth metacarpal and the extra metacarpal.
Progressive distalward shortening of the tubular bones with short, broad middle phalanges and hypoplastic distal phalanges.

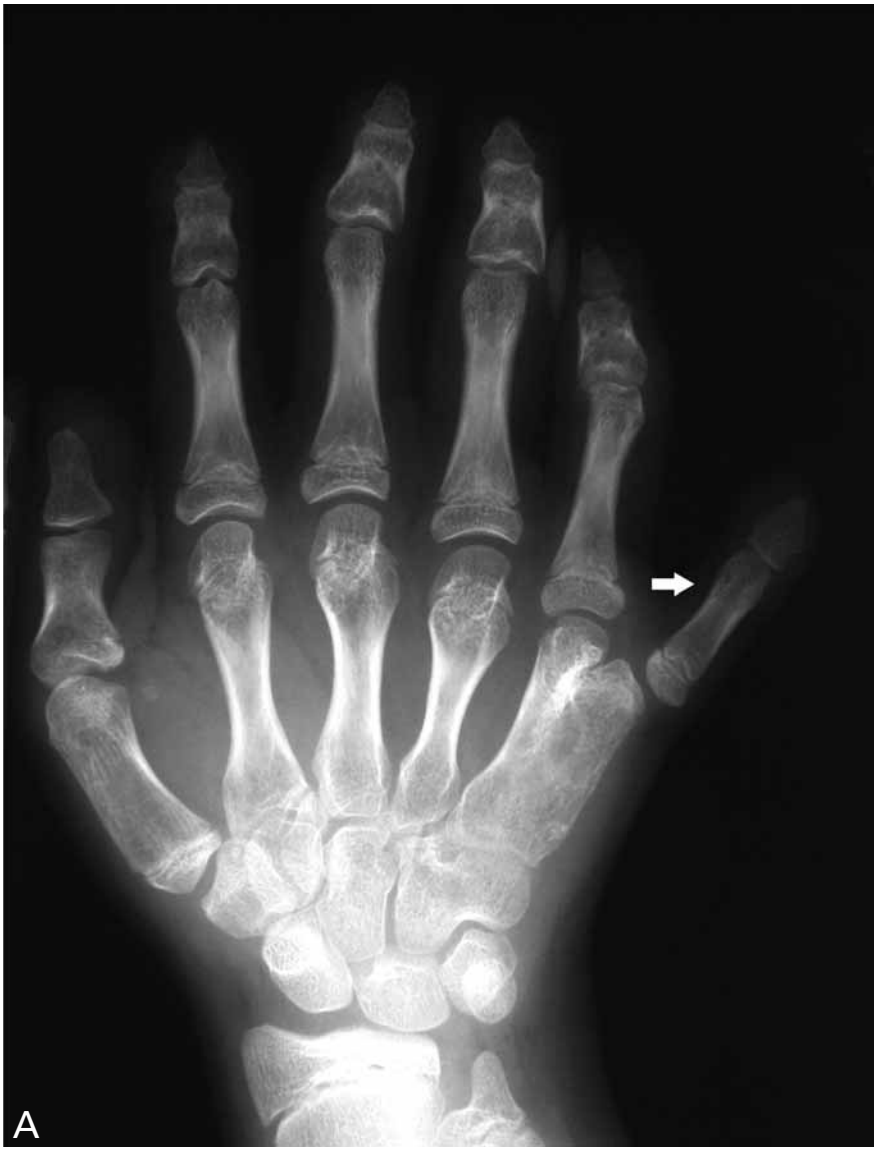

Based on the positive family history, clinical and radiographic findings, the diagnosis of **Ellis-van Creveld Syndrome (EvC)** or chondroectodermal dysplasia can be made.
EvC belongs to the short rib dysplasia group of osteochondrodysplasias, and is inherited on an autosomal recessive basis.
Clinically it is characterized by a disproportionate short-limb dwarfism, postaxial polydactyly of the fingers (and toes), hypoplastic nails, dental anomalies, multiple labiogingival frenula, cardiac abnormalities and knock-knee deformity. The chest is usually short.
Its main differential diagnosis includes asphyxiating thoracic dysplasia.
Hexadactyly of the hands is a constant finding in EvC syndrome, but is rare in asphyxiating thoracic dysplasia.

JBR–BTR, 2007, 90: 444.

Case 49

Clinical information: 11-month-old female with multiple congenital malformations, including an atrial and ventricular septum defect, renal agenesis on the left side, and anorectal malformation, presenting with a deformity of the hand and forearm on both sides.

Fig. A. PA radiography of the left hand and arm.

There is an aplasia of the thumb including the first metacarpal bone (*oligodactyly*). The radius is missing and the ulna is foreshortened and slightly bowed.

Fig. B. AP radiography of the thoraco-lumbar spine.

There are multiple congenital vertebral anomalies, including hemivertebrae of Th4, L1 right and L3. Due to these hemivertebrae there is a scoliosis of the lower thoracic and lumbar spine. Furthermore, there is a partial sacral dysgenesis.

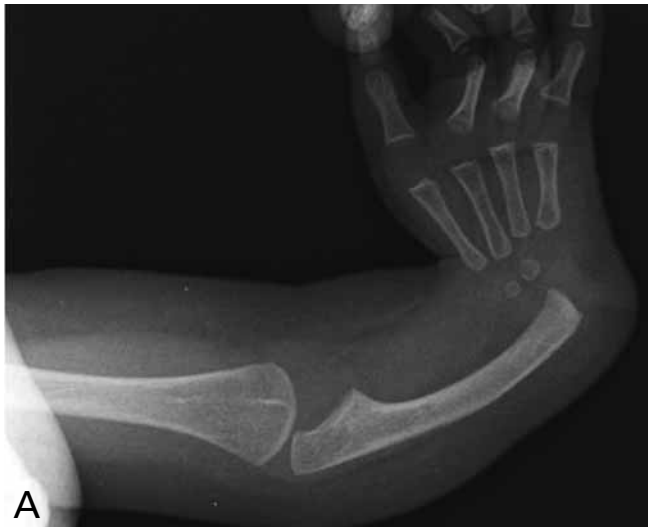

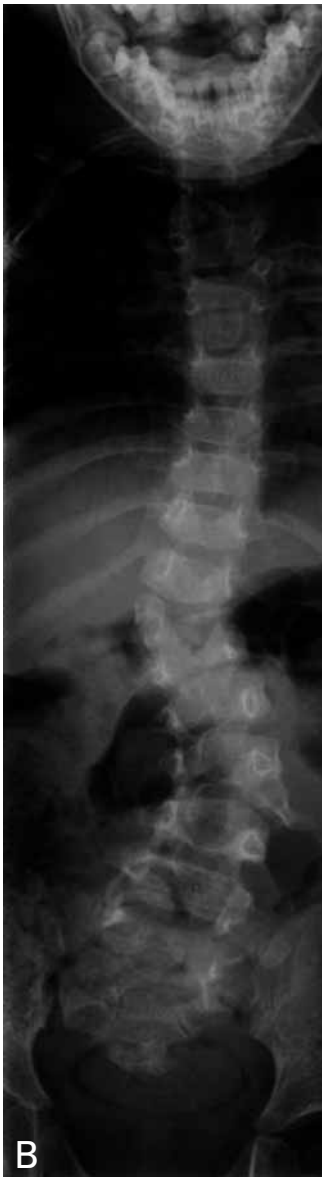

Based on the clinical and radiographic findings, the diagnosis of **VACTERL association** with **radial ray** deformity can be made.

This abbreviation stands for **V**ertebral (or **V**ascular), **A**norectal of (**A**uricular), **C**ardiovascular, **T**racheo-**E**sophageal fistula, **R**enal (or **R**adial, **R**ib), and **L**imb anomalies. The frequency of anomalies in this association is: vertebral (37%), anal (63%), cardiac (77%), tracheal (40%), renal (72%) and radial ray deformity (58%). In the literature there is some tendency to reserve the diagnosis of a VACTERL association to those patients with at least three of the six anomalies. In the presented case except of the TE-fistula all other criteria were present. In addition to the above described anomalies, MRI did show a tethered cord with a large intraspinal cyst at the level of the sacrum.

JBR–BTR, 2007, 90: 445.

Case 50
This elderly gentleman complained of a painless swelling of his left ring finger. He is known to have osteoarthritis and ischemic heart disease.
Look carefully at the hand radiographs (Fig. A).Three abnormalities are present.

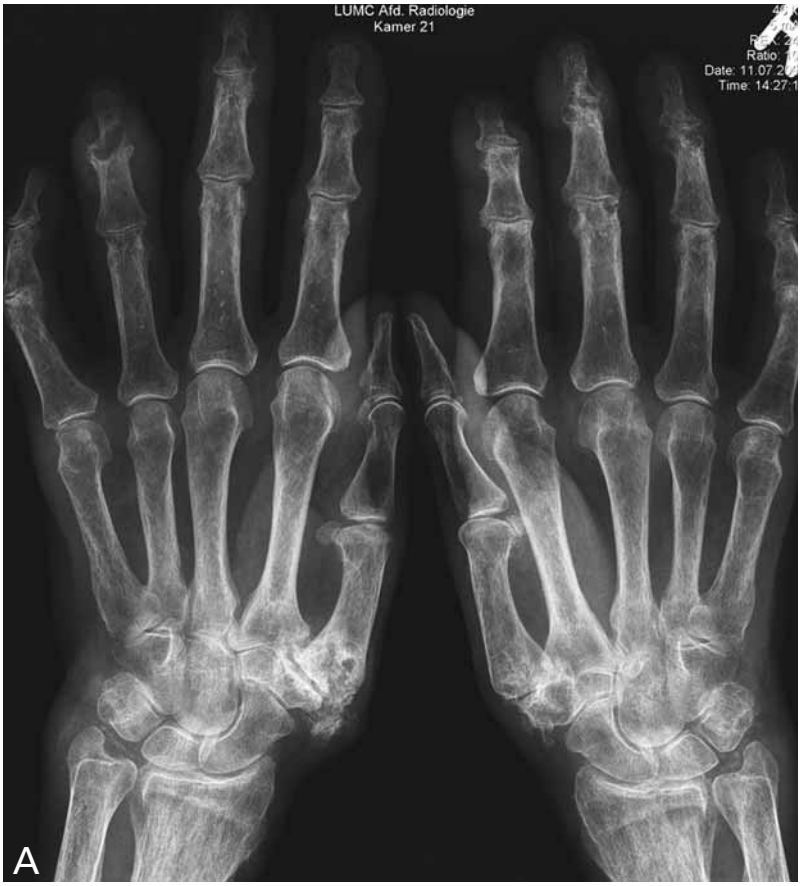

Firstly he has marked, hypertrophic Osteoarthritis (OA) of the thumb carpometacarpal joints. Secondly, he has chondrocalcinosis (CPPD) involving the triangular fibrocartilages.The combination of hypertrophic OA and CPPD has been described as **pyrophosphate arthropathy**. However, CPPD is associated with osteophyte formation, not hyaline cartilage loss. So this association may be coincidental, especially as CPPD deposition is age-related, as is OA. The third, and most important finding, is the destructive arthropathy of the interphalangeal joints, especially the DIPJ of the left ring finger. The clue is the well-defined nature of these lesions and the soft tissue swelling so typical of **gouty tophi**. Diuretic associated gout is usually painless and presents as swelling often misdiagnosed as OA alone. It is not unusual to have two types of crystal deposited in an elderly patient.

JBR–BTR, 2007, 90: 446.

Case 51
A 24-year-old male presents with left wrist pain on the lateral side after a bicycle accident.
Routine radiography shows no abnormalities (Fig. A).
After inclusion in a trial evaluating the value of acute MRI (within 12 hours after the accident) an abnormal signal is seen in the radius on T1- (Fig. B) and fat suppressed T2-weighted images (Fig. C).
Twenty-four hours later, a bone scintigraphy was performed (Fig. D).

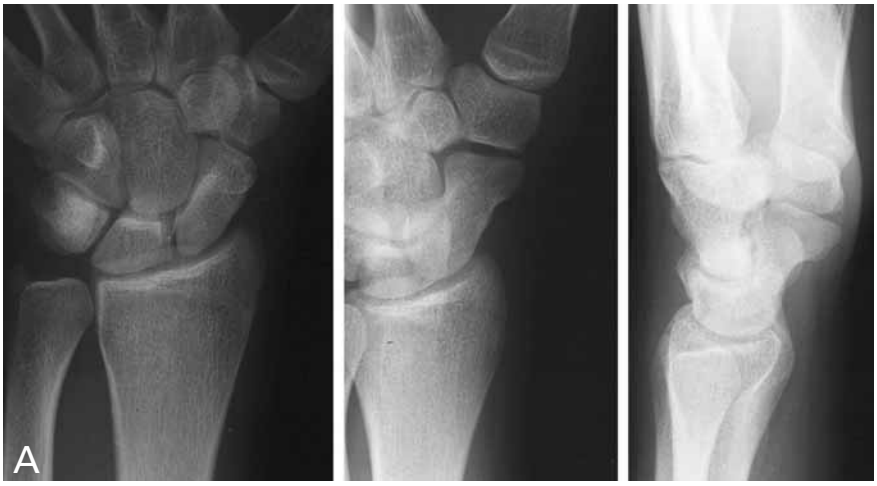

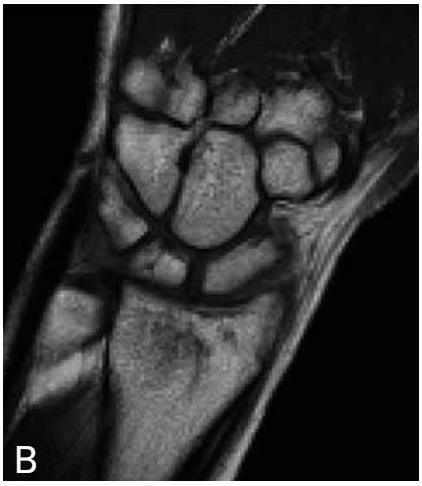

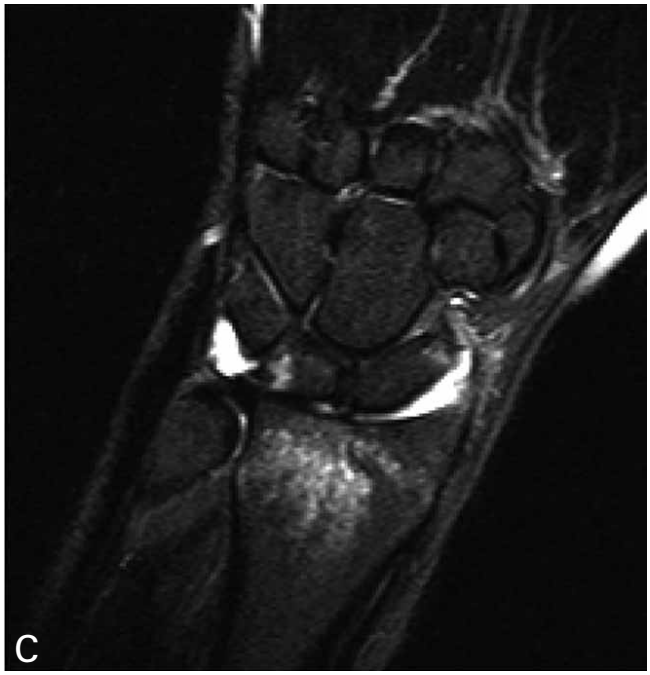

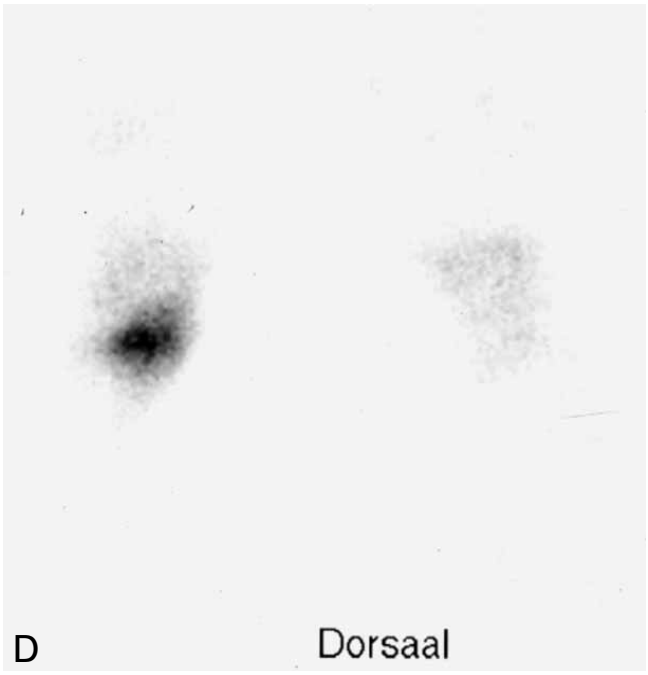

Occult fracture of the distal radius.

JBR–BTR, 2007, 90: 447.

Case 52
A 31-year-old male presenting with diffuse left wrist pain on the lateral side after a motorbike accident. Routine radiography shows a wide space between scaphoid and lunate (Fig. A).

MRI was performed within 12 hours after the accident. Fat suppressed T2-weighted image confirms carpal effusion (Fig. B). There is an abnormal position of the lunate on a sagittal T1-weighted image. The lunate is in DISI-position (Fig. C).

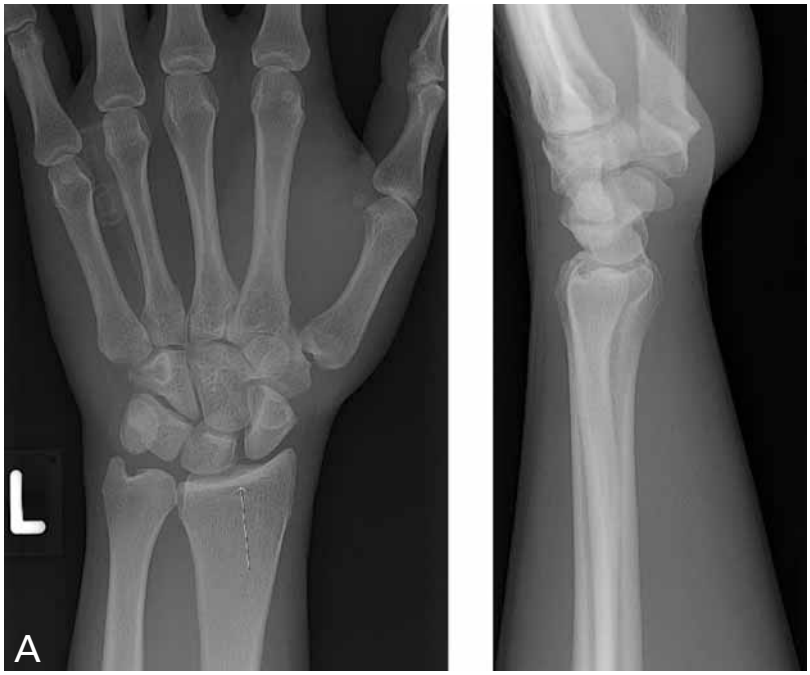

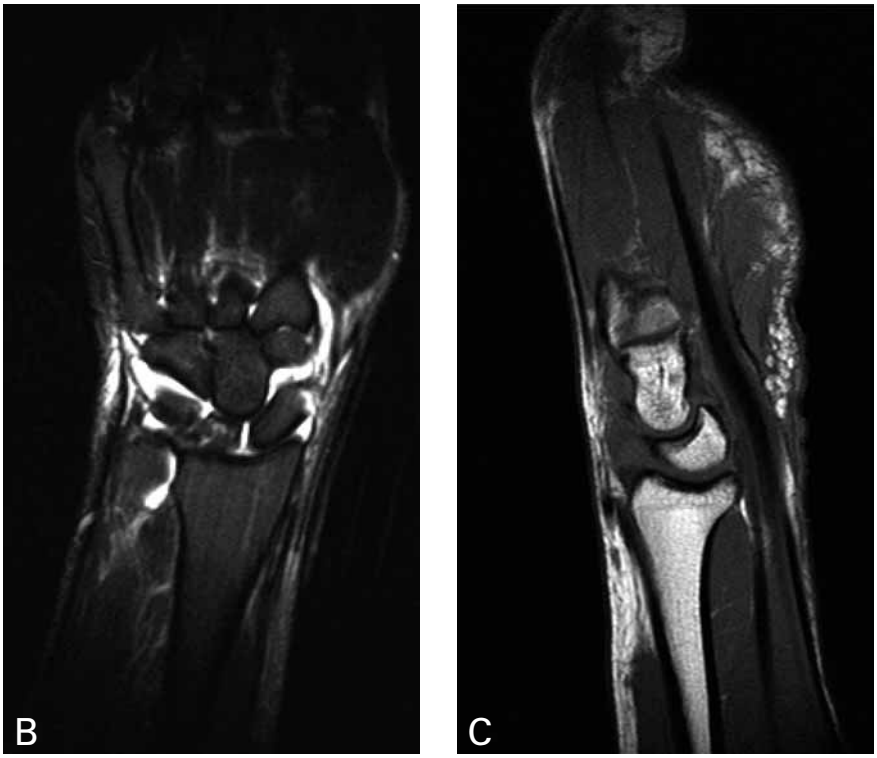

DISI, due to an injury to the intercarpal ligaments after longitudinal compression of the carpus.

JBR–BTR, 2007, 90: 448.

Case 53
30-year-old football player sustained acute pain in the right ring finger when pulling the shirt of an opponent during a soccer game. Immediately afterwards, he lost active motion at the proximal and distal interphalangeal joint.
Clinical examination showed swelling of the finger and tenderness in the palm of the hand.
Plain radiography showed no abnormalities.
An urgent MRI was done. Sagittal and coronal T1-weighted MR images were performed (Fig. A and B)
Fig. C demonstrates surgical findings.

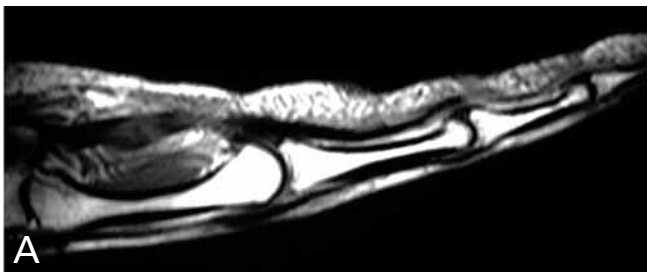

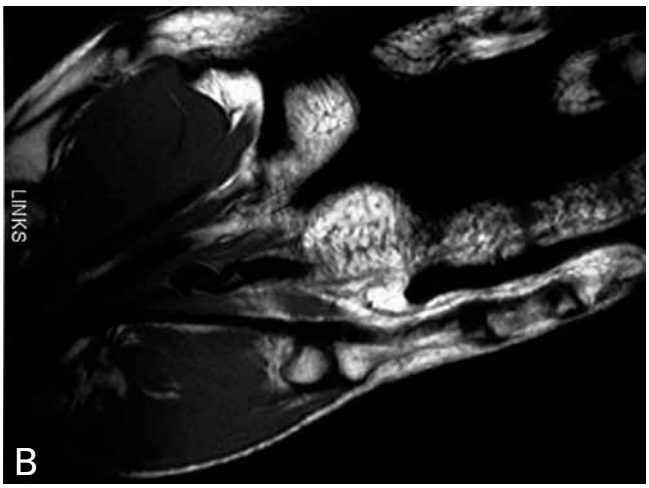

This patient has an **avulsion of both the superficial and deep flexor tendon** of the ring finger, with retraction of the superficial tendon into the palm of the hand. This very rare injury requires immediate operative repair to restore normal function of the finger.

JBR–BTR, 2007, 90: 449.

Case 54

A 30-year-old pilot was involved in a car accident and sustained a complex fracture of the left forearm. He was treated with a combination of internal and external fixation (Fig. A). Immediately after surgery, he complained of complete loss of active flexion of the thumb (Fig. B). Passive range of motion was normal. This case was initially investigated with ultrasound, showing a normal flexor pollicis longus tendon. Subsequently a MRI was performed. Fig. C shows an axial fat suppressed T2-weighted image.

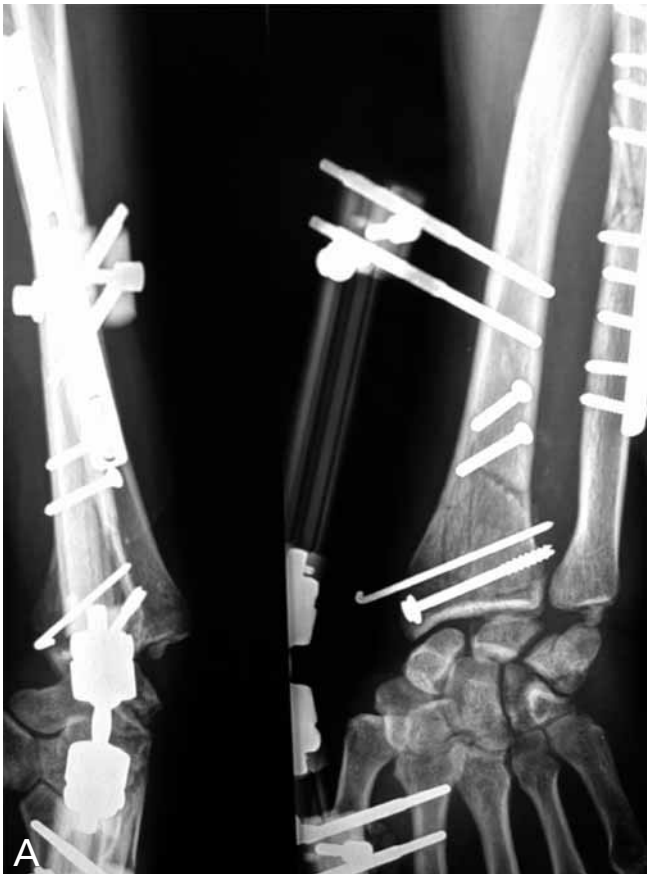

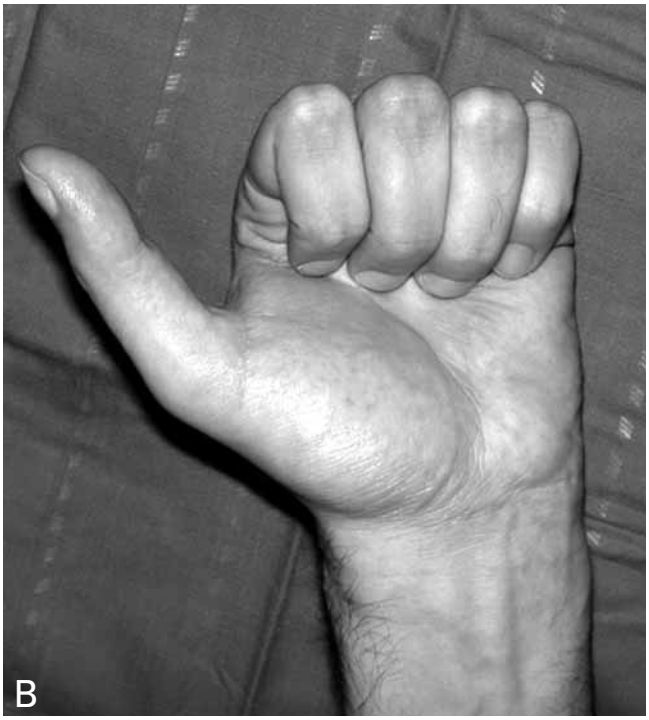

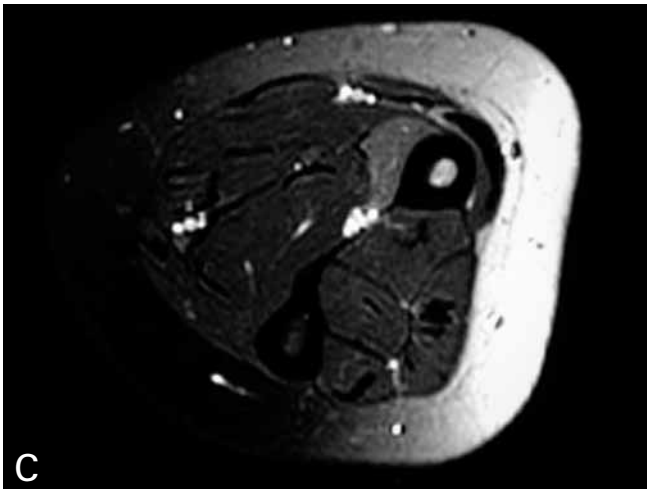

MRI shows an abnormal high signal in the flexor pollicis longus muscle, due to **denervation**. A subsequently done nerve conduction study and electromyography confirmed complete denervation of this muscle. This was caused by an injury of the branch of the anterior interosseous nerve, innervating the flexor pollicis longus muscle, by a proximal pin of the external fixator.

A tendon transfer was necessary to restore active thumb flexion.

JBR–BTR, 2007, 90: 450.

Case 55

A 45-year-old female complained of pain at the right wrist for more than 3 months, mainly while playing tennis. There was no acute injury.

Clinical examination shows pain on palpation in the hypothenar area, and with flexion of the small finger against resistance.

Plain radiography was normal, and an MRI was made. Coronal T1-weighted image (Fig. A) and axial fat suppressed T2-weighted image (Fig. B) demonstrated bone marrow edema in the hamate bone.

CT scan revealed cortical breakthrough at the base of the hook of the hamate bone (Fig. C).

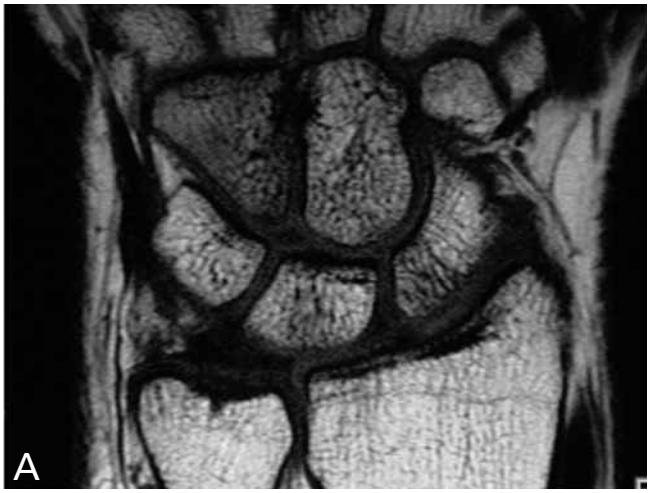

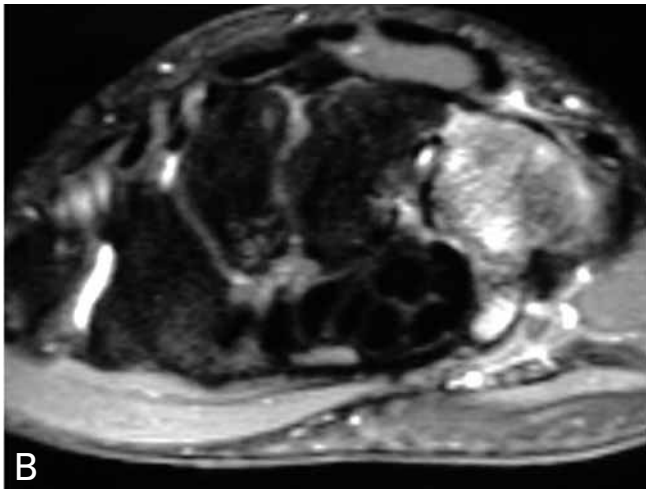

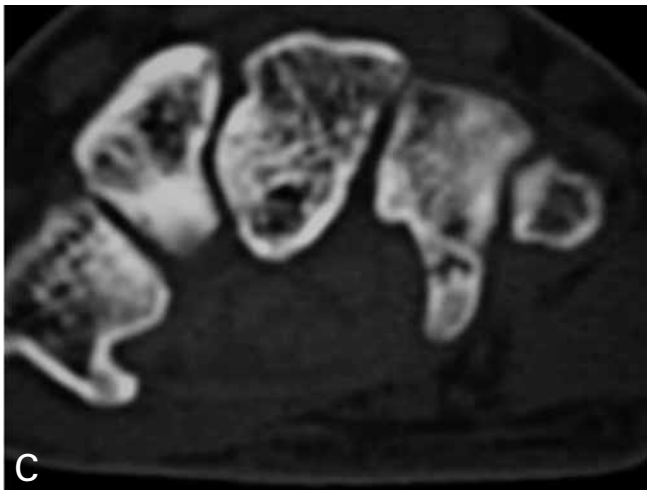

Although the report of the MRI suggested avascular necrosis of the hamate bone as most probable diagnosis, the history and examination were very suggestive for a **stress fracture of the hamulus**.

This was confirmed on CT scan. Although MRI is an excellent tool for demonstration of bone marrow edema, demonstration of the fracture line is better seen on CT.

The patient was subsequently treated with excision of the hamulus, when the fracture turned into a pseudarthrosis.

JBR–BTR, 2007, 90: 451.

Case 56
Clinical information: 2-year-old female with macrocephaly, mental retardation, multiple joint contractures and thoraco-lumbar gibbus.
Fig. A. PA radiography of the left hand:
There is some shortening and widening of the metacarpals. The second to fifth metacarpals are narrow at their bases. The cortices are thin. The distal metaphyses of the ulna and, less markedly, the radius are slanted toward each other.
Fig. B and C. Lateral radiography of the thoraco-lumbar spine (B) and magnification of Th12-L1:
There is a hook-shaped deformity of the vertebral bodies L2 and L3. The body of L2 is displaced dorsally and there is a thoraco-lumbar kyphosis.
Fig. D. AP radiography of the pelvis:
The basilar portions of the iliac bones are small, the acetabular fossa is dysplastic and shallow. The femoral necks are broad and in valgus, and there is a subluxation of the hip joint on both sides.

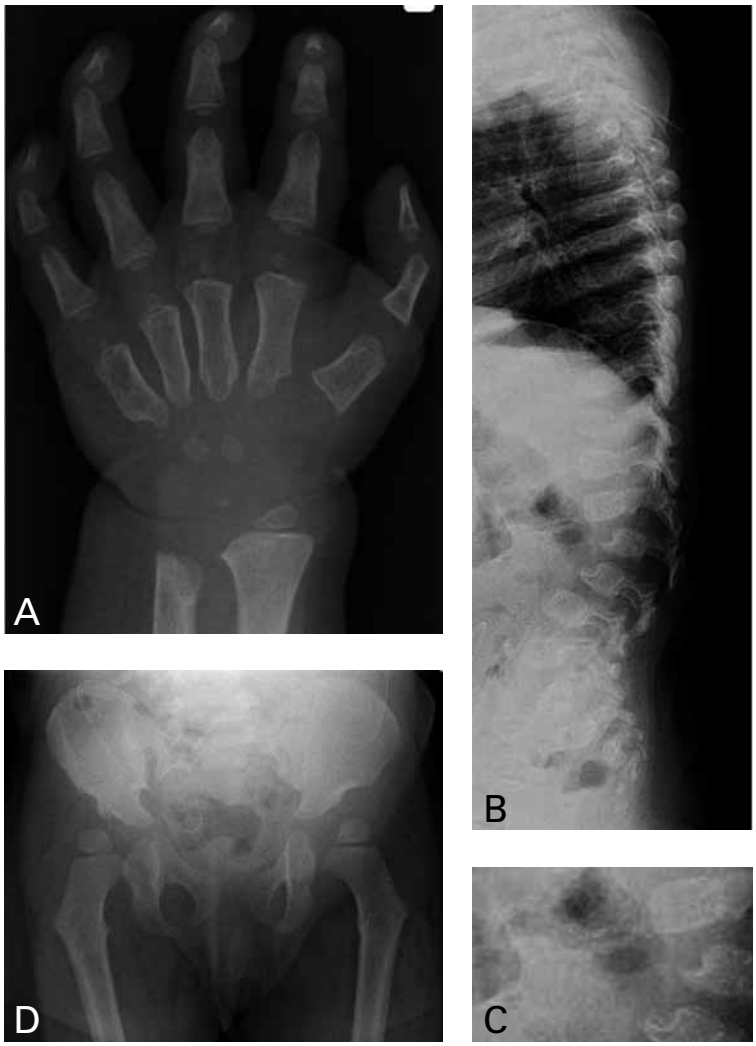

Based on the clinical and radiographic findings the diagnosis of a **mucopolysaccharidosis** can be made. Laboratory findings revealed that this patient was lacking the enzyme alpha-L-iduronidase, which is diagnostic for mucopolysaccharidosis type I, in this case type 1-H (Hurler disease).
Hurler disease is one of the Complex Carbohydrate Storage Diseases, which, depending on the type of stored material, have been classified as mucopolysaccharidoses, oligosaccharidoses and glycoproteinosis. The skeletal abnormalities in most of these disorders are summarized under the term "Dysostosis Multiplex" of which the major components are: macrocephaly, thick calvaria, wide (oar-shaped) ribs, oval-shaped or hook-shaped vertebral bodies, overconstriction of the lower iliac bones, dysplasia of the capital femoral epiphyses, coxa valga, irregular diaphyseal modelling, shortening of the long tubular bones, brachydactyly with metaphyseal widening, and proximal tapering of the second to fifth metacarpal bones. The skeletal abnormalities are relatively uniform in most of the Carbohydrate Storage Diseases, although its severity may differ.

JBR–BTR, 2007, 90: 452.

Case 57

A middle-aged male patient with a known chronic disease complains of pain in his hands and wrists. What differential diagnosis would you consider when looking at the radiographs (Fig. A and B)? Note the extensive involvement of the metacarpophalangeal joints and the numerous subchondral cyst-like radiolucencies. Hyaline cartilage is thinned but osteophytosis is minimal.

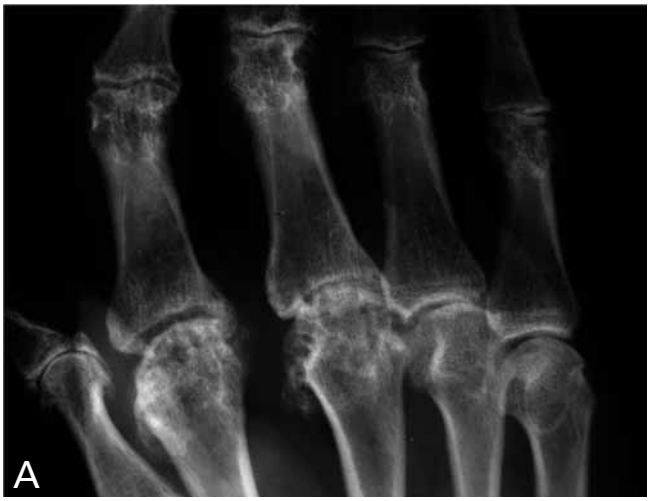

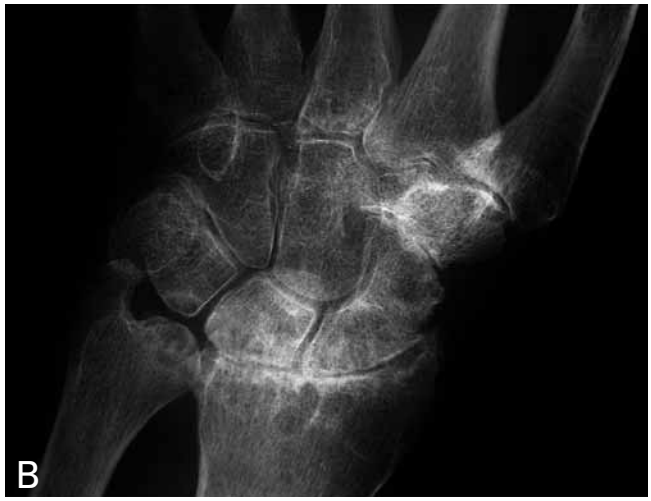

The diagnosis is **hemochromatosis**. This disease is one of a group in which subchondral 'cysts' are a hallmark. Others include hemophilia, CPPD deposition and Wilson's disease. Chondrocalcinosis may co-exist with these changes.

JBR–BTR, 2007, 90: 453.

Case 58
Longitudinal sonogram of the left middle finger in a 27-year-old man presenting with 'spring-finger' (Fig. A).
Small anechoic structure with diameter of 2,5 mm *(arrows)* is observed at the superficial aspect of the flexor tendon, at the level of the proximal phalanx. Posterior acoustic enhancement is observed.
During flexion *(not shown),* the lesion remains fixed to the superficial tissues, while excursion of flexor tendon was clearly observed.

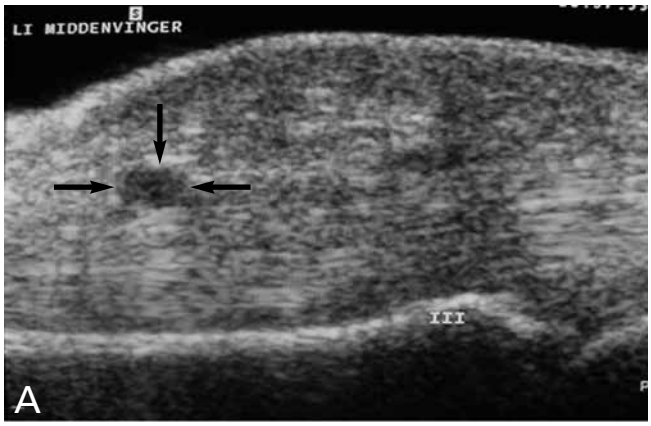

Together with history, the sonographic findings indicate tiny **tendon cyst** of the middle finger.

JBR–BTR, 2007, 90: 454.

Case 59
A 35-year-old man has complained of joint pains for several years. He has been able to continue his normal work and his general health is excellent. A recent radiography of his hands (Fig. A) is shown, together with a detail view of his right ring finger (Fig. B). What diagnosis would you consider?

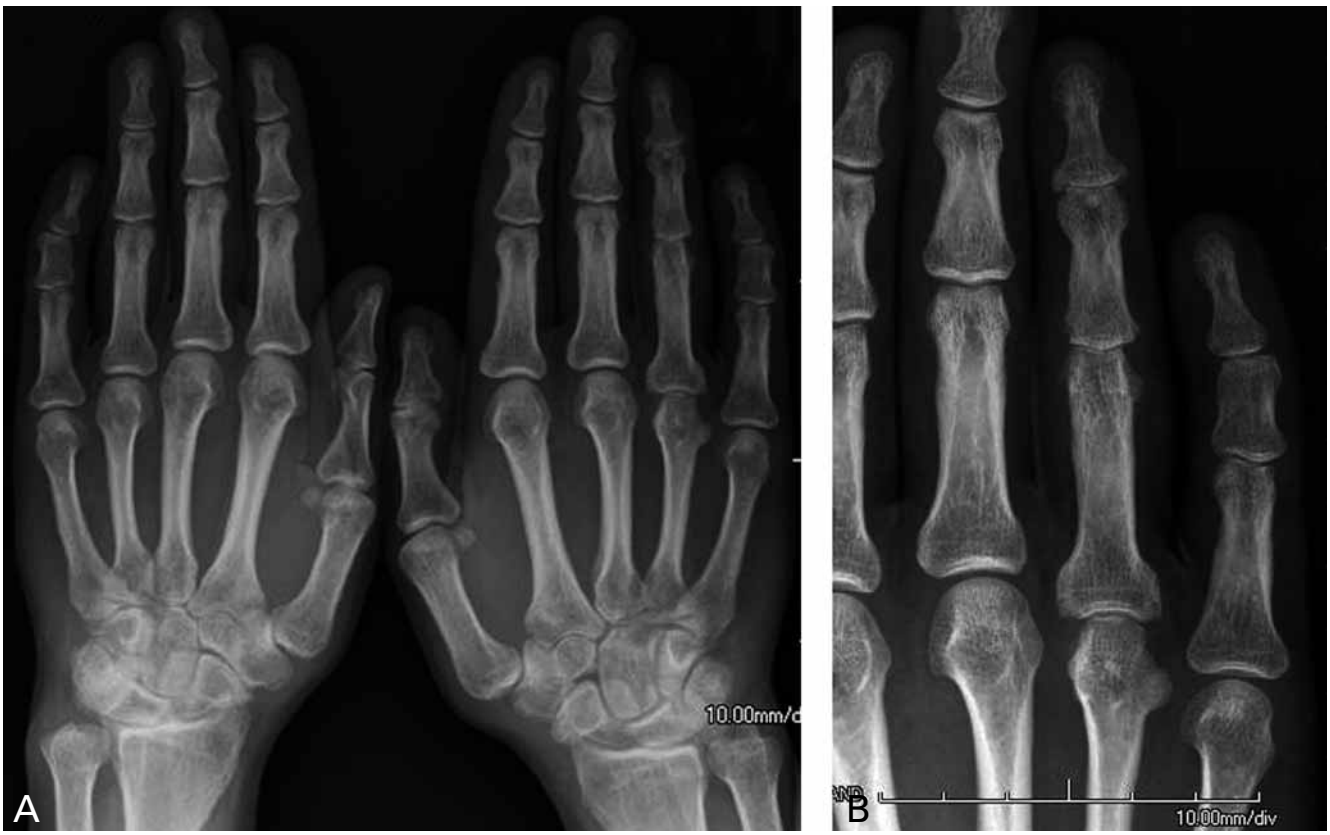

The major finding is that his ring finger is swollen and erosions are present at the 'bare areas' of the MCPJ and the IPJs. Note the associated new bone formation. The combination of synovial erosions with adjacent new bone formation strongly suggests either **psoriatic arthropathy** or, less likely, reactive arthritis. A patch of psoriasis was present above the patient's hair line at the back of his neck.

JBR–BTR, 2007, 90: 455.

Case 60
Radiograph of both hands (Fig. A) shows multiple osteolytic lesions, which are round or oval, well circumscribed and merely located in the periarticular regions. There is destruction of the distal phalanx of the left fourth finger and of the distal phalanx of the right thumb with associated soft tissue swelling (magnification). Scalloped lesion at the radial aspect of the middle phalanx of the right third finger. Similar lesions are seen at both feet.
Radiography of the chest shows widening of the mediastinum, probably due to enlarged lymph nodes.

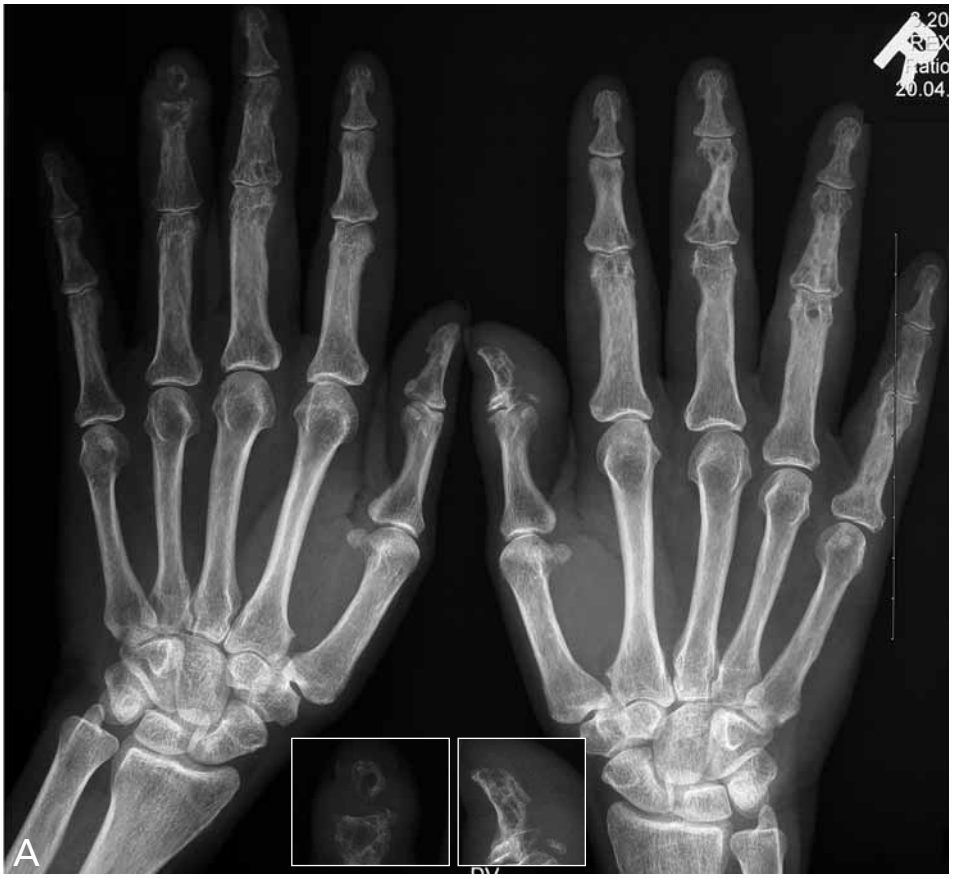

Biopsy specimen showed multiple non-caseating granulomas without acid-fast bacilli.
Radiography shows characteristic features of **chronic osseous sarcoidosis.**